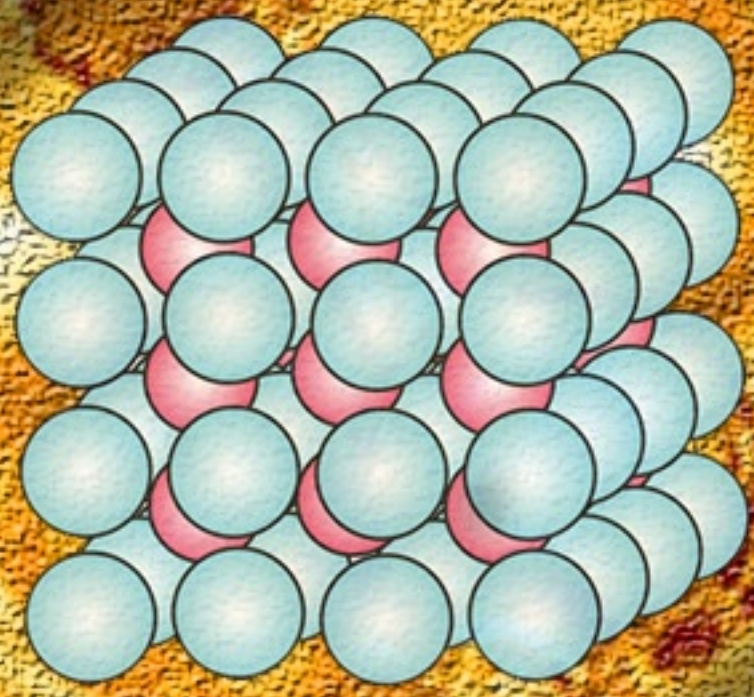
SCIENTIFIC TECHNICAL JOURNAL

# "MATERIAL SCIENCE"



## „NONEQUILIBRIUM PHASE TRANSFORMATIONS"

**ISSUE 2/2015**

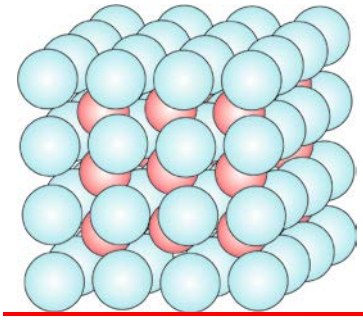
**YEAR I, ISSN 2367-749X**

PUBLISHER: SCIENTICIC TECHNICAL UNION OF MECHANICAL ENGINEERING

108 Rakovski str., 1000 Sofia, Bulgaria

tel./fax (+359 2) 986 22 40, tel. (+359 2) 987 72 90, www.mech-ing.com

e-mail: office@material-science.eu, http:/material-science.eu



**INTERNATIONAL JOURNAL**

# MATERIALS SCIENCE. NON-EQUILIBRIUM PHASE TRANSFORMATIONS

PUBLISHER:

**SCIENTIFIC TECHNICAL UNION OF MECHANICAL ENGINEERING**

108, Rakovski Str., 1000 Sofia, Bulgaria
**tel.** (+359 2) 987 72 90,
**tel./fax** (+359 2) 986 22 40**,**
office@material-science.eu

**ISSN 2367-749X**
**YEAR I, ISSUE 2 / 2015**

# EDITORIAL BOARD

## CHIEF EDITOR
Prof. Dimitar Stavrev – Bulgaria

## DEPUTY EDITOR:
Dr. Alexander Krugljakow, Germany
Prof. Sergey Dobatkin, Russia
Prof. Sergey Nikulin, Russia
Prof. Victor Anchev, Bulgaria

## RESPONSIBLE SECRETARY:
Assoc. Prof. Tsanka Dikova, Bulgaria

## MEMBERS:

Prof. Adel Mahmud, Iraq
Prof. Anna Proikova, Bulgaria
Prof. Bekir Sami Yilbas, Saudi Arabia
Prof. Dermot Brabazon, Ireland
Prof. Dipten Misra, India
Assoc. Prof.Eugeniy Grigoriev, Russia
Prof. F. W. Travis, United Kingdom
Prof. Gennagiy Bagluk, Ukraine
Assoc. Prof. Ibrahim E.Saklakoglu, Turkey
Prof. Iis Sopyan, Malaysia
Prof. Ivan Parshorov, Bulgaria
Prof. Ivanja Markova, Bulgaria
Prof. Janez Grum, Slovenia
Prof. Jens Bergstrom, Sweden
Prof. Leszek Dobrzanski, Poland
Prof. Ludmila Kaputkina, Russia
Prof. Nikolai Dulgerov, Bulgaria
Prof. Omer Keles, Turkey
Prof. Plamen Danev, Bulgaria
Prof. Rui Vilar, Portugal
Prof. Rusko Shishkov, Bulgaria
Prof. Saleem Hashmi, Ireland
Dr. Sefika Kasman, Turkey
Prof. Seiji Katayama, Japan
Prof. Souren Mitra, India
Dr. Sumsun Naher, United Kingdom
Prof. Svetlana Gubenko, Ukraine
Prof. Sveto Cvetkovski, Macedonia
Prof. Ventsislav Toshkov, Bulgaria
Prof. Yovka Dragieva, Bulgaria

# C O N T E N T S

**NANOSTATE PHENOMENON IN MATERIALS SCIENCE OF METAL-POLYMERIC SYSTEMS**
Assoc. Prof., Dr. Eng. Avdeychik S., Prof., Dr. Eng. Struk V., Assoc. Prof., Dr. Eng. Auchynnikau Y., Prof., Dr. Phys. Liopo V., Assoc. Prof., Dr. Eng. Ryskulov A. ..... 3

**SIZE FACTOR SELECTION MODIFIERS FOR FUNCTIONAL NANOCOMPOSITE MATERIALS BASED ON POLYMER MATRICES**
Assoc. Prof., Dr. Eng. Avdeychik S., Prof., Dr. Phys. Liopo V., Assoc. Prof., Dr. Eng. Auchynnikau Y., Prof., Dr. Eng. Struk V., Eisymont Y., , Pinchuk L. ..... 8

**NANOCOMPOSITE ENGINEERING MATERIALS BASED ON RECYCLED THERMOPLASTICS**
Burtsev A., Assoc. Prof., Dr. Eng. Auchynnikau Y., Struk A., Avdeychik O., Prof., Dr. Eng. Struk V. ..... 13

**METALLOGRAPHIC INVESTIGATION OF INDUCTION HARDENED PART TWO-SIDE LEVER**
Prof. Dr. Eng. Cvetkovski S., Asoc. Prof. Dr.Eng Nacevski G. ..... 17

**HARDENING OF AUSTENITIC STEELS WITH HIGH Mn AND Al CONTENT**
Prof. Dr. Phys.-Math. Kaputkina L.M., Prof. Dr. Eng. Svyazhin A.G., Cand. Eng. Bronz A.V., Cand. Eng. Smarygina I.V., Cand. Eng. Bazhenov V.E., Sen. Res. Cand. Eng. Kindop V.E. ..... 22

**EFFECT OF ALLOYING ELEMENTS ON THE MICROSTRUCTURE AND MECHANICAL PROPERTIES OF NiAl-Cr(Mo) EUTECTIC ALLOY**
Demirtas H. PhD.and Prof. Gungor A. ..... 25

**INVESTIGATIONS ON MAGNETRON SPUTTERED TANTALUM OXYNITRIDE THIN FILMS**
D. Cristea, L. Cunha, M. Pătru, D. Munteanu ..... 30

**INVESTIGATION OF PLASTIC DEFORMATIONS OF CARBURIZED ALLOY STEEL DURING HEAT TREATMENT**
Assoc. Prof. Dr. Kandrotaitė Janutienė R. ..... 34

**MECHANICAL PROPERTIES OF NANOSTRUCTURED B4C/C60 AND c-BN/C60 COMPOSITES PREPARED BY HPHT METHOD**
M.Sc. Prokhorov V. PhD., Prof. Blank V., M.Sc. Ovsyannikov D., M.Sc. Popov M. Dr., M.Sc. Levin V. PhD., M.Sc. Morokov E. ..... 38

**MICROSTRUCTURE AND THERMAL STABILITY OF 0.08%C-17.0%Cr-0.8%Ti STEEL AFTER HIGH-TEMPERATURE NITRIDING AND HIGH PRESSURE TORSION**
Ph.D. Rogachev S.O., Khatkevich V.M., Dr. Sci. Kaibyshev R.O., Ph.D. Tikhonova M.S., Dr. Sci. Dobatkin S.V. ..... 42

**THE COMPREHENSIVE TECHNIQUE FOR QUANTITATIVE ANALYSIS OF THE STRUCTURE IN COMPOSITE SUPERCONDUCTORS BASED ON Nb3Sn**
S.A. Nikulin, prof., Dr. Sc., A.B. Rozhnov, Ph.D., S.O. Rogachev, Ph.D., V.I. Zabolotnikova, postgraduate student, E.A. Dergunova, Ph.D, R.T. Aliev ..... 44

**INCREASE WEAR RESISTANCE HARD ALLOYS T15K6 BORIDE COATINGS**
Prof. Dr. Chernega S., Poliakov I., Grinenko K., Krasovskiy M. ..... 46

**MICROSTRUCTURE AND MECHANICAL BEHAVIOR OF TIG BIMETALLIC JOINTS**
M.F. Benlamnouar, R. Badji, M. Hadji, A. Boutaghane, N. Bensaid ..... 49

**HOT FORGING OF POWDERED Fe3Al INTERMETALLIC ALLOYS**
Prof., Dr.Sc. Bagliuk G.A., PhD. Tolochin A.I., PhD. Iakovenko R.V., M.Sc. Tolochina A.V., M.Sc. Kurikhin V.S. ..... 53

# NANOSTATE PHENOMENON IN MATERIALS SCIENCE OF METAL-POLYMERIC SYSTEMS

## ФЕНОМЕН НАНОСОСТОЯНИЯ В МАТЕРИАЛОВЕДЕНИИ МЕТАЛЛОПОЛИМЕРНЫХ СИСТЕМ

Assoc. Prof., Dr. Eng. Avdeychik S.[1], Prof., Dr. Eng. Struk V.[2], Assoc. Prof., Dr. Eng. Auchynnikau Y.[2], Prof., Dr. Phys. Liopo V.[2], Assoc. Prof., Dr. Eng. Ryskulov A.[3]
Molder LLC, Grodno, Belarus [1], Yanka Kupala State University of Grodno, Grodno, Belarus[2] , Tashkent automobile and road construction institute, Tashkent, Uzbekistan [3]
E-mail: molder.grodno@gmail.com, ovchin_1967@mail.ru, liopo@grsu.by, olimjong2008@mail.ru

**Abstract:** *There were considered the physical, structural and morphological prerequisites for the realization of the nanostate phenomenon of dispersed particles of condensed matter of different composition, nature and technology for production. It was shown the role of the size factor in the occurrence of the nanostate phenomenon due to the change of the energy parameters of the surface layers of particles that contribute to their effective modifying effect on the high-molecular matrix. Physical models of the formation of a particular energy state of dispersed particles and metallic and non-metallic materials substrates, characterized by the presence of local areas ("charge-mosaic") with a long relaxation time are proposed.It was considered practical application of the nanostate phenomenon when creating high-strength and wear-resistant materials based on thermoplastic matrices (PA6, PTFE, PET), consistent lubricant and lubricating oils, tribological and protective coatings for friction units and metalwares used in mechanical engineering, automotive and mining engineering. It was made the examples of the effective use of developed nanocomposite materials in practice.*
***KEYWORDS****: NANOSTATE, SIZE CRITERION, MODIFYING EFFECT, NANOCOMPOSITE MATERIALS, TRIBOTEHNICAL COATING, LUBRICANT.*

## *1. Introduction*

Cutting-edge areas of functional materials science of engineering is the practical realization of the phenomenon nanostate at different levels of structural organization, providing synergistic effects increasing the parameters of strength, tribological, thermal, adhesive and protective characteristics of composites by using nanoscale components of different composition, structure and technology of [1- 10].

Despite the significant progress made in the composite nanomaterials, there are considerable difficulties in their industrial production and industry use, due to the absence of uniform evidence-based approaches to the theoretical justification of engineering technology of nanomaterials that determine directional component selection, methods for their production and processing to ensure their industrial production scoped application.

Certain aspects of the structural and morphological characteristics and electrical energy in the form of nano-dispersed particles, thin films are considered in studies of domestic and foreign scientific schools [3, 5-10]. However, the transformation of phenomenological phenomenon nanostate in engineering technology functional nanocomposites based on macromolecular (polymeric, oligomeric, mixed) matrices is only possible in the implementation of a systematic approach that takes into account the effect of the characteristic features of the structure, the morphology, the energy state of nanoscale components on the structural organization of macromolecular matrices at the molecular, supramolecular and phase levels.

The purpose of this study was to develop criteria for evaluation of physical nanostate dispersed particles of condensed matter to justify the engineering technology of nanocomposite materials based on polymeric, oligomeric and common thermoplastic matrices.

## *2. Methods of research*

The main objects of the study were chosen nanoparticulate carbonaceous particles (graphite, UDAG, shungite, carbon fibers), metal (oxides, salts of organic acids) and silicon (mica, tripoli, opal clay) the compounds obtained by the process effects on natural and synthetic semi-finished products produced by industrial enterprises of Belarus and the Russian Federation. Nano-sized particles were prepared by mechanical grinding and heat treatment of disperse semis at temperatures 673-1473 K.

As matrix polymers used two basic types of materials. The first - with hereditary high viscosity (RGR) of the melt due to the chemical structure and molecular weight of the chain: polytetrafluoroethylene (PTFE), and ultra-high density polyethylene. The second group consisted of thermoplastic polymers PA 6, HDPE, EVA, PP, TPU, etc. With normal melt viscosity, this increases 2-3 times when the filling of nanoparticles - acquired high viscosity. Polymeric materials used in the state of industrial supplies as granules or powder produced by cryogenic dispersing granules at a temperature of 87 K.

The structure and properties of nanocomposite materials and their products investigated using modern methods of physical and chemical analysis: IR transmission and ATR (Specord), EPR spectroscopy (ER 1306, Brucer), X-ray diffraction (DRON 2.0, 3.0 DRON ), differential thermal (Q-1500) analysis, optical (MIM-10, MF-2), scanning electron (ISM-50A, Nanolab-7) and atomic force microscopy (Nanotop III). Energy state nanomodifiers and composite materials was evaluated by EPR spectra and the spectra of thermally stimulated currents (TSC) on the original installation of the GNU MPRI them. VA White NASB. The dielectric characteristics of materials after exposure to energy (laser, ion, temperature) were determined by an appropriate standardized methods. Regulation nanorelief surface layer of polymer samples was performed by short-pulse laser and accelerated ion impact with a given power density. Evaluation features crystal-chemical structures of nanoparticles was performed by the original method, developed on the basis of X-ray analysis.

## *3. Results and discussion*

To assess the role of the energy factor in mechanisms of formation of the structure at the molecular composite materials, and interface supramolecular structure parameters investigated dispersed particles, which are widely used as modifiers for oligomeric, polymeric matrices and combined.

Methods OM, AFM, SEM analysis of morphological features of dispersed particles of different composition, technology of reception, crystal chemical structure - oxide compounds metallurgical production (OM), the products obtained by a mechanical crushing silicate glasses (SS), carbon-fiber (CF), the products of detonation synthesis ( UDAG), carbon nanotubes (CNTs), silicon-containing natural particles (CN) - mica, tripoli, clays, schungite, talc.

It was found that, regardless of the technological history and crystal structure of the starting semi-dispersed particles form the cluster structures, and consisting of single particles with nanoscale parameters. This single particle morphology characterized by the presence of nanoscale spherical elements, plate or whisker habit forming nanorelief surface layer, contributing to the formation of the boundary layer at the interfacial interactions of the components in the formation of the nanocomposite material. Specific nanorelief surface layer due to crystal-chemical and technological prerequisites, is predominant factor in the choice of the original semi-finished product and technology of dispersed particles with optimal dimensional parameters. This dispersion of particles of a modifier can be in the range of micro, providing the necessary modifying effect due to the presence of nano relief with a characteristic structure forming elements. With this practical production nanocomposite materials based on polymeric matrices may use available intermediates, for example, silicon and carbon-containing minerals, with the widespread use of high-dispersion technologies.

Based on the classical concepts of the mechanisms of formation of boundary layers with optimal structure, defining the parameters of strength, tribological, thermal, and others service performance composites and products from them, found that the main factors influencing the mechanism and kinetics of their formation, are the mechanical and energy. Mechanical factors contribute to the formation of the adhesive bond and the polymer matrix modifier by crushing fragments melt penetrated under pressure form the workpiece or products nanofields topography of the surface layer of the particle. Power factor provides the course of adsorption and orientation process at the interface "matrix - filler", leading to the formation of an ordered (quasi-crystalline) structure of the boundary layer with high strength characteristics of the parameters.

The combined effect of both factors makes possible the realization of synergies, providing a comprehensive impact modifier dispersed nanocomposite structure at the molecular, supramolecular and interfacial levels, which leads to a simultaneous increase in its parameters of strength, tribological, protective, etc. Service characteristics.

The physical criteria for assessing nanostate dispersed particles of condensed matter of varying composition and crystal structure. Studies Ajayan P.M., N. Kobayashi, Suzdaleva I.P., Trefilov V.I., Gusev A.I., Poole Ch., Owens F., Stroscio M.A., Dutta M. and employees, according to the determining role of size factor in moving the particles of condensed matter from macro to nano-state that they exhibit specific energy parameters influencing the processes of structure-modified matrix [9, 10].

Currently, there are no uniform sound approaches to the definition of the boundaries of existence dimensional nanoparticles. Boundary size of nanoparticles used in 100 nm has no clear physical basis and is not correlated with the experimental results.

Nanoparticles have at least two characteristic features (taxa). Firstly, the nanoparticles should have a developed surface. Second, the performance parameters in the nanoparticle physical properties (S) depend on its linear dimensions (r), i.e. nanoparticles of various substances exists function S (r). To characterize the surface of the nanoparticle concept is crucial. Nanoparticles regarded as an independent object which can be isolated from a mixture with other objects or other mechanical means. Therefore, the nanoparticles can be regarded as a kind of nanophases with its specific features.

The term "surface" for macroscopic and low-dimensional particle has a different physical meaning. For macroscopic objects 'surface' is treated as an imaginary infinitely thin film on one side of which there are atoms of a specific substance, and on the other side they are missing. The surface at the equilibrium state of the object is treated as a statistical system, neglecting the thermal vibrations of the atoms. In the transition to the surface of the nano-sized objects to be regarded as a dynamic system. Since the period of atomic vibrations immeasurably less time any experiment, it is necessary to speak of the surface layer. If we consider that in addition to the surface atoms mutual atomic configuration changes just adjacent to the outer nuclear layer, this surface layer can be commensurate with the size of the particle itself.

The average (idealized) dependence of the parameters of the physical properties of the particle size (S(r)) is shown in Figure 1.

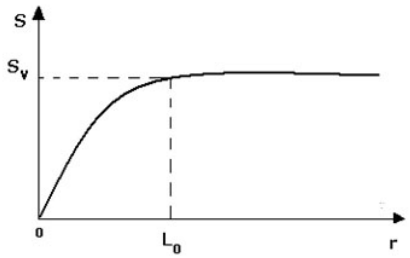



Figure 1 - The dependence of the parameter S of the physical properties of particle of size [S(r) function]

Figure 1 shows that a decrease in the size of the sample to a certain value $r = L_0$ the numerical value of the physical property $S(r) = S_V = const$, where $S_V$ - value characteristic of the bulk sample (table). If the $r < L_0$ parameter $S(r)$ decreases monotonically and if $r \to 0$ then $S(r) \to 0$.

Analytical dependence of the function has the form

$$(1)\ S(r) = \frac{S_V}{\left|\exp\left[\alpha\left(\frac{L_0 - r}{r}\right)^{3/2}\right]\right|} = \frac{S_V}{\left|\exp\left[\alpha\left(\frac{1-x}{x}\right)^{3/2}\right]\right|},$$

where $L_0$ - dimensional boundary between nanostate ($r < L_0$) and macrostate ($r > L_0$); $\alpha$ - parameter depending on the analyzed physical properties.

The presence of a sufficiently large volume of literature and our experimental data allows to confirm the consistency of the phenomenological formula (1). Obviously, if the parameter r passes through the dimensional limits $L_0$ of variation of the parameter S is not sharp. The more r different $L_0$, the more manifest the properties of the respective state. It can be concluded that when $r = L_0$ a substance is a change in the mechanism of physical processes or modified structural and energy characteristics of the particle compared to the bulk counterparts.

Based on the assumptions that the dimensional criteria nanostate $L_0$ should take into account the characteristic properties of substances that meet the basic understanding of the physical paradigm used tabulated values of the physical characteristics and is calculated by a simple formula, as the criterion for calculating the Debye temperature has been selected ($\theta_D$).

Debye temperature ($\theta_D$) as the $L_0$ parameter is not strictly a sharp boundary, but this option is entered in the modern physical paradigm. Debye theory of heat capacity indicates that the transition frequencies of quantum oscillators across the border $\omega_D$ there is a change in the mechanisms of the processes of substance. The atoms as quantum oscillators vibrate at a certain frequency. At low volumes on the geometrical dimensions of the frequency spectrum is influenced not only the structure of the substance, and the particle size. Vibrations of atoms to create a dynamic field that oscillates the electrons in the electron cloud with the same frequency.

Debye theory of heat capacity indicates that the transition frequencies of quantum oscillators across the border $\omega_D$ there is a change in the mechanisms of the processes of substance. The atoms as quantum oscillators vibrate at a certain frequency. At low volumes on the geometrical dimensions of the frequency spectrum is influenced not only the structure of the substance, and the particle size. Vibrations of atoms to create a dynamic field that oscillates the electrons in the electron cloud with the same frequency.

As part of the one-electron adiabatic approximation, we introduce the concept of Debye pseudo impulse $P_D$. We believe that the effective electron mass equal to the mass of a free electron. In this case

(2) $P_D = \sqrt{2mE_D}$

According to the formula of de Broglie Debye pseudo impulse $P_D$ allows you to calculate the value of the Debye length (wave):

(3) $\lambda_D = \frac{h}{P_D}$

Consequently, the Debye length $\lambda_D$ is the dimension of the boundary between the nano- and macrostate ($L_0 = \lambda_D$) substance in the condensed state.

Debye parameters $\omega_D$, $E_D$, $\theta_D$ are related to each other by the equations [22]:

(4) $E_D = \hbar\omega_D = k\theta_D = \frac{P_D^2}{2m} = \frac{h^2}{2m\lambda^2}$

where $\hbar$, $h$ ($h = 2\pi\hbar$) - Planck's constant, $k$ - the Boltzmann constant, $m$ - mass of the electron.

Note that in these terms the Debye length and the de Broglie wavelength coincide. Condition (4)

(5) $k\theta_D = \frac{\left(P_x^2 + P_y^2 + P_z^2\right)}{2m} = \frac{h^2}{2m\lambda_D^2}$

For an isotropic medium $P_x^2 = P_y^2 = P_z^2$. In this case, the parameter of the Debye length $\lambda_D$, for example, along the axis x (y or z) is defined by the expression:

(6) $L_0 = \lambda_D = \frac{\sqrt{1,5}h}{\sqrt{km}}\theta_D^{-1/2}$

After substituting the numerical values of physical quantities ($h$, $k$, $m$) received:

(7) $L_0 = 2,3\cdot 10^{-7}\left[m\cdot K^{-1/2}\right]\cdot\theta_D^{-1/2}[K] = 230\cdot\theta_D^{-1/2}[nm]$

Analysis of the expression to evaluate the dimensional border nanostate particles of condensed matter using the Bloch theorem, the Schrödinger equation, concepts of Debye wavelength $L_0 = \lambda_D$ indicates eligibility to use it to determine the parameters of nanoscale particles (NSP) of different composition and structure.

The expression (7) suggests the existence of a probability of correlation between the critical size $L_0$ of the nanoparticles and the Debye temperature $\theta_D$ of the crystal from which they were formed.

The shape of nanoparticles can have a different habit (spherical, needle, plate). For such particles the parameter $L_0$ value will depend on the direction, i.e. there are cases where "nanofeatures" particles will not occur in all directions (x, y, z), and one (needle habit), two (lamellar habit) or three (spherical habitus). Therefore, by using modifiers particles having a relatively large size and nanometer active sites may be achieved by modifying effects inherent in the "classical" nanoparticles at least energy rich techniques for their preparation by synthesis or dispersing the intermediate product.

With the use of the proposed analytical expression (7) carried out calculation of critical parameter $L_0$ for particle single-element and multi-element materials - metals, non-metals, halides, semiconductor compounds. The results are in good correlation with literary sources, and allow us to determine the most effective technology for nanoscale modifiers for use in materials of polymer nanocomposites.

Analysis features nanostate particles of condensed matter using quantum theory allowed to show that for each substance there is an energy parameter $E_0$ differentiating the process. When $E > E_0$ dimensional effects do not play a role and true volumetric approach to describe the properties of the substance; when $E < E_0$ it need to take into account the size effects. The influence of the size factor on the energy characteristics of dispersed particles of silicon and carbon-containing components that have found the most widely used as a functional polymer modifiers and oligomeric matrix in the development of nanocomposites with enhanced service performance parameters.

The quantum-mechanical analysis of bulk and surface states of the particles showed that the potentials of the near-surface areas are not simply scrap the wave functions of the potential in the volume, but also have their own characteristics that appear in the manifestation of the electron work function of metals and a number of surface effects in dielectrics and semiconductors. The mechanism of formation of a particular energy state of the metal and dielectric samples, leading to the appearance of the surface mosaic observed experimentally.

The analysis of the crystal-formation mechanisms of nanoparticles in an active state by thermal or mechanical stress on the semi-finished products of natural layered silicates, frame and chain structure (mica, clay minerals, natural opals, tripoli). Among the most common are geosilikates laminates comprising various modifications of the mica and clay minerals. A common feature of this type is the presence of specific minerals of the crystal lattice with a perfect cleavage, consisting of layers of silicon-oxygen tetrahedra $SiO_2$, connected by a layer of metal-oxygen octahedra, and the interlayer cations.

With the destruction of the block layered minerals interlayer cations $Na^+$, $K^+$ to pass one of juvenile surfaces and form localized regions with a charge so-called " charge mosaic" such a structure of juvenile surfaces of layered silicates with charge areas, the area of which is many times the size of the cations causes the flow of intense processes of interaction with the environment of Nanophase particle. The presence of active centers on juvenile surfaces, form the basis of tetrahedra $SiO_2$, changes the course of adsorption processes on the surface of the particles and affects the structural ordering of molecules in contact with them and oligomeric polymeric macromolecules. Thus, the specific structure of the crystal-phyllosilicates creates the preconditions for the formation of nanoscale dispersion of the active particles, which have a modifying effect on the polymer matrix.

The actual particles of natural silicates are nonequilibrium structure, determine the existence of uncompensated charge. By EPR spectroscopy and TSC spectroscopy revealed the presence of uncompensated charge and the possibility of thermostimulated nanocuttent in powder samples of silicate minerals (opal, white and blue clay) (Figures 2, 3). Thermal effects on particulate phyllosilicates leads to a restructuring of their structure. On thermograms silicate minerals of various composition and structure can mention a few endoeffect at temperatures 373-423 K 523-623 K, 723-823K, 1023-1123 K, due to the processes of dehydration and dehydroxilation. The effect of 523-623 K characterizes the selection of interlayer water. When exposed to process blocks phyllosilicates mode thermal shock dehydration processes, water and interlayer separation degidroksilatsii occur virtually simultaneously, resulting in macrodestruction crystals due to rupture of the interatomic bonds. Product image type noncrystalline oxides and X-ray amorphous phases of different composition. The size of the particles formed during thermal processing products does not exceed 100 nm, according to modern concepts it allows to refer them to the nanoscale.

The special characteristic of the energy state and carbonaceous particulate matter (UDDG, carbon nanotubes, shungite). A characteristic feature of these low-dimensional particles of different composition, structure and technological history is the dependence of the energy state characterized by the magnitude of thermally stimulated currents, temperature. Therefore, when choosing the modifier to obtain nanocomposite materials with desired functional parameters (tribological, of strength, adhesion) must take into account the temperature range of manifestations of its maximum activity. Practical implementation of the established principles of the Energy of the respective components of nanocomposite

materials based on polymeric matrices can achieve significant effects as in the doping content nanomodifier (0.001 - 1.0 wt.%), And the powers of filling 20 - 40 wt.%.

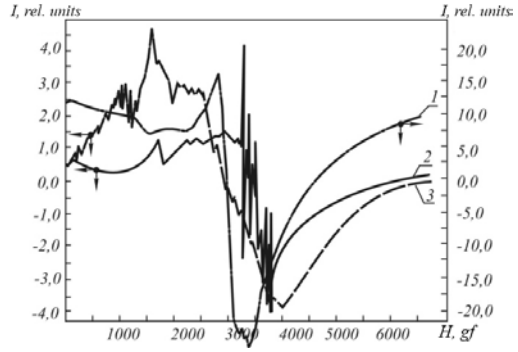



Figure 2 EPR spectra of opal (1) and clay minerals of different composition (2, 3)

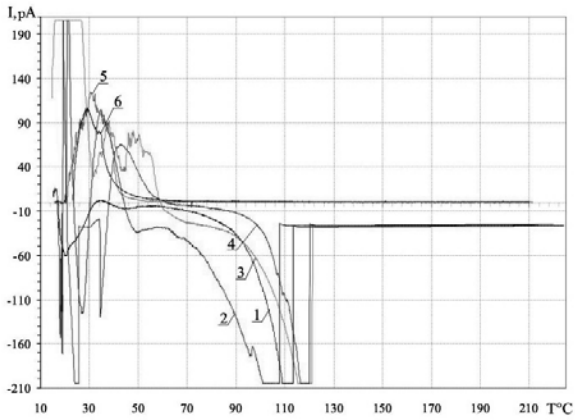



Figure 3 Characteristic form TSC-spectrum shungite source (1) and heat-treated at 100 ° C (2) 200 ° C (3) 300 ° C (4), 600 ° C (5) 800 ° C (6)

The mechanism of action of modifying nanoparticles in polymer matrices and different oligomeric structure. Based on the developed model, involves the formation of the adsorbed layer under the action of the active centers of the spherical nanoparticles form macromolecules, analytical expressions for calculating the concentration of modifier enough to transfer the entire matrix in an ordered state. The matrix will be in a modified form, if the nanoparticle influences the matrix macromolecule in the boundary layer thickness L:

$$(8)\ L = r_1\left[1+\frac{\rho_н}{\rho_n}\right]\left(\frac{1}{C_m}-1\right)^{1/3},$$

where $r_1$ - particle size.

Even if the content of doping nanofiller (0.001 - 1.0 wt.%) And the ratio of its modifying effect for at least 2 - 3 layers adjacent macromolecules achieved significant technical effect of improving the parameters of strength and tribological characteristics of nanocomposites based on thermoplastic matrices.

It is found that the efficiency of modifying action NSP affect not only the parameters of size, composition and structure, and form. When using a layered particles (flaky), whisker and the spherical shape of varying degrees of modification of the matrix M defined by the ratio of the total volume of the modified to the total volume of the composite. Taking into account the different energy states of various shapes NSP obtained degree of modification ratio of scaly ($M_{sc}$), whisker ($M_w$) and spherical ($M_{sp}$) particles at the same concentrations in the composite:

$$(9)\ M_{sc} : M_w : M_{sp} = 1 : 0,4 : 0,8$$

From this expression that when creating malonapolnennyh nanocomposites based on polymer matrices is the most effective use of layered modifiers, which include natural silicates - clay, mica.

The experimental and theoretical studies are based on the assumption of constancy of the structure, composition and habit NSP introduced into the polymer matrix. However, there are classes NSP (metal, oxide, metallic) that can be transformed under the influence of physical and chemical processes occurring in the boundary layers of the composites under the influence of operational factors (temperature, mechanical, mechano-chemical, etc.) To give the product a different composition and structure. Therefore informed choices NSP for modifying the target polymer or oligomer matrix involves a systematic analysis of the structural phase transitions with the energy, chemical and physical aspects of the formation and operation of metal-system.

A systematic approach to the analysis of the features of the modifying action of nanoscale objects of different composition, structure and technology for the development of scientific principles has led to the creation of functional engineering of nanocomposite materials based on commercially available thermoplastics (polyolefins, polyamides, polyacetals, fluoropolymers, and mixtures thereof) and technology of their processing in products with higher performance parameters.

To apply tribological and protective coatings of the developed nanocomposite materials based on polyamides developed the technology and installation for cryogenic grinding granular semifinished providing manufacturing powders with a given degree of dispersion of energy and activity (Figure 4).

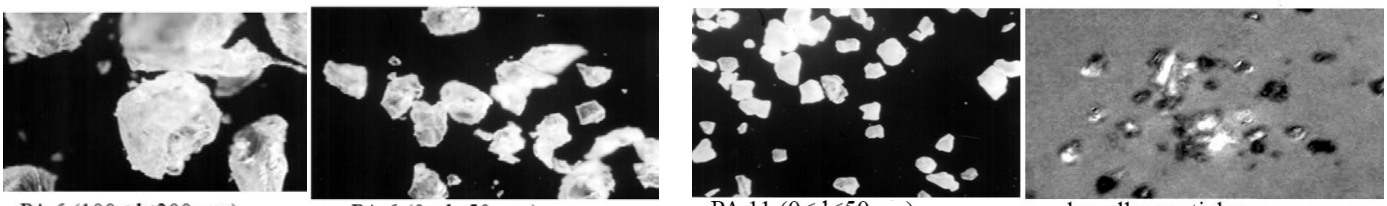



Figure 4 - The characteristic morphology of the particulate fraction of nanocomposites based on PA 6 and PA 11

The resulting powder semifinished provides functional coatings with the necessary operational parameters as they are formed by methods of the fluidized bed and flame spraying.

The compositions of tribological coatings used in the construction of automobile units to improve the wear resistance of splines driveshafts transport and special equipment, the protection of the elastic members of brake chambers trucks from corrosion and mechanical wear and fatigue failure and to prevent jamming in the mechanism of the drive lathe chuck technology metalworking equipment. Application of nanocomposites based on polyamide 6 (JSC "GrodnoAzot") instead of imported counterpart PA 11 («Rilsan») provided to obtain significant economic effect on the JSC "Belcard", JSC "BelTAPAZ 'products are used for the assembly of automotive engineering and metalworking equipment produced in the Russian Federation [11].

For the manufacture of nanocomposite materials based on polytetrafluoroethylene developed the original tooling and equipment for the implementation of effective activation of

components in the process of filling the system of training, cold pressing, hot monolitization and calibration. The technological methods to eliminate or minimize the negative effect of structural factors at various levels, enhancing defect nanocomposites and products of them as a result of the clustering of the particles of the reinforcing filler (HC) and their inefficient wetting polymer binder being in viscoplastic state at temperatures monolitization (573 - 673 K) pieces .

The effectiveness of the developed nanocomposite materials based on polytetrafluoroethylene due to a decrease in the content in the composite costly filler - carbon fiber (CF), while maintaining the required performance parameters and a decrease in energy consumption due to optimization of the technological cycle of manufacturing products (billets) . In addition, the use of technology Cold monolitization to reduce the loss of the composite due to allowances. Application of the developed nanocomposite materials for the manufacture of elements moving seals compressor equipment for compressed and liquefied gases (JSC "Grodno Azot", JSC "Sumy Scientific-Technical Center", JSC "Frunze Sumy Machine Building Scientific Production Association") provides an increase in the service life of less than 2 times [14-16].

Increased resistance to spike universal joint propeller shaft brinnelling achieved by using plastic lubricants designed for heavy duty units containing polymer fibers and low-dimensional nanoporous carbon particles or metal particles thermoplastics. Developed based lubricant base oils and industrial-20, I-40 at ANTI characteristics and resistance to mechanical degradation far superior lubricant used CIATIM 201, №158, Lithol-24 [16].

To ensure the technical performance of the brush attachment drive road cars developed abrasion composite material based on PP-doped doping additives (0,01-2,0 wt.%) Geomodifiers layered, chain or frame structure. Introduction into the polymer matrix of the active particles geosilikate reduces melt index composite 1.5-2.0 times and stabilizes the extrusion of strands at the multislot head. The structure of the composite with physical crosslinks oriented uniaxial stretching with the formation of the ordered area, increases the strength of 1.3-1.5 times and 1.5-2 times material to the resistance to abrasion. Designed nanocomposite composition allowed to apply to PP as the base material for general technical purposes instead copolymer doped with a thermoplastic elastomer having almost twice higher value [16].

Conducted testing of the developed nanocomposite formulations of engineering materials based on thermoplastic matrices at industrial enterprises of Belarus and Russia testifies to their high efficiency and expediency of application in the construction of automotive engineering, process equipment and valves.

## *4. Conclusion*

Based on a systematic approach to the study of the impact of the structural features and the energy state of nano-sized particles of condensed matter the mechanisms of physical and chemical processes in polymer matrices that define the parameters of their structure at the molecular, supramolecular and interfacial levels. Methodological approaches to the creation of nanocomposite materials with high engineering parameters of strength, tribological, adhesive and protective characteristics on the basis of industrial thermoplastics and their production technology and processing into products.

Methodological principles of obtaining nanocomposite materials based on thermoplastics industry, consisting in:

- crystal-established assumptions selection of natural and synthetic carbon-containing, silicon metal and semi-finished products for directional formation of active nanoparticles with desired structural and morphological and energetic parameters for optimum technological impact (mechanochemical, thermal, laser);
- implementation of the conditions prevailing energy nanomodifiers compliance mechanism of the optimal structure of the polymer, oligomeric matrices and combined at different levels - molecular, supramolecular and interfacial;
- ensuring the development conditions of the preferred mechanisms of interfacial physico-chemical interactions of the components with the formation of boundary layers optimum structure, defining mechanisms of destruction of the nanocomposites under the influence of various operational factors [11-16].

## *5. Literature*


1. Skaskevich, A. Structure and technology malonapolnennyh engineering materials based on engineering thermoplastics modified with carbon nanoclusters author. diss. ... cand. tehn. sciences, Minsk BGTU, 2000. - 18 p.
2. Avdeychik, S. The polymer-silicate materials engineering, physico-chemistry, technology, use, Minsk: Tehnalogiya, 2007. 431 p.
3. Pokidko, B. Adsorptive modifying of laminated silicates for reception polymer-silicate nanocomposites. dis. ... cand. chemical. science, Moscow, 2005. - 154 p.
4. Vinogradov, A. Creation and research of tribological engineering materials based on PTFE and ultrafine sialon. diss. ... dr. tehn. sciences,Gomel, 1993. - 293 with.
5. Okhlopkova, A. Plastics filled with ultrafine inorganic compounds. Gomel, MPRI of NAS B, 1999. - 164.
6. Petrova, P. Development engineering tribological materials based on polytetrafluoroethylene and natural zeolite deposits in Yakutia. diss. ... cand. tehn. science, Gomel, 2002. – 125 p.
7. Bouznik, V. Status of domestic chemistry fluoropolymers and possible prospects for development. - Russian Chemical Journal. - 2008. - T. LII. - №3. - P. 7-12.
8. Avdeychik, S. Introduction to the physics of nanocomposite engineering materials, Grodno, GGAU, 2009. -439 p.
9. Guozhong, Cao Nanostructures and Nanomaterials. USA, World Scientific, 2011 - Science - 581 p.
10. Gusev, A. Nanomaterials, nanostructures, nanotechnology. Moscow, FIZMATLIT, 2005. - 416 p.
11. Avdeychik, S. Innovative coating technology. Moscow, Publishing House. House "Spectrum", 2012. - 272 p.
12. Avdeychik, S. Innovative engineering technology. Volume II. Moscow, Publishing House "Spectrum", 2012. - 336 p.
13. Avdeychik, S. The nanocomposite and nanostructured materials engineering and technology for their production. Moscow, Publishing House "Spectrum", 2013. - 224 p.
14. Avdeychik, S. Machine-building fuorcomposites: structure, technology, application Grodno, YKSUG, 2012. - 339 p.
15. Avdeychik, S. Fluorinated inhibitors of wear metal-tribosystems. Minsk Tehnalogiya, 2011. - 270 p.
16. Avdeychik, S. Nanocomposite materials engineering: experience in development and application. Grodno, YKSUG, 2006. – 403 p.

# SIZE FACTOR SELECTION MODIFIERS FOR FUNCTIONAL NANOCOMPOSITE MATERIALS BASED ON POLYMER MATRICES

## РАЗМЕРНЫЙ ФАКТОР ВЫБОРА МОДИФИКАТОРОВ ДЛЯ ФУНКЦИОНАЛЬНЫХ НАНОКОМПОЗИЦИОННЫХ МАТЕРИАЛОВ НА ОСНОВЕ ПОЛИМЕРНЫХ МАТРИЦ

Assoc. Prof., Dr. Eng. Avdeychik S.[1], Prof., Dr. Phys. Liopo V.[2], Assoc. Prof., Dr. Eng. Auchynnikau Y.[2], Prof., Dr. Eng. Struk V.[2], Eisymont Y.[2], Pinchuk L.
Molder LLC, Grodno, Belarus [1], Yanka Kupala State University of Grodno, Grodno, Belarus2
E-mail: molder.grodno@gmail.com, liopo@grsu.by, ovchin_1967@mail.ru, gffh@mail.ru

**Abstract:** *On the basis of modern concepts of condensed matter physics and quantum physics considered the criteria for inclusion of dispersed particles of different composition, structure, and technological background to nanomodifiers of polymeric, oligomeric and combined matrices. There were proposed an analytical expression for the evaluation of limiting size of the dispersed particles $L_0$, which characterizes the manifestation of a particular energy state - nanostate.There was implemented the analysis of experimental and literature data confirming the adequacy of the calculated value of the size of particles in nanostate obtained using relation $L_0=230 \bullet \theta_D^{-1/2}$, where $\theta_D$ - Debye temperature. It is shown that the provision of effective modification of macromolecular matrices necessary and sufficient condition is the presence of dispersed particles of different composition and structure of nanoscale structural fragments of the surface layer, which ensure the implementation of synergies through a combination of energy and mechanical factors in the formation of boundary layers of the optimal structure.*

***KEYWORDS**: DISPERSED PARTICLE, NANOSTATE, SIZE FACTOR, DEBYE TEMPERATURE, NANOSIZED FRAGMENTS. SURFACE.*

## *1. Introduction*

In the first half of the last century, in the scientific paradigm of condensed matter physics, including materials science, underlie the notion that the physical properties of the substances assessed by parameters characteristics affect their structural and chemical characteristics, environmental factors and individual characteristics of structure of concrete objects, called defects. Defects are considered as deviations of atomic structure and mutual configuration from their average structures called ideal structural models [1, 2]. The numerical values of the characteristics of the properties of substances called parameters given in the table without specifying the size of the sample on which they are defined. But in certain size ranges of particulate matter values of characteristics of the physical properties begin to differ from the parameters of bulk material analogs, and often fine particles acquire new properties, which allows them to achieve new effects, including in materials science and other practical applications.

For example, nanoparticles are not only provided the basis for the miniaturization of microelectronic components and shaped the direction of nanoelectronics, but also began to be used as functional additives to conventional substances used in materials science as matrixes. Such additives are responsible for structural changes of matrices at different levels, which leads to a significant effect of improving performance parameters: tribological, deformation-strength, thermal and others. [3]. Intensively began to develop methods of producing nanoparticles, as well as the creation of composite materials, in which these particles are included as a modifying components. There are new terms: nanostructures, nanotechnology, nanomaterials, nanophysics et al. [4, 5]. It should be noted that the effect of particle size on the parameters of the various materials and their incorporation has been known for a long time. Nanomaterials in the form of glass, painted metal colloidal particles, produced in ancient Egypt. Light scattering such glasses studied Michael Faraday. In 1906-1910 P. Veimarn research found that "... between the world of molecules (atoms, ions) and microscopically visible particles there is a special form of matter with a complex of the physical and chemical properties inherent to this form - ultrafine or colloidal state, produced when the degree of dispersion (fragmentation) in $(10^5 \div 10^7)$ $cm^{-1}$, wherein the films have a thickness and fiber and particle size diameter in the range of (1,0 ÷ 100) nm "[6].

Nanotechnology, as a branch of colloid chemistry, known from the middle of the XIX century. In 1935, W.J. de Haas and T. Birmash found that the thermal conductivity of the low-dimensional particles is different values macro sized counterparts values. In 50-ies of XX century, it was confirmed by R. Berman, and attempt was made by R. Peierls to explain these results [7]. At the turn of XX and XXI centuries, the amount of basic knowledge of physics, chemistry and related sciences has led to the realization that the prefix "nano" actually forms new research areas that are of great practical significance [8].

## *2. Nanoparticles (definition)*

Despite the fact that in recent years nanophysics and nanotechnology achieved unquestionable success, up to date no generally accepted definition of the term "nanoparticle" [4, 5]. Probably one of the first sources that indicated the dimensional boundaries of nanoparticles 1,0 ÷ 100 nm is above cited paper P. Weimar [6]. Follow-known studies have not paid enough attention to the justification of the size range of nanoparticles. Moreover, this dimension of the boundary between the nano- and macro-particulates adopted the same regardless of the composition and structure of matter. This approach lacked a sufficient physical justification. With the same 'success' can take any temperature as the melting temperature for all substances. At the convention dimensional border 100 nm indicated in a number of papers (eg, [9]). In this monograph when considering the impact of size on the properties of the dispersed particles rather cautiously said that "the effect of significant changes in the properties appears when the grain size is less than 100 nm, and is most clearly seen when the grain size is less than 10 nm". Boundary 100 nm can be applied to characterize the nanocrystal when describing it in a general way. We proceed from the fact that not everyone nanoobject is nanoparticle.

Nanoparticle must have at least two major features (taxa). Firstly, the nanoparticles should have a developed surface. Second, the performance parameters in the nanoparticle physical properties (S) depend on its linear dimensions (r), i.e. nanoparticles of various substances exists characteristic function S(r) (Figure 1). For the nanoparticle concept of the surface is crucial. Nanoparticles regarded as an independent object which can be isolated from a mixture with other substances by mechanical, chemical or other means. Therefore, the nanoparticles can be regarded as a kind of nanophases with its specific features due to the composition, structure, technology acquisition and others factors.

A number of studies [4, 5, 8] suggested that the main role in the formation of specific properties parameters of nanoparticles plays their surface. In the macroscopic objects of atomic and molecular

mutual configuration in the surface layer is different from that which is structurally identical characteristic surface atomic planes in the crystal [9, 10]. It is believed that the influence of the surface as a two-dimensional defect applies to 5 - 7 atomic layers [11-13].

The concept of "surface" for macroscopic and low-dimensional particle has a different physical meaning. For macroscopic objects 'surface' is treated as an imaginary infinitely thin film on one side of which there are atoms of a specific substance, and on the other side - they do not exist. Of course, the surface atoms vibrate, but the amplitude of the thermal vibrations is so small compared to the size of macroobject that it is neglected. The surface at the equilibrium state of the real object is treated as a static system. Surface to be regarded as a dynamic system in the transition to the nano-sized objects. Since the period of atomic vibrations immeasurably less time any experiment, it is necessary to speak of the surface layer. If we consider that in addition to the surface atoms mutual atomic configuration changes just adjacent to the outer nuclear layer, this surface layer can be commensurate with the size of the particle itself. With further decrease the size of the concept of the surface loses its meaning. A particle moves in atom-cluster state [13]. It must be noted that the surface can be absent not only in low-dimensional particles, but also the objects of a size reaching hundreds of meters or more. For example, in the strict sense, surface did not exist for such macroscopic objects as clouds.

The dependence of the numerical values of the parameters of the physical properties of the particle size is observed by many investigators [1, 2, 8, 14-18]. The average (idealized) dependence of the parameters of the physical properties of the particle size (S(r)) is shown in Figure 1.

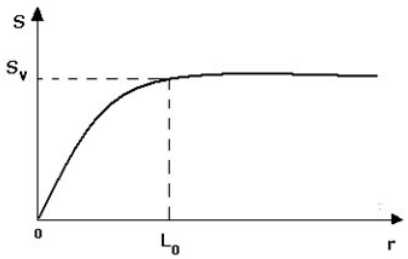



Figure 1 - The dependence of the parameter S of the physical properties of particle of size [S(r) function]

Figure 1 shows that a decrease in the size of the sample to a certain value $r = L_0$ the numerical value of the physical property $S(r) = S_V = const$, where $S_V$ - value characteristic of the bulk sample (table). If the $r < L_0$ parameter $S(r)$ decreases monotonically and if $r \to 0$ then $S(r) \to 0$.

Analytical dependence of the function has the form

$$(1)\ S(r) = \frac{S_V}{\left|\exp\left[\alpha\left(\frac{L_0 - r}{r}\right)^{3/2}\right]\right|} = \frac{S_V}{\left|\exp\left[\alpha\left(\frac{1-x}{x}\right)^{3/2}\right]\right|},$$

where $L_0$ - dimensional boundary between nanostate ($r < L_0$) and macrostate ($r > L_0$); $\alpha$ - parameter depending on the analyzed physical properties.

Equation (1) shows that when $x = 1$ ($r = L_0$) value $S(r) = S_V$. Further $x$ decreases ($r < L_0$) $S(r)$ function decreases monotonically and $\lim_{r \to 0} S(r) = 0$.

If the value $r > L_0$, that is $(1 - x) < 0$, the exponent becomes an imaginary quantity. As

$$(2)\ \left|e^{ia}\right| = \left|e^{ia} \cdot e^{-ia}\right|^{1/2} = 1$$

then $x > 1$ the value of the function $S(r) = S_V = const$.

The presence of a sufficiently large amount of experimental data allows you to check the consistency of the proposed phenomenological formula (1). For this purpose, is used the following method.

After taking the logarithm of the formula (1) and substituting

$$(3)\ \begin{cases} Y = \ln\dfrac{S(r)}{S_V}; \\ X = \left(\dfrac{1-x}{x}\right)^{3/2}; \end{cases}$$

for the site $r < L_0$ ($x < 1$) we obtain

$$(4)\ Y = \alpha X.$$

In [18] the results of the analysis of the literature data. Distribution $X$, $Y$ points corresponds to a linear regression with a correlation coefficient $C > 0,70$, with more than 60% of the pixels have a correlation coefficient $C > 0,90$. Reducing the linear correlation due to the fact that the particles have investigated nanoobjects unequal size, and was such that part of the distribution area included in $r > L_0$ [19]. The described method allows determining the $\alpha$ ratio in formula (1).

All of the above makes it possible to confirm the presence of dimensional boundaries between nano- and macrostate particles of condensed matter. However, it remains unclear why this boundary $L_0$ lies in the nanometer range, and how to influence the $L_0$ parameter individual properties of nanoparticles substance.

## *3. Calculation dimensional boundaries between nano- and macro-state.*

The formula for calculating the parameter $L_0$ should, in our view, meet three basic requirements:

- Firstly, the formula should be derived based on the basic concepts of condensed matter physics and quantum physics, known facts and theories;
- Secondly, it should include parameters characteristics of the substance which determine its basic properties;
- Thirdly, the formula should be simple enough for practical use, and easily verified experimentally.

Obviously, if the parameter $r$ passes through the dimensional limits $L_0$ of variation of the parameter is not sharp. This fact was rightly pointed out in [19], which states that "... the boundary of nanometers in size may not be correct criteria nanostructured state of matter ..." as well as a number of studies [20].

The more $r$ different from the $L_0$ value, the more manifest the properties of the respective state. It can be concluded that when in a substance $r = L_0$ there are any changes in the mechanisms of physical processes, or changing the structural characteristics of the energy-fine particles compared to the bulk counterparts.

From the theory of thermodynamics it is known that the molar heat capacity at constant volume of all substances is $C_V = 3R$, where $R = 8,3144$ J / $(K \cdot mol)$ - the universal gas constant. The $C_V$ parameter does not depend on the temperature $T$ to determine its value ($\theta_D$). Then $C_V$ decreases monotonically and when $T = 0$ K $C_V = 0$.

Dulong and Petit law, which establishes the connection $C_V$ and $R$ parameters the ratio $(C_V)_\mu = 3R$ is obtained based on classical statistics Maxwell-Boltzmann-Gibbs when using the ideal gas model. Einstein and Debye P. came to the conclusion that the temperature is lowered to a certain value classical statistics should be replaced by quantum. Atoms must be seen not as a colliding balls, but as quantum oscillators. Einstein proposed the condition that all the oscillators for monatomic substances have the same $\omega_E$ frequency. P. Debye model is considered in which frequencies are

allocated according to the law $P(\omega) \square \omega^2$ up to a certain frequency $\omega_D$. When the ratio of the model is $\omega > \omega_D$ applicable to describe the classical statistics.

Upon cooling agent treble "freeze." If the substance is heated from a low temperature, the low frequency "burn out." The theory of Debye to describe model systems were accurate Einstein's theory. In condensed matter physics began to use the concept of value of the Debye $\omega_D$ - frequency, $E_D$ - energy, $\theta_D$ - the temperature [21].

The $C_V(T)$ dependence is different for different substances. The resulting function $C_V = f(\mathrm{T}/\theta_D)$ has been set, the graph of which is shown in Figure 2. When in Formula (1) take $x = T/\theta_D$, $C_V = const$ ($C_V$ at $T >> \theta_D$), then as shown in [18], the analytical relationships $S(r)$ and $C(T)$ coincide.

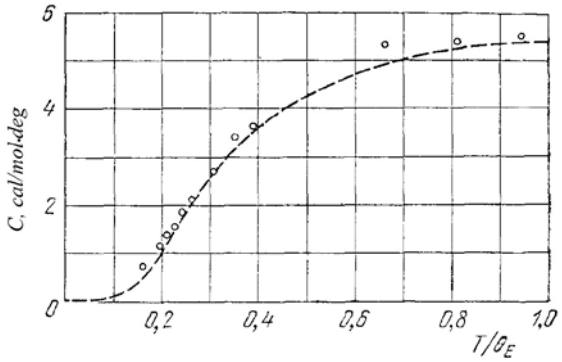



Figure 2 - The function $C_V = f(\mathrm{T}/\theta_D)$ in the P. Debye's theory of heat capacity [18]

Debye temperature ($\theta_D$) as the parameter $L_0$ is not strictly a sharp boundary, but this option is entered in the modern physical paradigm and used in the Mendeleev periodic system to describe its elements.

Debye theory of heat capacity indicates that the transition frequencies of quantum oscillators across the border $\omega_D$ there is a change in the mechanisms of the processes of substance. The atoms as quantum oscillators vibrate at a certain frequency. At low volumes on the geometrical dimensions of the frequency spectrum is influenced not only the structure of the substance, and the particle size. Vibrations of atoms to create a dynamic field that oscillates the electrons in the electron cloud with the same frequency.

As part of the one-electron adiabatic approximation, we introduce the concept of Debye pseudo impulse $P_D$. We believe that the effective electron mass equal to the mass of a free electron. In this case

(5) $P_D = \sqrt{2mE_D}$

According to the formula of de Broglie Debye pseudo impulse $P_D$ allows you to calculate the value of the Debye length (wave):

(6) $\lambda_D = \dfrac{h}{P_D}$

Wavelength Debye defines the scope of the electron on the surrounding areas of the sample [7]. Consequently, when $r << \lambda_D$ the adiabatic model of a free electron is not applicable. It should be replaced by a model of "electronic jelly" [22].

Dynamic processes describes the flow of phonons, the mean free path which is commensurate with the $\lambda_D$ [23, 24]. If values $r < \lambda_D$ we can talk about a kind of "phonon vacuum" as a phonon can pass from one end to the other particles, followed by the process of flipping the border. When particle sizes $r < L_0$ and $r > L_0$ in the former case requires to consider model of "electronic jelly" and "phonon vacuum" in the second case, the substance exists in a macroscopic phase.

As an example of the effect of particle size on the performance parameters of its properties shows the width of the plasmon peak for spherical gold particles (Figure 3).

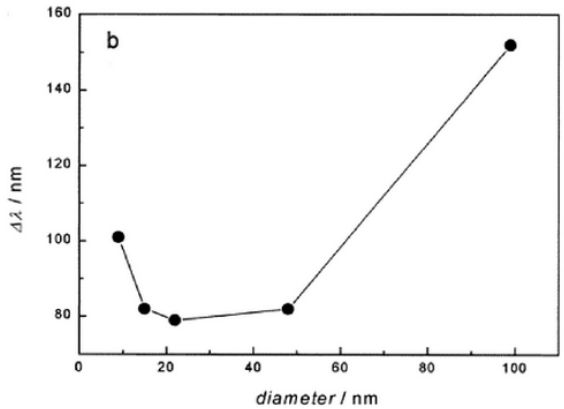



Figure 3 - Dependence of the maximum width of the plasmon ($\Delta\lambda$) on the diameter of the spherical gold nanoparticle [5]

Consequently, the Debye length $\lambda_D$ is the dimension of the boundary between the nano- and macrostate ($L_0 = \lambda_D$) substance in the condensed state.

Debye parameters $\omega_D$, $E_D$, $\theta_D$ are related to each other by the equations [22]:

(7) $E_D = \hbar\omega_D = k\theta_D = \dfrac{P_D^2}{2m} = \dfrac{h^2}{2m\lambda^2}$

where $\hbar$, $h$ ($h = 2\pi\hbar$) - Planck's constant, $k$ - the Boltzmann constant, $m$ - mass of the electron.

Note that in these terms the Debye length and the de Broglie wavelength coincide. Condition (7)

(8) $k\theta_D = \dfrac{\left(P_x^2 + P_y^2 + P_z^2\right)}{2m} = \dfrac{h^2}{2m\lambda_D^2}$

For an isotropic medium $P_x^2 = P_y^2 = P_z^2$. In this case, the parameter of the Debye length $\lambda_D$, for example, along the axis x (y or z) is defined by the expression:

(9) $L_0 = \lambda_D = \dfrac{\sqrt{1,5}h}{\sqrt{km}}\theta_D^{-1/2}$

After substituting the numerical values of physical quantities ($h$, $k$, $m$) received:

(10) $L_0 = 2,3\cdot 10^{-7}\left[m\cdot K^{-1/2}\right]\cdot\theta_D^{-1/2}[K] = 230\cdot\theta_D^{-1/2}[nm]$

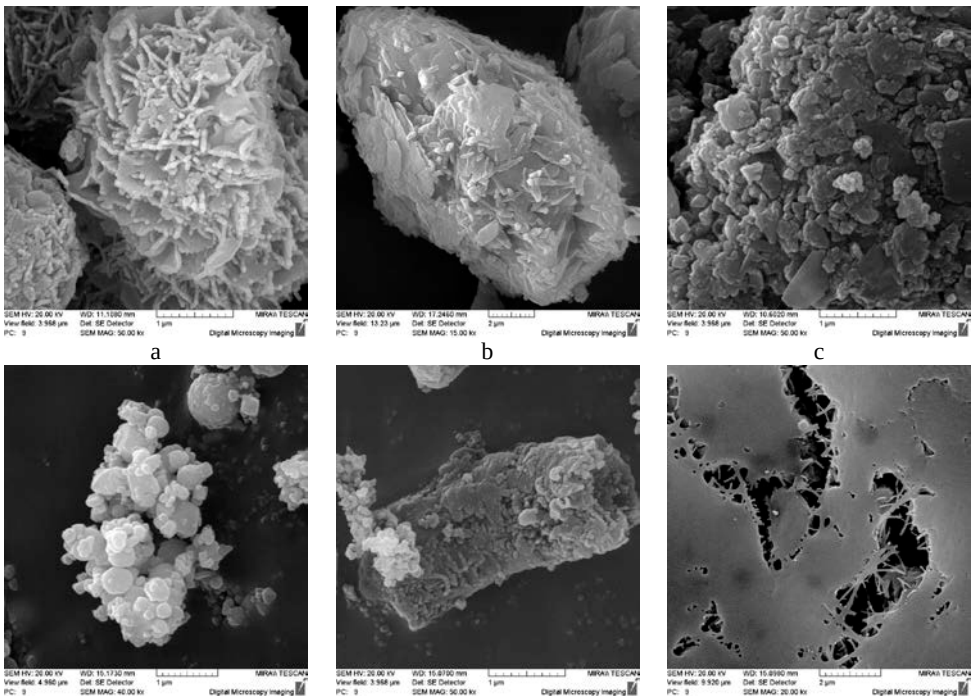
It is this formula has been used by us to calculate the $L_0$ parameter of the experimental results obtained by many researchers [5, 5, 17].

Note that $\theta_D = 170$ K for gold. Therefore, the value $L_0$ is equal $L_0 = 17,6$ nm to the gold particles, which agrees well with the results presented in [5], and given in Figure 3.

Debye temperature $\theta_D$ - table setting. Experimental dependences for the $S_V(r)$ characteristics parameters of the various physical properties are described in the literature. The experimental plots easy to determine the $L_0$ value. This dimension corresponds to the start point of the $S(r)$ deviation from the values of macroscopic matter. The parameter values $L_0$ obtained experimentally and calculated by the formula (10) to coincide with an error not exceeding 10%. Therefore, we can say that when $r = L_0$ there is a

kind of transition to the macroscopic phase of nanophase particulate matter [3, 25].

The proposed analytical expression (10) allows the evaluation of characteristics of the dispersed particles used in functional materials science to create composites based on metal, ceramic, silicate, organic macromolecular matrix. By scanning electron microscopy (SEM), it can be shown that the dispersed particles of micron dimensions range obtained with different technologies, are clustered structures containing nanoscale components (Figure 4). Nanocomponents whisker, plate and a spherical habitus characterized for inorganic particles obtained by dispersing (mechanical crushing) of natural semi-finished products - tripoli (Figure 4 a), clay (Figure 4 b), shungite (Figure 4c), and the oxide sublimation products melts carbon and alloy steels (Figure 4 d), carbon nanotubes (Figure 4e) and polytetrafluoroethylene (Figure 4 f). Therefore, when assessing the effectiveness of modifying action of the dispersed particles in matrices of various kinds need to take account of their tendency to cluster formation and morphology and specific parameters of the surface layer comprising nanoelements. Obviously, significant role ratio of the surface layer particles and nanocomponents total since physico-chemical and structural processes occurring at the interface "matrix - the modifier" depend on a set of various factors affecting the kinetics of adsorption, crystallization and adhesion interaction.



a b c d e f

Figure 4 - A typical particle morphology tripoli (a), clay (b), shungite (c) metal oxide (d), carbon nanotubes (e), polytetrafluoroethylene (f)

## 4. Conclusion

The experimental parameters depending on the characteristics of the numerical values of physical properties of substances from the sizes of the particles shows that these values correspond with tabular particle sizes $r > L_0$ where $L_0$ - dimensional macroscopic phase boundary between the state and nanophase particulate matter.

As part of the one-electron approximation for adiabatic electron with $m$ mass can introduce the concept of the Debye pseudo impulse $P_D$ and Debye wavelength $\lambda_D$. The relationship between Debye parameters: energy $E_D$, frequency $\omega_D$, temperature $\theta_D$, pulse $P_D$, wave length $\lambda_D$, is given by: $E_D = \hbar\omega_D = k\theta_D = \frac{P_D^2}{2m} = \frac{3P_x^2}{2m(\lambda_D)_x^2} = \frac{3h^2}{2m(\lambda_D)_x^2}$. For an isotropic medium $L_0$ value proposed is calculated as: $L_0 = \lambda_D = \frac{\sqrt{1,5}h}{\sqrt{km}}\theta_D^{-1/2} = 230 \cdot \theta_D^{-1/2}$.

When the particle size $r > L_0$ is possible to use the classic one-electron adiabatic model. If $r < L_0$ you must to use the model of "electronic jelly". The proposed formula allows the estimation of the modifying action of the dispersed particles in the parameters of the surface layer of the particle morphology formed by nano-components of different habitus.

## 5. Literature


1. Belov, N. Essays on structural mineralogy. Moscow, Nedra, 1976, 344 p.
2. Belov, N. Essays on the structural crystallography and space groups of symmetry. Moscow, Nauka, 1986, 379 p.
3. Avdeychik, S. Introduction to the physics of engineering of nanocomposite materials. Grodno, GGAU, 2009, 439 p.
4. Gusev, A. Nanomaterials, nanostructures, nanotechnology. Moscow, Nauka, 2007, 416 p.
5. Guozhong, Cao, Ying Wang Nanostructures and nanomaterials. USA: World Scientific. 2011, 581 p.
6. Veimarn, P. On the doctrine of the state of matter (the base of the crystallization theory of irreversible colloids), St. Petersburg, 1910, 188 p.
7. Kittel, Ch. Introduction to Solid State Physics. Moscow, Gos. ed. physical and mathematical lit., 1967, 696 p.
8. Ajayan, P. Nanocomposite science and technology. NY, Willey. 2004, 230, p.
9. Wolkenstein, F. Electronic processes on the surface of the semiconductor in chemisorption, Moscow, Science, 1987, 380 p.
10. Goodman, F. Wachmann, the dynamics of the scattering surface of the gas. Moscow,Mir, 1980, 423 p.
11. Dzheykok, M.. Chemistry of the interface. Moscow,Mir, 1984, 269 p.
12. Dunk, H. Quantum Chemical adsorption on the surface of solids. Moscow,Mir, 1980, 288 p.

13. Kiselev, N. Properties conductivity of bismuth, tellurium doped at low temperatures. Solid State Physics, 2005, T. 47, Vol. 3, pp 404-411.
14. Liopo, V. Dimensional boundary between the nanoparticles and the atomic cluster states of matter. Bulletin YKSUG, 2012, Series 2, № 1, pp 100-105.
15. Poole, Ch. Nanotechnologies, Moscow, Technosphere, 2005, 334 p.
16. Rodulgin, V. Fractal properties of disperse systems, Russian Chemical Reviews, 2004, T. 73, №2, pp 123-156.
17. Liopo, V. The mechanism of formation of the structure of nanocomposite materials based on oligomeric and polymeric matrices. - Advanced engineering technology. Volume 2, Section 4, Moscow,Spectrum House, 2012, pp 159-248.
18. Liopo, V. The dependence of physical quantities on the size of particles in the nanometer range, YKSUG Bulletin, 2009, Ser. 2, № 2, pp 60-67.
19. Liopo, V. Evaluation of dimensional nanoscale inhomogeneities modifiers YKSUG Bulletin, 2011, Ser. 6, № 1, pp 13-18.
20. Buchachenko, A. Nanochemistry - a direct path to the high technology of the new century. Russian Chemical Reviews, 2003, T. 72, № 5, pp 419-437.
21. Ashcroft, N. Solid State Physics. Moscow,Mir, 1979, Vol.1, 399 pp., T. 2, 422.
22. Animalu, A. Quantum theory of crystalline solids, Moscow, Mir, 1981, 574 p.
23. Reyslend, J. Physics of phonons. Moscow,Mir, 1965, 365 p.
24. Stroscio, M. Phonons in nanostructures. Cambridge: Univ. Press., 2011. 298 p.
25. Pinchuk, L. Physical criteria nanodimension dispersed materials. Bulletin YKSUG 2012, Series 6, №4. - S. 80-89.

# NANOCOMPOSITE ENGINEERING MATERIALS BASED ON RECYCLED THERMOPLASTICS

## НАНОКОМПОЗИЦИОННЫЕ МАШИНОСТРОИТЕЛЬНЫЕ МАТЕРИАЛЫ НА ОСНОВЕ РЕНЕГЕРИРОВАННЫХ ТЕРМОПЛАСТОВ

Burtsev A.[1], Assoc. Prof., Dr. Eng. Auchynnikau Y.[2], Struk A.[2], Avdeychik O.[2], Prof., Dr. Eng. Struk V.[2]
CJSC "Soligorsk Institute for problems of resources savings with Pilot production"[1], Yanka Kupala State University of Grodno, Grodno, Belarus[2]
E-mail: ipr@sipr.by, ovchin_1967@mail.ru, proffi2011@yandex.by, ol_avd.78@mail.ru

**Abstract:** *There were studied features of the structure of composite materials on the basis of recycled thermoplastic (HDPE, LDPE, PP) modified by components of different composition and dispersion. It was established the hardening effect of the matrix of the composite with the introduction of the highly oriented fragments that preserve the structure after the completion of the technological cycle of manufacturing products by injection molding or extrusion. It was proposed the technology of thermo-mechanical combining of thermoplastic components while simultaneous modifying by components of different composition and structure. When modification of fluorinated nanoparticles ablation products is provided the effect of increasing the rate of extrusion and formation of hydrophobized surface layer of products. Nanoscale silicate modifiers (clay, tripoli, metals phosphates and oxides,) contribute to the thermodynamic compatibility of the matrix and the modifier polymer due to formation of a spatial network of physical binds in the volume of the composite. The obtaining technologies for products based on recycled composites that the parameters of deformation strength and tribological characteristics are not inferior to raw materials, but have a significantly lower cost of production.*
***KEYWORDS****: RECYCLED THERMOPLASTICS, COMPOSITES, THERMO-MECHANICAL COMBINING, MODIFICATION, RECYCLING TECHNOLOGIES.*

## *1. Introduction*

The main elements of belt conveyors used in various branches of the mining, chemical, construction, processing industries are the conveyor belt and the supporting roller.
In light duty conveyor belts used in warehousing operations particulate product (eg. sylvite potash or on the basis thereof, ε-caprolactam, expanded clay, and others. Materials) storage technology waste processing mineral and synthetic products it is advisable to use elements from thermoplastic composite materials that Composites based on superior oligomers crosslinking resins (including on the basis of phenol-formaldehyde, epoxy, polyester) for manufacturability and processing and have high enough parameters of strength characteristics of the manual provides technical requirements [1]. A special perspective to create such materials are recycled thermoplastics class polyolefins (HDPE, LDPE, PP) and polyamide (PA 6, PA 66), industrial production which the number of companies specializing in the recycling of industrial and household waste. To adjust the parameters of strength and tribological characteristics of the reclaimed polymer matrix it is advisable to use traditional approaches to the management of the parameters of structural organization at the molecular, supramolecular and interfacial levels [2].
The objective of this work was to study the mechanisms of modifying the regenerated thermoplastic components of different molecular weights, dispersion and activity.

## *2. Methods of research*

As binders for composites using thermoplastic polymers - polyamide 6 (PA 6) and polyamide 11 (PA 11), high density polyethylene (HDPE), polypropylene (PP), polytetrafluoroethylene (PTFE) in the state of industrial supply (JSC "Grodno Azot" JSC "Polymir", JSC "HimvoloknoMogilev"). Most of the experiments were carried out with the regenerated thermoplastic (HDPE, PP, LDPE) obtained at JSC "Belvtorpolimer" in accordance with the existing standard documentation.
To obtain composite materials used highly dispersed, including nanosized particles of carbonaceous (UDD, UDAG, nanotubes, colloidal graphite, TRH), silicon (mica, clay, flint, shungite, tripoli), fluorides (UPTFE) and metal (oxides of Fe, Cu, Zn) compounds prepared according to the manufacturer's proprietary technology (JSC "Sinta", SSI " Lykov Institute of Heat and Mass Transfer", Institute of Chemistry FEB RAS), or as a result of special technological effects on the semi-finished product (mechanochemical dispersion, sublimation).
For modifying the regenerated basic primary and matrixes used primary and recycled thermoplastic elastomers (TPE) (polyurethane TPU, micro-cellular polyether urethane MPEU, divinil styrene DST), and thermoplastic polymers - a copolymer of ethylene and vinyl acetate (EVA), copolymer of formaldehyde with dioxolane (UDF) in granular or powder state.
Physical and chemical processes at the interface "matrix-filler", "coating-substrate" in the preparation and processing of composites and coatings and use of the products were evaluated using the methods of IR spectroscopy (Tensor-27), X-ray diffraction (DRON 2.0, DRON 3.0), DTA (Thermoscan-2) by conventional means. The morphological parameters of the particles and substrates subjected to different types of energy impact, examined using an atomic force (NT-206), scanning electron (Mira, Tescan), optical (MDS) microscopes. Energy state of dispersed particles, samples of composites, coatings and substrates investigated by thermally stimulated currents (TSC-analysis) on the original installation (ODL "Microtestmachines").

## *3. Results and discussion*

An analysis of the literature devoted to the problem of functional materials science, evidence of the intensive development of the two principal directions of modifying the basic matrix. For composites, used in the manufacture of products that are subject to the cumulative effects of operational factors, it is advisable to use modifiers tiered mechanism of action, which will allow the formation of an aggregate due to the structure of the composite to ensure the inhibition of adverse physical and chemical processes that lead to the destruction or wear of metal-elements.
One of the most promising areas of creating binders for composite materials with improved performance characteristics, first of all, tribological and of strength is the modification of polymer resins by mechanical action on the mixture in a solid or viscous fluid state [2-6].
Currently multitonnage production of polymer blends that combine with the thermomechanical effect, created only for a limited number of compositions, primarily for nylon, polyolefin, thermoplastic polyolefin - divinil styrene. Meanwhile, the leading foreign firms to

increase production of composite materials based on thermoplastics, thermoplastic elastomers, oligomers, resins of different composition [7-15].

The effective direction of the target modification of thermoplastics by thermo-mechanical alignment (Fig. 1) [2, 7-15].

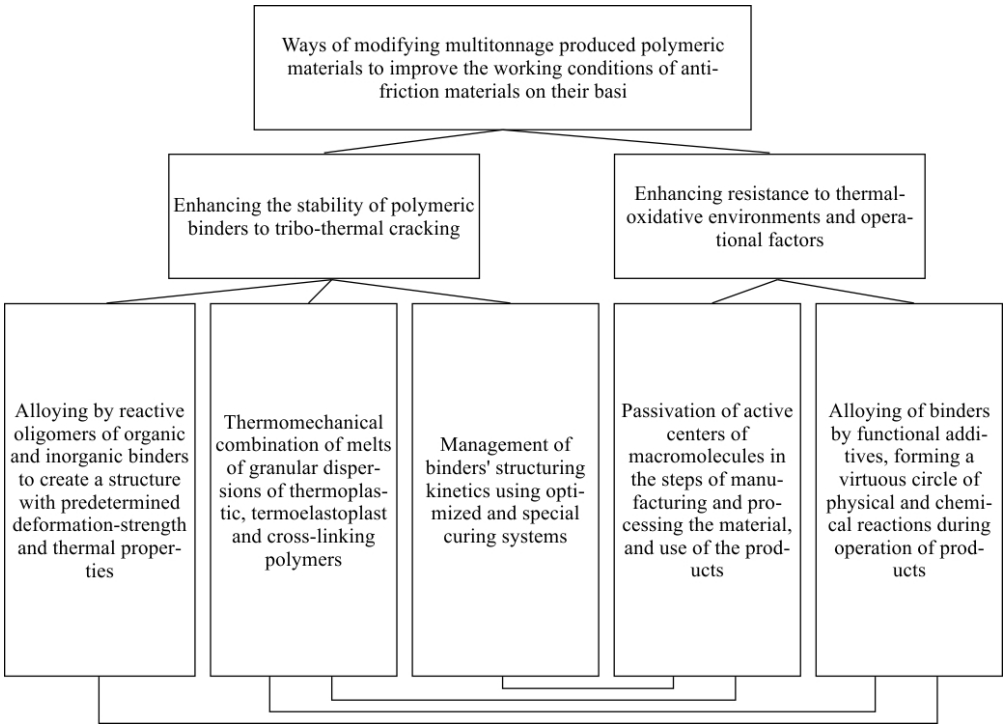



Figure 1 - Some areas of tonnage produced modification of polymer materials [2]

Among the mixtures of thermoplastic polymer materials most widely used compositions based on polyamides and polyacetals. Advantageously, the technology for producing such materials is a mixture of powdery components followed by homogenization in the melt and pelletizing. It was found that the implementation of such technology makes a manifestation of a number of effects that lead to a change in a non-additive properties of composite materials. Thus, the observed effect of abnormal increase physical and mechanical characteristics in two-component systems at low concentrations of each component. The cause of the effects associated with the occurrence of morphological changes in the contact area of the two polymers, leading to the formation of transition layers. A number of studies indicated appearance in processing the polymer blend fiber-aggregates, the shape and size of which depend essentially on the viscosity of the melt components and modes of processing technology. The formation of such ultrathin fibers improves the physical and mechanical characteristics of the composites. The possibility of the formation of copolymeric products of thermomechanical impact on mixtures of thermoplastic polymers. It was necessary to assess the extent to which the marked effects peculiar composite materials made from a mixture of components of the regenerated pellets, and the feasibility of practical application of the technology of combining thermomechanical bead polymers for the manufacture of binders for antifriction and constructional materials.

Samples for research were produced by injection molding on injection molding machine with screw kneader at a temperature conditions typical of a high melting component of the mixture.

The mechanical action performed on the melt by a screw injection molding machine, the speed of which was varied from 0.42 to 2.0 $s^{-1}$. The shear rate in a screw channel of the screw and between the crest of the screw and the inner wall of the sleeve is suitably from 18 - 89 $s^{-1}$ and 83 - 398-1 $s^{-1}$.

The results of physical and mechanical tests show a non-monotonic dependence of the parameters tensile strength and toughness of the component content in the material. The presence of two extrema on the experimental curves in good agreement with published data [2], which indicates the modification of community processes that take place in mixtures of polymers of different compositions, both primary and regenerated, when combining components of different technologies.

Depending on the content of the doping component in a mixture of its distribution changes significantly. Thus, in compositions PA6 + 5% SFD copolymer is distributed mainly in the form of spherical structures with a diameter of 1-5 microns, and are present as individual fiber-like aggregates with a diameter of 10-13 microns (Fig. 2c).

With increasing content of SFD up to 50% observed the emergence of larger diameter of Education 80-120 microns (Fig. 2d), the uniformity of distribution of the components in this case is considerably deteriorated.

A similar pattern of distribution of alloying components and destruction inherent in sample composition of HDPE-UDF, PP SFD, both primary and regenerated.

The research revealed that the combination of thermomechanical granular dispersions engineering thermoplastics can not only control the physical and mechanical properties of materials, but also significantly change their thermal stability and resistance to thermal oxidation. Combined binary relationships on the basis of the regenerated thermoplastic can be used for the manufacture of composite materials of different functionality with improved performance, including tribological [2]. Thermomechanically combined matrix based on regenerated polyolefins were tested as binders for the production of structural components of belt conveyors.

Modern technology allows the recycling of the polymer product, the parameters of strength and tribological characteristics is not inferior to the primary raw materials. This aspect is determined by a combination of several factors, the most important of which concerns the preparatory process for the high quality of the recovered materials, which removes components of different composition and structure (dyes, residues of organic and inorganic substances, etc.), have an adverse effect on the kinetics of thermal-oxidative and destructive remelting processes in regenerable raw materials for the manufacture and use of many single-use products (films, packaging, components of medical devices and others.) of high-quality raw materials with high requirements on the parameters of service characteristics.

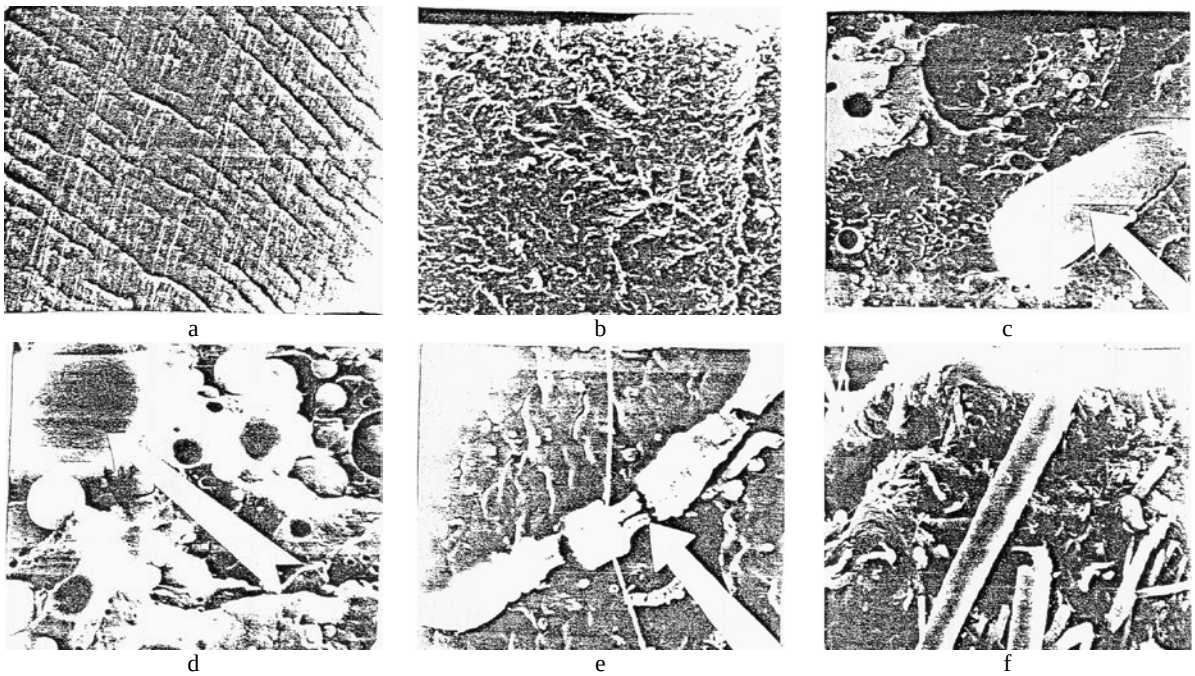



Figure 2 - The typical form of chips in liquid nitrogen (a-d) and fracture surfaces after uniaxial tension (d-f) samples from PA6 (a) SFD (b), the compositions PA6 + 5% wt. SFD (c, d) and PA6 + 50% by wt. SFD (e, f)

For the development of composite materials for metal-roll shells used recycled thermoplastics produced by JSC "Belvtorpolimer".The main attention was paid to the polypropylene (PP), which is in the parameters of strength and tribological characteristics clearly superior to other types of polyolefins (HDPE, LDPE, EVA) and can serve as a basis for range of engineering materials for various purposes, including for the manufacture of shells of metal-rolls of conveyor belts.

Conducted by IR spectroscopy studies have shown that the secondary (recovered) PP composition and thermal characteristics virtually identical to the primary.

The IR spectra of granular polypropylene after recycling has not revealed the presence of intense absorption bands belonging to the oxide compounds (1710-1740 cm-1), as well as significant amounts of impurities or additives. This confirms that the process of preparation of high quality secondary raw material for processing, comprising multistage dispersing and washing to remove unwanted impurities.

Thermophysical studies confirm the relatively high structural parameters of recycled polypropylene (Fig. 3). However, it should be noted there is a wide endoeffects the DTA curves in the temperature range 165-205 ° C, which appears to indicate the presence in the regenerate several fractions with different molecular weight and correspondingly melting point.

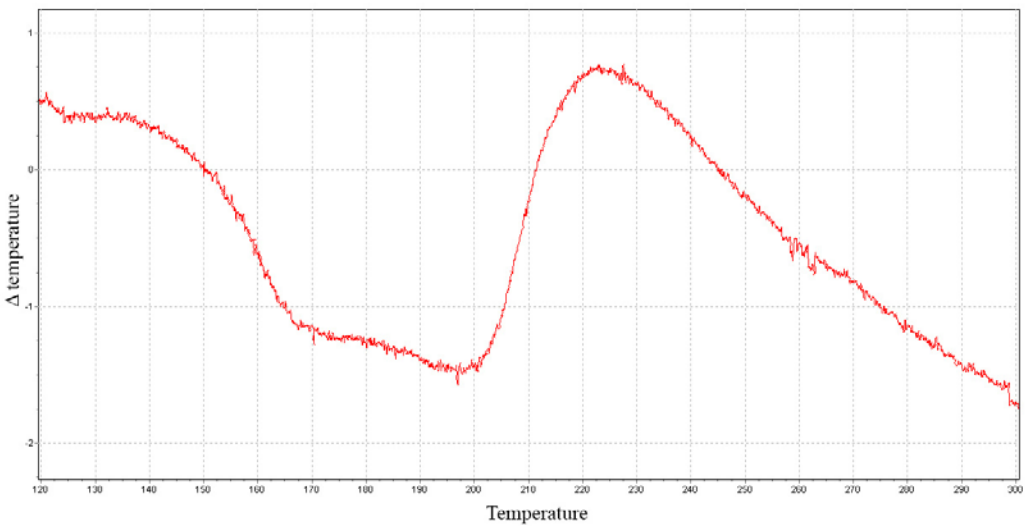



Figure 3 - DTA curve of polypropylene subjected to recycling

This may be due to the use of regeneration for the different types of waste - film packaging and tissues (packages) of flat oriented yarns which are markedly different in the parameters of strength characteristics, as They have different structures obtained using the processes of orientation of the hood.

For the development of composite materials for the elements of metal-rolls of conveyor belts (shell) used a regenerated polypropylene produced at JSC "Belvtorpolimer" on multistage recycling technologies depreciated packaging products of flat oriented fibers. As functional modifiers used nanoparticulate particles of metal oxides, which are the waste of metallurgical production (JSC "Severstal"), silicate particles produced by mechanical dispersion of glass semi-finished products of polytetrafluoroethylene termogazodinamicheskih synthesis - ultrafine polytetrafluoroethylene (UPTFE). In addition, high molecular weight components used class of polyolefins (HDPE, LDPE, EVA), polyester (PBT) and styrenic polymers (DST) both

primary and secondary (recycled), which lets you adjust the parameters of strength characteristics, including toughness and resistance to alternating loads in the optimal range. Composite materials prepared by combining the components in a thermomechanical material cylinder injection machine with a screw kneader at temperatures typical for processing thermoplastic base.

For the manufacture of shells has been tasked to create a composite thermoplastic material based on a mixture of thermodynamically incompatible polymers of polypropylene and high-density polyethylene with high abrasion resistance, resistance to shock and alternating loads. The problem is solved in that the composite material based on a thermodynamically incompatible mixture recycled polypropylene and recycled polyethylene containing silicate filler and modifier as a mechanically activated silicate-containing filler in the grinder of impact type pulverized glass, and as a modifier - olefin oligomer or polymer with a molecular weight in the following ratio, wt.%:

silicate filler - 0.1 - 3%;

modifier - 0.5 - 2%;

secondary polyolefin - rest.

The essence of the developed technical solution is as follows. In the manufacturing process and the glass-based products various types of waste processing is formed in the form of dispersed particles of 0.3 microns to 50 microns. Subsequent mechanical dispersion on various types of data dismembrator particles acquire a stable electret state, as formed uncompensated charge with great relaxation time. Own charge particles dispersed in the glass determines the orientation of the macromolecules in the melt mixture of regenerated polyethylene and polypropylene, which leads to homogenization of the polymer blend and stabilize the rheology of the melt, the formation of quasicrystalline boundary layer upon cooling of the melt in the mold cavity of the mold or forming the filter head.

The simultaneous increase and stabilization of the rheological parameters and physico-mechanical properties of the composite material on the basis of thermodynamically incompatible polymer recovered due to the synergistic effect observed with the introduction of the activated glass particles. Particles of silica filler with its own charge fulfill the role of a coupling agent, as a result of which the spatial grid formed labile physical connections throughout the volume of the composite material that provides increased friction characteristics, resistance to alternating loads and stress cracking.

An important aspect of the manifestation of synergy in the system is the ordering of the amorphous component mixtures of the polymer matrix, increasing the crystalline medium co-processing recycled polypropylene, polyethylene and recycled glass-modifier. Formed low-defects structure with high ductility in comparison with a primary polypropylene leads to an increase in frost resistance of the composition. Modifying the secondary polypropylene mixture and fillers recycled polyethylene-based olefin polymer or oligomer component contributes to the thermodynamic compatibility of the material because of the proximity of the molecular structure of the matrix and modifier.

As the finely divided active modifier regenerated thermoplastics may be used and other types of fine particles having a characteristic morphology, the surface layer consisting of nanocomponents different habit. Such particles, as follows from [16] exhibit characteristic symptoms of nanoscale particles which display increased activity in the processes of modifying macromolecular matrices at different structural levels. Due to the effect of modifying the appearance of the complex is possible to achieve the required parameters of strength, tribological, adhesive, etc.. Service characteristics of composite materials based on thermoplastic regenerated, which allows them to be used as a full-fledged alternative to the primary composite.

The developed composite materials based on polyolefins regenerated capable of processing both molding and extrusion because matrix comprise polypropylene extrusion type and additives which allow to adjust the parameters of the rheological characteristics (paraffin, chloroparaffin wax, mineral oil). Extruded pipe blanks were made necessary for the geometric dimensions of the shell metal-roll belt. These shells were used for belt conveyors operated at RUE "Belaruskali". Bench and production tests have shown high efficiency roller carriage with shells made of composite material based on a modified polypropylene to replace conventional metal counterparts.

## *4. Conclusion*

Recycled thermoplastic materials based on polyamides and polyolefins can be used as templates for making compositions with predetermined parameters of service characteristics. For modifying regenerated target thermoplastics advisable to use a method of modifying a multi-level, allowing to control the parameters of the structure at the molecular, supramolecular and interfacial levels. Effective use of the combination of modifiers with different mechanisms of action – low-dimensional active particles and polymer components are able to form dispersed aggregates in the matrix binder and copolymerization products under the effect of operational parameters of the extrusion process or injection molding process in conventional equipment. Functional composite materials with multi-level modification based on recovered thermoplastics are valuable alternative to the primary materials while providing significant economic benefits.

## *5. Literature*


1. Dyachenko, V. Research and reliability of carrying rollers of belt conveyors Transport lumpy cargo: author. ... dis-ta tehn. sciences. Moscow, Horn Institute, 1981. - 13 p.
2. Struk, V. Tribochemical concept of anti-friction material on the basis of tonnage produced binders: author. dis. ... doctor. tehn. Sciences, Minsk, 1981. - 36 p.
3. Sysoev, P. Scientific fundamentals of developing polymer and metal-engineering materials and high resistance to friction fatigue: author. dis. ... dokt..tehn sciences, Minsk, 1981. - 36 p.
4. Hull, V. The structure of the strength of the polymer L - Moscow, Chemistry, 1978, - 316.
5. Savkin, V. The role of structural tribomehaniki polymers in the creation of composite self-lubricating materials: author. dis. doctor tehn sciences Moscow, 1984 - 35,
6. Lisowski, V. Development and research of composite materials for high-speed friction units: author, dis. cand. tehn. sciences - Minsk, 1979 – 12 p.
7. Kuleznev, V. Mixtures of the polymers. - Moscow, Chemistry, 1980. - 304 p.
8. Blinnikov, V. Polymer composite materials. Overview. - Moscow, VNIIPO, 1984. - 62 p.
9. Manson, J. Polymer blends and composites. Moscow, Chemistry, 1979. - 440 p.
10. Lipatov, Y. Physical chemistry of polymers. Moscow, Chemistry, 1977. - 304.
11. Keber, M. Modification of polymeric materials during processing. - Plastics, 1971, № 5, - p. 59-66.
12. The polymer mixture / Ed. D. Paul and S. Newman, Vol. 1 - Moscow, Mir, 1981.- 550.
13. The polymer mixture / Ed. D. Paul and S. Newman, Vol. 2 - Moscow, Mir, 1981. - 455 p.
14 Mujiri, B. Structural and chemical modification of high density polyethylene in the recycling process. - Plastics, 1973, № 10 - p. 79-80.
15. Akutin, M. Regulation of properties of the polypropylene during extrusion. - Plastics, 1971, № 2, -. 23-25.
16. Avdeychik, S. Introduction to the physics of nanocomposite engineering materials. Grodno, GGAU, 2009. – 439 p.

# METALLOGRAPHIC INVESTIGATION OF INDUCTION HARDENED PART TWO-SIDE LEVER

Prof. Dr. Eng. Cvetkovski S.[1], Asoc. Prof. Dr.Eng Nacevski G.[1]
Faculty of Technology and Metallurgy, Ss. Ciril and Methodius University, Skopje, Macedonia
E-mail: sveto@tmf.ukim.edu.mk, goran@tmf.ukim.edu.mk

***Abstract:*** *Basic idea in this metallographic investigation is checking the effect of induction (surface) quenching of produced part, two-side lever made of 42CrMo4 steel. This part is build in railway wagon. According its production assignation it has to be surface hardened just in some positions. Formerly surface hardness of this part was realized by chemical-heat treatment i.e. case hardening of 16MnCr5 steel. But because of specific form of the part and increased britlness which appear in the thinnest parts of lever (between the rounded opening and the surface) and idea was obtained to change the case hardening with induction quenching. Efficiency of performed induction quenching i.e. hardness values and depth of quenched layer was controlled by optical microscopy and hardness measurement.*
***KEYWORDS:*** *TWO-SIDE LEVER, INDUCTION QUENCHING, CASE HARDENING, TEMPERING,MARTENSITE*

## *Introduction*

Investigated material has designation 42CrMo4 according EN10083-2 [1]. Material number is W.NR 1.7225. According chemical compositions it is low alloyed steel (CrMo) steel. Molibdenum aditions improve its temper britlness [2]. It is mostly delivered in quenched and tempered condition (Q&T) [3]. It belong to the group of steels intended for surface hardening. 42CrMo4 steel is versatile material. Its main application is automotive industry, transportation and mechanical engineering. Production of parts which possess very good impact toughness, wear resistance and fatique is the main implementation of this steel. It is ultrahigh strength steel and in the same time enable production of high stressed components. The most often produced components are crankshafts, gears and similar parts. One of its characterics is very good machinability. Chemical composition and mechanical properties of 42CrMo4 are given in tables 1 and 2. Because this steel is used for different methods of heat treatment in table 3 are given characteristic heat treatment (temperature points) [4].

***Table 1*** *Chemical composition of 42CrMo4 (DIN EN 10083-2)*

| 42CrMo4 | C | Si | Mn | S | P | Cr | Mo |
|---|---|---|---|---|---|---|---|
| Comp, % | 0.38 - 0.45 | 0.40 | 0.60 - 0.90 | 0.035 | 0.025 | 0.90 -1.20 | 0.15-0.30 |

***Table 2*** *Mechanical properties of 42CrMo4 steel in quenched and tempered condition (Q&T) accoding (DIN EN 10083-2)*

| 42CrMo4 | values | | |
|---|---|---|---|
| Diameter, mm | <16 | >16-40 | >40-100 |
| Thickness, | <8 | 8<t<20 | 20<t<60 |
| Yield strength, Re N/mm$^2$ | min 900 | min 750 | min 650 |
| Ultimate tensile strength, Rm, N/mm$^2$ | 1100-1300 | 1000-1200 | 900-1000 |
| Elongation, A, % | min 10 | min 11 | min 12 |
| Contraction, Z, % | min 40 | min 45 | min 50 |
| Toughness, CVN, J | min 30 | min 35 | min 35 |

***Table 3*** *Recomended temperatures for heat treatment of 42CrMo4 [5]*

| Operation | Temperature, $^0$C |
|---|---|
| Soft anealing | 680-720 |
| Normalization | 850-880 |
| Hardening | 820-850 |
| Forging | 1100-900 |
| Isothermal anealing | 850-900 |
| Subcritical anealing | 680-720 |
| Tempering | 550-650 |

*Critical points (temperatures) of 42CrMo4 steel, which are of crucial importance for regular choice of heat treatment temperature are given in table 4 [4].*

***Table 4*** *Critical points of 42CrMo4 steel*

| | |
|---|---|
| Ms: | 325°C |
| $AC_1$: | 735°C |
| $AC_3$: | 780°C |

Induction quenching is heat treating process implementing for surface hardening of the heat treatable steel. The basic principles of induction quenching are: strengthening of surface layer, heating to ferrite-austenite transformation, fast cooling in order to perform martensitic transformation. Heating is very fast and there is not phase transformation in middle part of the treated material.

Adventages of this process are the following: energy saving, increasing of wear resistance, very small dimension change and minimising machining of part after quenching.

Induction quenching of 42CrMo4 can be accomplish in: oil, water or air water spray. Main intention of the process is increasing of surface hardness. Typical examples of parts intended for induction quenching

are gears and similar parts. Alternative current is used for surface heating of parts. Heated area is quenched after that. Finaly, the surface hardness of the quenched area is significantly increased. The process itself lasts very short. Tempering process which follow after that is accomplish at temperature of 550-650 $^0$C [5].

Type of steel, its microstructure and performances of the part determine required hardness and internal stress. On the contrary of carburizing, induction quenching don't require heating of whole part. During inductive quenching only specific surfaces of the parts are heated. Success rate of quenched parts is function of the type and shape of of inductor as well as the heating way.

The aim of induction quenching is obtaining fine martensite after quenching while the microstructure od the remaining part, primarily the core stay unchanged.

Besides hardness, wear resistance, contact fatique and impact strength are increased as result of surface quenching. Basic factor which influence efficiency of induction quenching are: inductor power, frequency and current, voltage, temperature of austenitization, cooling rate, heating time, tempering temperature, pick temperature. Frequencies used for induction quenching are in range between 1-30kHz [6]. Knowing this characteristic of 42CrMo4 steel and induction quenching, preliminary treatment and investigation investigation of two-side lewer were performed.

***2 Metallographic analyze of two-side lever***

*2.1 Preparation of part for metallographic analyze*

As was point out two-side lever is produced from 42CrMo steel. For production was used bar with diameter □50 according EN10060 standard .

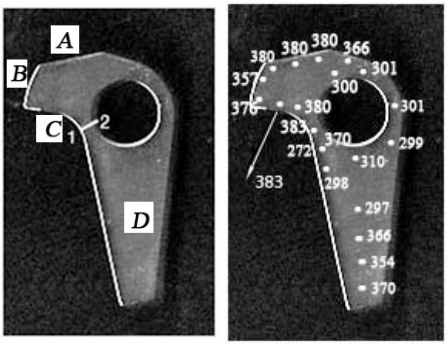
The aim of this metallographic analyze was the following:

- to check cleanliness of material concerning non metallic inclusions;
- to analyze initial microstructure of base material;
- to determine the thickness of quenched layer;
- to measure the hardness of surface quenched layer.

The first step in metallographic preparation of specimen was longitudinally cutting of specimen in two equal parts. One half was prepared for metallographic analyze (micro and macro). Appeaeance of metallograpahy prepared specimen is given in figure 1a. Surfaces (positions) of the two-side lever which need increased hardness in the exploratory conditions are marked with capital letter. In figure 1b are given measuring positions and obtained hardness values after induction quenching of the part implementing Vickers method (HV10). In figure 1c are presented hardness values obtained by implementing HRC method. HRC method is most often used for hardness measurement of the heat treatable steel. But with this method, load of 100 kg (HRC100) is used and biger imprints at the specimen surface is obtained. From another point of view thickness of quenched layer is pretty thin. Because of that, in order to be sure in the credibility of obtained values both method are used. For comparasion of obtained results, conversion of results from HV to HRC was made too (Table 5). All hardness measurement were realized on metallographic specimen.

***Table 5*** *Conversion of hardness values from HV10 too HRC100*

| HV10 | HRC |
|---|---|
| 442 | 46 |
| 420 | 43 |
| 400 | 41 |
| 383 | 39 |
| 380 | 39 |
| 376 | 39 |
| 370 | 38 |
| 366 | 38 |
| 364 | 37 |
| 357 | 37 |
| 310 | 31 |
| 300 | 30 |
| 299 | 30 |
| 297 | 29 |



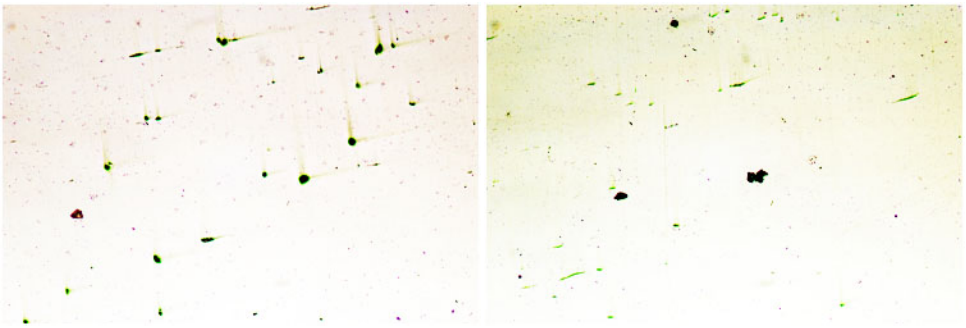

a b




c

***Figure 1*** *(a - c) Metallographic specimen and measured hardness values according Rockvel and Vickers method*

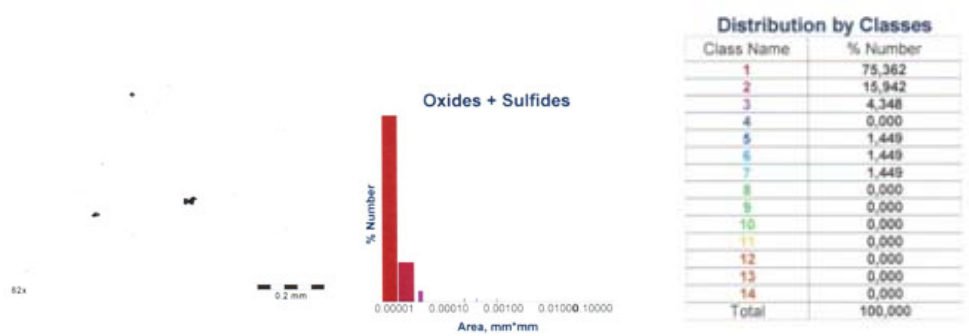
Metallographic preparation of specimen consists of mechanical grinding using different grinding abrasive papers: 180, 220, 280, 400, 600, 800 и 1200. After finishing grinding, specimen was polished with suspension of $Al_2O_3$. Polished specimen was subdued to analyze of nonmetallic inclusions at magnification of x100. This investigations were performed by automatic analyze using VideoTestMetal softver based on EN12457 standard. Automatic Quantitative and qualitative examination was performed for determination of type size and distribution of non metalic inclusions. In figure 2 (a and b) are given micro metallografic photos from polished specimen x100.



a b

***Figure 2*** *(a and b) Non metallic inclusions present in the investigated specimen, x100*

*Results from automatic analyze of inclusions are given in figure 3.*




**Distribution by Classes**

| Class Name | % Number |
|---|---|
| 1 | 75,362 |
| 2 | 15,942 |
| 3 | 4,348 |
| 4 | 0,000 |
| 5 | 1,449 |
| 6 | 1,449 |
| 7 | 1,449 |
| 8 | 0,000 |
| 9 | 0,000 |
| 10 | 0,000 |
| 11 | 0,000 |
| 12 | 0,000 |
| 13 | 0,000 |
| 14 | 0,000 |
| Total | 100,000 |

***Figure 3*** *Analyze of non metallic inclusions*

Next phase in metallographic preparation of specimen was chemical etching. First used etchant was Nital. But obtained results was not satisfactory. Next attempt was etcing with Kallings reagent. Something beter results were obtained (figure 4). The best revaling of microstructure was achieved with Villela etchant. This etchant is recommended for etching of heat treated steels. So further on this etchant was used. Initial microstructure of 42CrMo4 steel is given at figure 5 (a and b.)

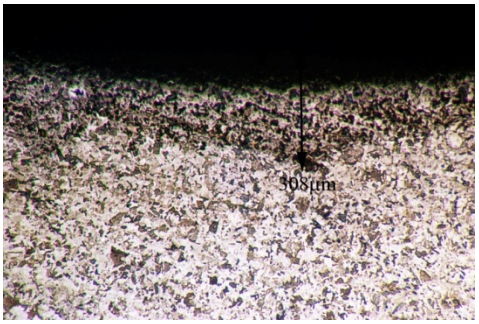
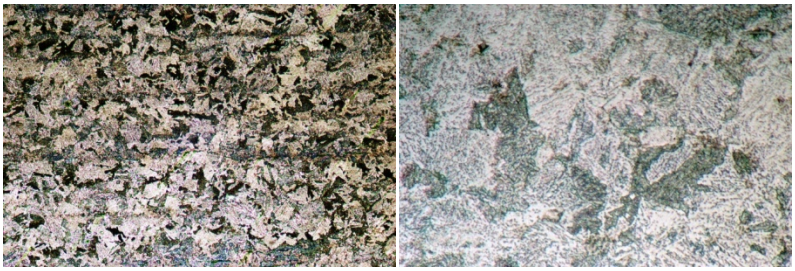



***Figure 4*** *Microstructure of induction quenched layer, x100, Kalings reagent*

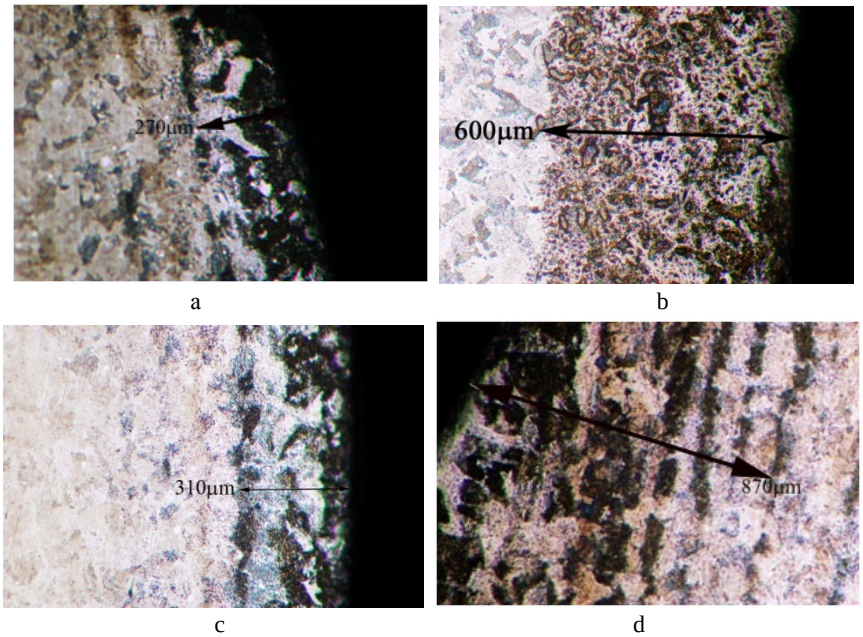


*a* *b*

***Figure 5*** *(a and b) Microstructrure of initial material, Villela reagent*
*a. x100* *b. x200*

Microstructural photos of induction quenched layers taken from different position of specimen. 6 (a-d). Measurment are performed using Photoshop programe.

Figure 7 presents micro photo from the outer surface until to round opening. See figure 1b, position 1-2




a b

c d

***Figure 6*** *(a-d) Microstructure surface (quenched layer) at different positions of specimen*




***Figure 7*** *Microstructure of the specimen from the outer surface to the opening, position 1-2, microphotos 2b*

## Discusion

Analyze of poslished surface of specimen confirmed that oxidic and sulfidic inclusions are present. According to size and distribution it can be said the very fine inclusion uniformly distributed are presented. Generally performed analyze showed that base material is pretty clean concerning non metallic inclusions. Principaly steel for induction hardening steel are cleaner concerning many othe types. In the middle of the lever there is no microstructural changes because heat treatment (induction heating) happen only on the surface of the part.

Initial microstructure of the two-sided lever consists of fine grained temepered martensite (Q&T), figure 5(a and b)) Hardness of initial microstructure according to literature dates should be 28–35 HRC. It was confirmed in our investigations too where hardness value is (29-30 HRC) [7].

Max measured hardness value is 383 HV10 (39 HRC). It means that requirement from technical documentation of 30-38 HRC are fulfilled. Probably hardness on the surface of part is something higher, because there is hardness gradient from the surface to the interior of the specimen.

There is no doubt that with optimal choice of quenching parameters higher values can be achieved (figure 8. It can be seen from the same figure (CCT diagram) that max mardness for 42CrMo4 steel can be reach during very high cooling speeds is 660 HV10 (56 HRC). Here we have to take in consideration that this steel contain 0.45 %C. For comparison, 16MnCr5 steel which was formerly used for production ow two-side has carbon concentration of 0.16%. Because of that this steel was subjected to case hardening [7]. There is migration of carbon atoms from the surface towards interior of part during carburisation and increase hardness. Max hardness which can be reached during quenching of 16MnCr5 is 46 HRC (continous cooling diagram figure 9). For obtaining higher hardness values case hardening is necessary. In that case hardness of 60HRC can be obtain [7].

According appropriate literature dates, deepness of quenched layer could be 0.25-2.3 mm. Measurments performed in this research are in the range 0.21 до 0.87 mm [8].

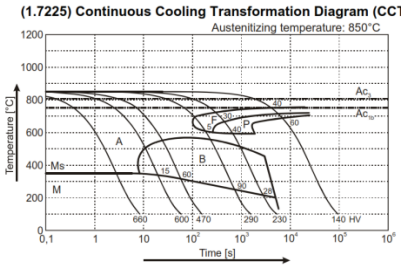



***Figure 8*** *Diagram of continous cooling (CCT) for 42CrMo4 steel [9]*

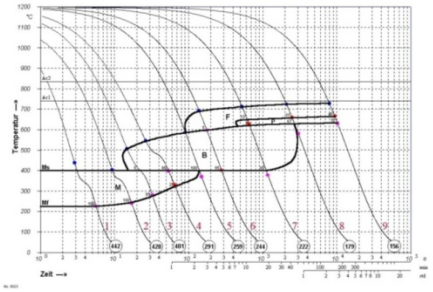


***Figure 9*** *Diagram of continous cooling (CCT) for 16MnCr5 steel [10]*

## *Conclusion*

Microstructural analyse of polished surface of the specimen show presence of sulfidic and oxidic inclusions. Concerning the presence on non-metalic inclusions it can be said that material is very clean which is characteristic for this type of steel (heat tratable).

Microstructure in the middle of the specimen consists of fine grained tempered marteniste (Q&T). There is not any changes in the initial microstructure of material because induction quenching change the microstructure only in the surface.

Deepness of the quenched layer is different in different position of the two side lever. Measured values are between 210 до 870 □m. Different thickness is result of the iregular shape of the two-sided lever and the fakct that only determined surfaces has to be inductive quenched.

Max measured hardness value is 39 HRC, and it satisfy requirement of technical documentation. But according to characteristics of 42CrMo4 much higher hardness values can be reached by induction quenching.

## *Literature*


1. EN 10083-1 steel for quenching and tempering
2. EN 10084: 2008 Case hardening steels. Technical delivery conditions for case hardening steels
3. BS EN 10060:2003 Hot rolled round steel bars for general purposes. Dimensions and tolerances on shape and dimensions
4. ISO 6508-3 Metallic Materials – Rockwell hardness test (scales A, B, C, D, E, F, G, H, K, N, T) – Part 3: Calibration of reference blocks, 1999-09-01
5. F. Nürnberger, Microstructural Behaviour of Tempering Steels during Precision Forging and Quenching from Hot-forming Temperatures, © Metallurgical and Mining Industry, 2011, Vol. 3, No.
6. Harichand, Krishan Kumar and S.K. Jha, Heat Treatment for 16 MnCr5Material International Journal on Emerging Technologies 3(1): 60-64(2012)
7. Prof. Dr-ing Jurgen Maier, Induction hardening of Gear wheels made from 42CrMo4 hardening and tempering steel by employing water-air spray cooling Project A3 IRTG 1627 „Virtual Materials and Structures and their validation“
8. Sascha Brill, DirkM. Schibsch, Induction, Hardening Versus Case Hardening – A Comparasion, REPORTS, Induction Technology 15 Hu Zhizhong, The Handbook of Steel and Its Heat Treatment Curve. Beijing: Defence Industry Press,1987.
9. Hu Bao Xintao, Practical Handbook of Heat Treatment of Steel, Shanghai: Science and Technology Press of Shanghai, 2009.

# HARDENING OF AUSTENITIC STEELS WITH HIGH Mn AND Al CONTENT

## УПРОЧНЕНИЕ АУСТЕНИТНЫХ ВЫСОКОМАРГАНЕЦАЛЮМИНИЕВЫХ СТАЛЕЙ

Prof. Dr. Phys.-Math. Kaputkina L.M.[1], Prof. Dr. Eng. Svyazhin A.G.[1], Cand. Eng. Bronz A.V.[2],
Cand. Eng. Smarygina I.V.[1], Cand. Eng. Bazhenov V.E.[1], Sen. Res. Cand. Eng. Kindop V.E.[1]
National University of Science and Technology «MISIS»[1];
S.P. Korolev RSC «Energia»[2] , Russia
E-mail: kaputkina@mail.ru

**Abstract:** *Estimates and experimental study of aluminum, carbon and nitrogen content effect for thermally and mechanically stable austenitic alloys based on Fe-(20–25)%Mn-(5–10)%Al-(0–10)%Ni-C-N, and hardening efficiency of these alloys by nitrogen addition are conducted. It is shown that the alloys based on the investigated system with C content of >1.2% for nickel-free system and ≥1.4 % for 5% and 10% of Ni can be proposed as high-strength non-magnetic cryogenic both in heat-treated and aged states. Nitrogen addition in the alloy containing 5% Al can be considered as micro-alloying, enhances dispersion of the cast structure. Ni enhances the dispersion hardening effect due to increase in carbide release rate resulted from the reduction of C solubility in austenite. Rational content of nickel equals to ~5%.*

***KEYWORDS:*** *IRON-MANGANESE ALLOYS; TRIPLEX ALLOYS; NITROGEN MICROALLOYING; HIGH-STRENGTH ALLOYS; MULTIPHASE STRUCTURE.*

### *1. Introduction*

In the past few decades, the efforts of many researchers focused on the development of the advanced high-strength steel (AHSS) with adequately high ductility and toughness. It is often trying to get the heterogeneous structure with ultrafine particles (up to nanosizes) and one or several of such particles should be metastable to deformation under load [1]. It provides high mechanical hardening and enhanced ductility.

The alloys based on Fe-Mn-Al-C system, or so called TRIPLEX alloys with high Mn and Al content satisfy this requirement and can be applied as light high-strength steels.

This work is directed to calculation assessment and experimental research of the effects of Al, Ni and C content on the thermally and mechanically stable austenitic steels based on the Fe-(20–25)%Mn-(5–10)%Al-(0–10)%Ni-C systems.

### *2. Material and Experiment*

Fe-20%Mn-(5–10)%Ni-10%Al-C system is chosen as the basic calculation system in order to provide the maximum strengthening due to the Al alloying.

Thermo-Calc software using thermodynamical database TCFE7 for the chosen basic content is applied to plot the polythermal section of phase diagrams and to determine the thermal-concentration regions of equilibrium phase existence such as austenite, carbides nitrides and intermetallides. Generalized Hall-Petch law is used to assess the influence of the chemical and phase-changing content of the alloy under the thermal treatment, more specifically, the solid-state and dispersion strengthening, as the effect of structure strengthening of the steels with different content is generally determined by technological parameters of metal production processes.

Experimental researches on the influence of the content on the mechanical properties and phase content in cast and deformed steel are made for certain alloys (see Table 1 for the chemical content).

Mechanical properties are tested for flexture under GOST 14019-2003 on the Instron 3300 test system under the normal temperature.

### *3. Results and Discussion*

Phase diagrams show that all Fe-20%Mn-10%Al-(0–10)%Ni-C alloys with low carbon content crystallize according to L+α→L+α+γ→α+γ method and when C content exceeds 1.3 and 1.4 % the crystallization finishes with γ-phase formation.

Addition of 5 % of Ni does not influence the type and sequence of different carbides formation. The higher the C content the higher the temperature of carbide formation in alloy structure. Addition of 10 % of Ni supports the extension of γ-region and the reduction of required concentration of C till 1.05 % under 1000 °C and 1.35 % under 1200 °C.

For the sake of further assessment the C content of 1.4 % is taken as the basic content since it allows to create and treat the alloys in the fully austenitic state (without proeutectoid constituent) ant their dispersion strengthening as the result of aging.

In Fe-Mn-Al-Ni-C-N nitrides of aluminum are formed at temperatures considerably exceeding the liquidus temperature, therefore, the nitrogen content in the aluminum is its solubility at this temperature. The solubility of nitrogen in the melt and in the solid δ- and γ-phases decreases with decreasing temperature and increasing content of aluminum [2].

Table 2 shows the assessed temperatures of the martensite transformation initiation for steels $M_S$ as well as temperatures allowing the formation of 50 % of martensite under the deformation of 30 %, $M_{d30}$ according to [3, 4].

It is clear, that thus received assessments are very rough, but in this case only evaluation of assessment changes due to the austenite content change is important.

As we see, the full solution hardening results in the stability of all alloys up to the temperatures close to 0 K. The reduction of $M_S$ and $M_{d30}$ due to addition of 10 % Ni is about 200–250 K. This allows significant dispersion hardening of such alloys in case the stable austenite matrix is persistent till the cryogenic temperatures.

The volume of released phases f and the change of austenite content under the aging calculated using the Thermo-Calc software are indicated in Table 2.

***Table 1.*** *Chemical composition of investigated alloys*

| No. | Alloys | Chemical composition, wt. % | | | | | |
|---|---|---|---|---|---|---|---|
| | | Mn | Al | Si | Mo | C | N |
| 1 | 35K | 21,2 | 6,2 | 0,50 | 0,20 | 1,10 | 0,006 |
| 2 | 33K | 19,1 | 9,0 | 0,50 | 0,03 | 2,18 | 0,001 |
| 3 | 34K | 23,9 | 4,0 | 0,54 | 0,01 | 1,80 | 0,032 |
| 4 | 44K | 24,1 | 5,3 | 0,32 | <0,001 | 0,04 | 0,024 |

* – base is Fe

***Table 2.*** *Estimation of temperatures* $M_S$ and $M_{d30}$ estimated alloys Fe-20%Mn-10%Al-1.4% of C-x%Ni*

| Ni, % | After treatment for solid solution | | After aging | | | | | | | |
|---|---|---|---|---|---|---|---|---|---|---|
| | $M_S$, K | $M_{d30}$, K | T, °C | f, % | The content of elements in the austenite, % wt. | | | | $M_S$, K | $M_{d30}$, K |
| | | | | | C | Ni | Mn | Al | | |
| 0 | 17 | <4 | 800 | 1,17 | 1,34 | 0 | 19,77 | 10,06 | 40 | <4 |
| 5 | <4 | <4 | 790 | 5,67 | 1,20 | 5,3 | 20,75 | 9,90 | <4 | <4 |
| 10 | <4 | <4 | 827 ($T_1$) | 4,95 | 1,24 | 10,52 | 21,04 | 9,83 | <4 | <4 |
| | | | 773 | 10,44 | 0,96 | 11,16 | 21,31 | 9,84 | <4 | <4 |
| | | | 721 ($T_2$) | 14,77 | 0,72 | 11,73 | 21,30 | 9,90 | <4 | 30 |

* for the calculation of temperatures $M_S$ and $M_{d30}$ for austenite solution heat treatment we take the content corresponding to the chemical compound of the alloy, for the condition after aging – considering the release of proeutectoid constituents from austenite

Results of calculation of $M_S$ and $M_{d30}$, possible number of proeutectoid constituents after aging for certain experimental alloys content and the actual phase content are shown in Table 3.

Calculated temperatures of $M_S$ and $M_{d30}$ for heat-treated high-carbon steels 33K, 34K and 35K are very low, i.e. austenite in such compounds is thermally and mechanically stable till cryogenic temperatures. Under the complete release of carbides from austenite $M_S$ in 34K alloy or $M_{d30}$ in 33K and 35K increase to the values above normal temperature. This proves that hardening of such alloys due to aging should be done in regimes maintaining the proper stability of austenite. In order to prevent the release of carbides in cast alloys higher cooling rates are needed after the casting and solidification.

Under the experiment the cast alloys 33K, 34K and 35K under cooling rate of ~$10^2$ K/s show the existence of austenite in the form of matrix phase (by X-ray method), 35K alloy shows c-carbide traces and 33K exhibit the significant amount of c-carbide (see Table 3).

High-carbon alloys 33K and 34K exposed to the cold deformation using three-point bending method remain austenitic under the normal temperature and 35K showed small amount of α-martensite.

The total content of N in researched experimental alloys is very low (less than 0.01–0.03%) and is represented in the form of AlN nitrides. So, it can be expected that the influence of N on steel properties is similar to the influence of other proeutectoid constituents.

Estimation of the alloy flow limit is calculated by the following relation [5]:

$$(1) \qquad YS\,(UTS) = S_0 + \Delta S_{S.S.} + \Delta S_d + \Delta S_G + \Delta S_{S.G.} + \Delta S_\rho,$$

where $S_0$ = YS of pure iron (30–40 MPa); $\Delta S_{S.S.}$ – solid-solution hardening; $\Delta S_d$ – dispersion hardening due to the second constituent particle; $\Delta S_G$ – grain boundary strengthening; $\Delta S_{S.G.}$ – hardening due to formation of subgrain structure upon polygonization; $\Delta S_\rho$ – hardening due to increase in ρ dislocation density.

Solid solution hardening may be estimated by equation $\Delta S_{S.S.} = \Sigma K_i \cdot C_i$, where $K_i \cdot C_i$ – hardening due to each dissolved element. Empirical expressions are used to assess the certain effects of austenite content on flow limit and ultimate strength, see [4].

Calculated assessment of the austenite content influence on mechanical properties after the treatment on solid solution and after the aging, as well as assessment of dispersion hardening due to the particles of released constituents upon aging (see Table 2, Figures 1 and 2) for estimated (model) and experimental steels.

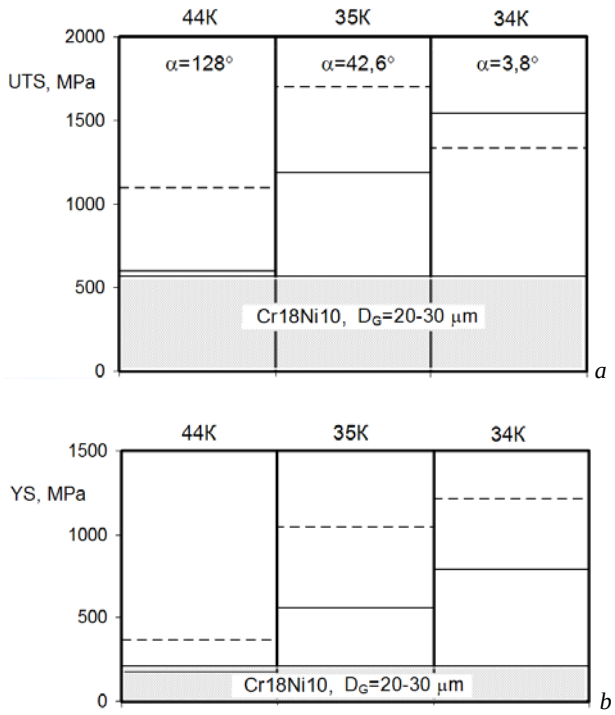
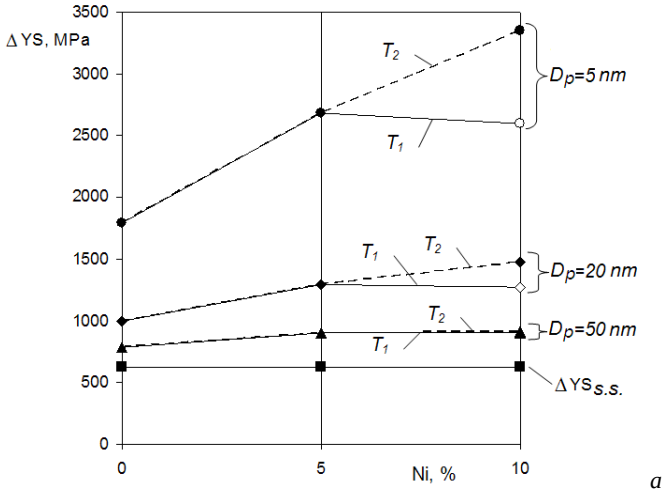



***Fig. 1.*** *Comparison of calculated (solid lines) and experimental (dashed) values of strength UTS (a) and YS (b) for alloys 44K, 35K and 34K and traditional corrosion-resistant austenitic steel Cr18Ni10 [6]*

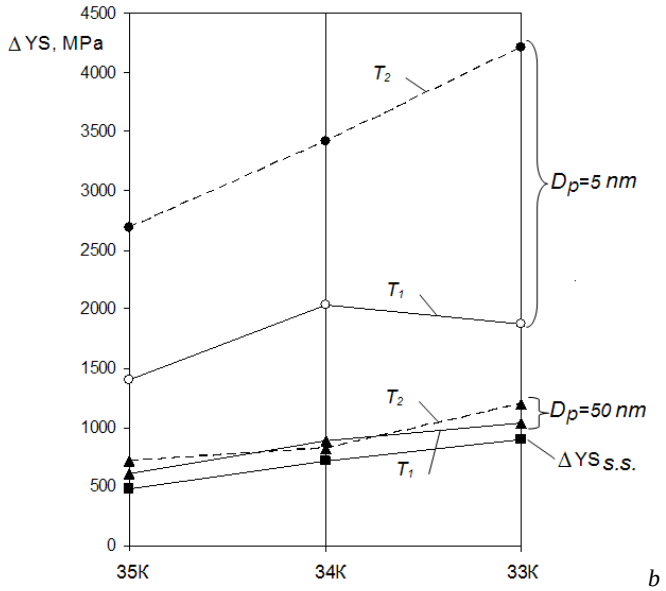
***Table 3.*** *Phase composition and temperature rating* $M_S$ and $M_{d30}$ experimental Fe-Mn-Al-C alloys*

| Alloys | The phase composition of the alloys | | After treatment for solid solution | | After aging | | | |
|---|---|---|---|---|---|---|---|---|
| | in the cast state | after cold deformation | $M_S$, K | $M_{d30}$, K | T,°C | f, % | $M_S$, K | $M_{d30}$, K |
| 35K | γ+[κ]** | γ+α | 54 | 79 | 804 ($T_1$)<br>691 ($T_2$) | 0,628<br>7,612 | 73<br>234 | 104<br>310 |
| 33K | γ+κ | γ+κ | <4 | <4 | 971 ($T_1$)<br>757 ($T_2$) | 0,711<br>29,430 | <4<br>153 | <4<br>122 |
| 34K | γ | γ | <4 | <4 | 985 ($T_1$)<br>660 ($T_2$) | 1,664<br>17,769 | <4<br>321 | <4<br>376 |
| 44K | γ | γ | 234 | 542 | – | – | – | – |

* for the calculation of temperatures $M_S$ and $M_{d30}$ for austenite solution heat treatment we take the content corresponding to the chemical compound of the alloy, for the condition after aging – considering the release of proeutectoid constituents from austenite;
** trace (less 1 %)




*a*




*b*

***Fig 2.*** *The growth of values alloy yield strength ΔYS Fe-20%Mn-10%Al-1,4%C-x%Ni (a) and experimental alloys (b) due to aging at different temperatures ($T_1$ and $T_2$ denote as in tables 2 and 3) and obtain different particle size $D_P$*

It is clear that solid-solution hardening provides significantly high strength of the alloy class under research (for model alloys $\Delta YS_{S.S.} \approx 622$ MPa and $\Delta UTS_{S.S.} \approx 950$ MPa), such austenite hardening level due to particles may be realized if the size of particles equals ≤20 nm only. The cumulative hardening effect $\Delta YS = \Delta YS_{S.S.} + \Delta YS_d$ for regular particles of 50 nm for aged austenitic alloys equals to 786–906 MPa for Ni-free alloys and 900 MPa for alloys with 10% Ni.

Results of the estimation and mechanical tests of experimental alloys proved the rationality of estimations and considerations.

In order to increase the hardness efficiency and to compensate the reduction of solid-solution hardening due to reduction of alloying addition content we need to get significantly smaller particles $D_{cr} \leq 20$–30 nm.

This is realized in [7, 8] and works described in [9]. After aging or thermal deformation followed by the release of carbides of type $Me_xC_y$ and c-carbide of 20–30 nm the strength values are twice higher than values calculated for cast metal. The strength values under 550ºC equal to YS=1200–1300 MPa, UTS=1600–1800 MPa. The hardness of thermal deformation equals to 550–600 HV. Besides, the reduction of alloy density per 10–14% results in the increase in their corresponding specific tenacity.

## *4. Conclusion*

Alloys based on Fe-20%Mn-10%Al-(0–10)%Ni-C with C content of >1.2% for nickel-free system and ≥1.4 % for 5% and 10% of Ni can be proposed as high-strength non-magnetic cryogenic steels both in heat-treated and aged states.

Nitrogen addition in the alloy containing 5% Al can be considered as micro-alloying, enhances dispersion of the cast structure.

Ni enhances the dispersion hardening effect due to increase in carbide release rate resulted from the reduction of C solubility in austenite. Rational content of nickel equals to ~5%.

Results of experiments confirmed the adequacy of phase content calculation as well as the assessments of solid-solution and dispersion hardening of alloys based on Fe-(20–25)%Mn-(5–10)%Al-(0–10)%Ni-C.

Cast high-carbon alloys Fe-(19,1–23,9)%Mn-(4,0–9,0)%Al-(1,1–2,18)%C allow to reach the high strength and adequate ductility under deformation conditions at normal temperature. Strength values: YS=1000–1200 MPa, UTS=1300–1600 MPa upon deformation of ε=10%.

## *5. References*

1. De Moor, E., P.J. Gibbs, J.G. Speer, and other. Strategies for third-generation advanced high strength steel development. – AIST Transactions, Iron and Steel Technology, 7 (11), 2010, pp. 133–144.

2. Svyazhin, A.G., V.E. Bazhenov, L.M. Kaputkina, and others. Critical concentration of nitrogen in steels high, providing a dense ingot. – Metallurg, 11, 2014, pp. 41–46. (in Russian)

3. Birman, S.R. Economically alloyed maraging steel. Moscow, Metallurgy. 1974. 208 p. (in Russian)

4. Pickering, F.B. Physical Metallurgy and the Design of Steels. London, Applied Science Publisher Ltd., 1978, 104 p.

5. Goldshtein, M.I., S.V. Grachev, Y.G. Veksler. Special steel: Textbook for universities. Moscow, MISiS, 1999. (in Russian)

6. Marochnik steels and alloys /Ed. by V. G. Sorokin. Moscow, Mashinostroenie, 1989. (in Russian)

7. Mazancova, E., Z. Jonsta, K. Mazanec. Structural metallurgy properties of high manganese Fe-Mn-Al-C alloy. – Hutnicke Listy, 61 (2), 2008, pp. 60–63.

8. Frommeyer, G., U. Brux. Microstructures and mechanical properties of high-strength Fe-Mn-Al-C light TRIPLEX steels. – Steel Research International, 77 (9–10), 2006, pp. 627–633.

9. Bronze, A.V., L.M. Kaputkina, V.E. Kindop, and others. Experimental study of high temperature strength of the alloys Fe-Mn-Al-C-N. – Problems of ferrous metallurgy and materials science, 3, 2012, pp. 57–62. (in Russian)

*This work was financially supported by the Ministry of education and science of the Russian Federation in the framework of the project of the state assignment in the sphere of scientific activity, task No. 11.1943.2014/K.*

# EFFECT OF ALLOYING ELEMENTS ON THE MICROSTRUCTURE AND MECHANICAL PROPERTIES OF NiAl-Cr(Mo) EUTECTIC ALLOY

Demirtas H. PhD.[1]and Prof. Gungor A.[1]
Karabuk University, Engineering Faculty, Metallurgical and Materials Engineering Department, Karabuk-Turkey [1]
hdemirtas@karabuk.edu.tr

***Abstract:*** *Microstructure and mechanical properties of NiAl-Cr(Mo) eutectic alloy and the effect of 0.1Fe,1Nb,4Ti additions are investigated at room temperature (RT) and high temperature (1000°C). The alloys are prepared by arc melting method and then homogenized at 1300°C in Ar atmosphere for 24 h. In addition to the room temperature and high temperature compression tests and X-ray diffraction measurements, hardness measurements and microscopic analyses at room temperature are performed. NiAl-Cr(Mo) alloy exhibit fine cellular eutectic structure with coarse eutectic at interdendiric regions. However, the Nb and Ti addition reduced the formation of eutectic structure. $Cr_2Nb$-type Laves and $Ni_2AlTi$-type Heusler phases are observed in the XRD patterns of the Nb and Ti containing alloys respectively. Addition of Fe does not have important effect on the room and high temperature yield strength of the alloy, while the Nb and Ti increase the yield strength of the alloys at both temperatures.*

**Keywords**: NiAl-Cr(Mo), LAVES PHASE, HEUSLER PHASE, MECHANICAL PROPERTIES

## *1. Introduction*

Ordered intermetallic materials have taken considerable attention for high temperature structural applications last two decades. Among the ordered intermetallics, NiAl intermetallic compound with B2 crystal structure has excellent properties including high melting point, low density, good thermal conductivity and excellent oxidation resistance up to 1300°C [1–5]. Such attractive properties make NiAl an attractive candidate for high temperature structural applications. However, low ductility and fracture toughness at room temperature and poor elevated temperature strength of the NiAl limit its commercial applications significantly [6,7]. Some strengthening and toughening approaches such as alloying, second-phase strengthening and single crystal preparation were proposed to overcome the drawbacks of NiAl [8–12]. Previous studies on NiAl revealed that the additions of refractory metals like Cr, Mo, V and Ta, etc. can improve the room temperature toughness and elevated temperature strength of NiAl simultaneously [13–15]. Walter et al. [13] showed that directionally solidified NiAl–Cr eutectic alloy strengthened by the Cr fiber had better toughness and creep strength than NiAl. In addition, Cline et al. [16,17] showed that adding Mo to the NiAl–Cr eutectic alloy would lead to a change of microstructure from Cr fibers to Cr(Mo) lamellae.

Among the eutectic alloys, NiAl–28Cr–6Mo alloy is very attractive due to its good room temperature ductility and fracture toughness as well as good high temperature strength [18]. The low temperature and high temperature mechanical properties of NiAl–28Cr–6Mo eutectic alloy can be further improved with micro alloying. Therefore, it is of interest to investigate the room and high temperature microstructure and mechanical properties of Fe, Nb and Ti containing NiAl-Cr(Mo) eutectic alloys since there are not enough studies on the arc melted and micro alloyed eutectic alloys. Here, we present low and high temperature microstructure and mechanical properties of arc melted NiAl–28Cr–6Mo, 65.99(NiAl)-28Cr-6Mo-0.1Fe and Ni(33-X)Al-28Cr-6Mo-X (X=1 at % Nb, 4 at % Ti) eutectic alloys.

## *2. Experimental Procedures*

NiAl–28Cr–6Mo eutectic alloy with X=0.1 at % Fe, 1 at % Nb and 4 at % Ti nominal composition are prepared by vacuum arc melting using Edmund Buhler Vacuum Arc Melter. The purity of metal powders used in this work is 99.9 % for Ni, 99.9 % for Al, 99.99 % for Cr, 99.95 % for Mo, 99.98 % for Fe, 99.99 % for Nb and 99,9 % for Ti. Before melting the alloys, the mixture of metal powders are cold pressed. All arc melted buttons are turned over and remelted at least four times to get homogeneous specimens. In addition, homogenization heat treatment of the alloys has been performed at 1300°C for 24 hours in Ar atmosphere (40 L/h). After that, all alloys are furnace cooled. Before the homogenization heat treatment, the atmosphere of the furnace is purged three times by filling high purity Ar and then vacuuming to $6.5x10^{-2}$ mbar. Since the weight loss for each sample is less than 0.5%, the alloy compositions have been considered to be equal to their nominal compositions.

Wire electro-discharged machine (EDM) is used to get specimens for microstructure analyses and compression tests. For microstructure analyses, specimens are cut along the longitudinal and transverse directions of arc melted buttons. The sections are mechanically polished and then etched in a 5 % nital solution. The microstructures are observed by optical microscope (OM) and scanning electron microscope (SEM, Carl Zeiss Ultra Plus Gemini FESEM) with attached energy-dispersive X-ray spectrometer (EDS). The room temperature and high temperature (1000°C) X-ray diffraction (XRD, Rigaku Ultra IV diffractometer) measurements have been conducted at a rate of 4°/min. between 25°-85° using 40kV and 30mA. The Brinell hardness (HB2.5/31.25/10) of the alloys is determined using Qness/Q250M hardness device. For each alloy, the average hardness of the alloys is obtained from three hardness measurements. In compression tests, cylindrical specimens with 3 mm in diameter and 5 mm in height have been used. The room temperature compression tests are performed at a strain rate of $5x10^{-4}$ $s^{-1}$ in a Zwick/Roell Z600 static/dynamic test machine. The high temperature (1000°C) compression tests are performed at a strain rate of $5x10^{-3}$ $s^{-1}$ in a Shimadzu AG-IS 250 test machine.

## *3. Results and Discussion*

### *3.1. Microstructure characteristics*

Fig. 1 shows the typical SEM microstructures of four alloys produced for this study. In the first and second alloy (Fig.1 a and b) consisted of NiAl and Cr(Mo) phases and the structure was fully eutectic. In the eutectic cells, dark NiAl and gray Cr(Mo) lamellas radiate from the cell center to the cell boundaries. The interlamellar spacing of the Cr(Mo) and NiAl phases near the cell center is smaller than that near the cell boundary. Some coarse and irregular plates formed at the cell boundaries. Figure 1. c and d show the microstructure of the Nb and Ti bearing alloys respectively. In addition to the eutectic phases, a Nb-rich phase formed in the Nb bearing alloy. Introduction of Ti reduced the formation of lamellar microstructure. Ti addition essentially changed the structure of NiAl-Cr(Mo) alloy by forming Cr(Mo) rich dendrites and Ti bearing NiAl solid solution.

The EDS point analyses taken from all alloys are given in Fig. 2. NiAl-Cr(Mo) eutectic and Fe added alloy show similar results except that small amount of Fe distribution in eutectic phases. Existence of Ni and Al in the Cr(Mo) phase and Cr and Mo in the NiAl phase show that small NiAl precipitates are present in the Cr(Mo) phase and similarly Cr(Mo) precipitates exist in the NiAl

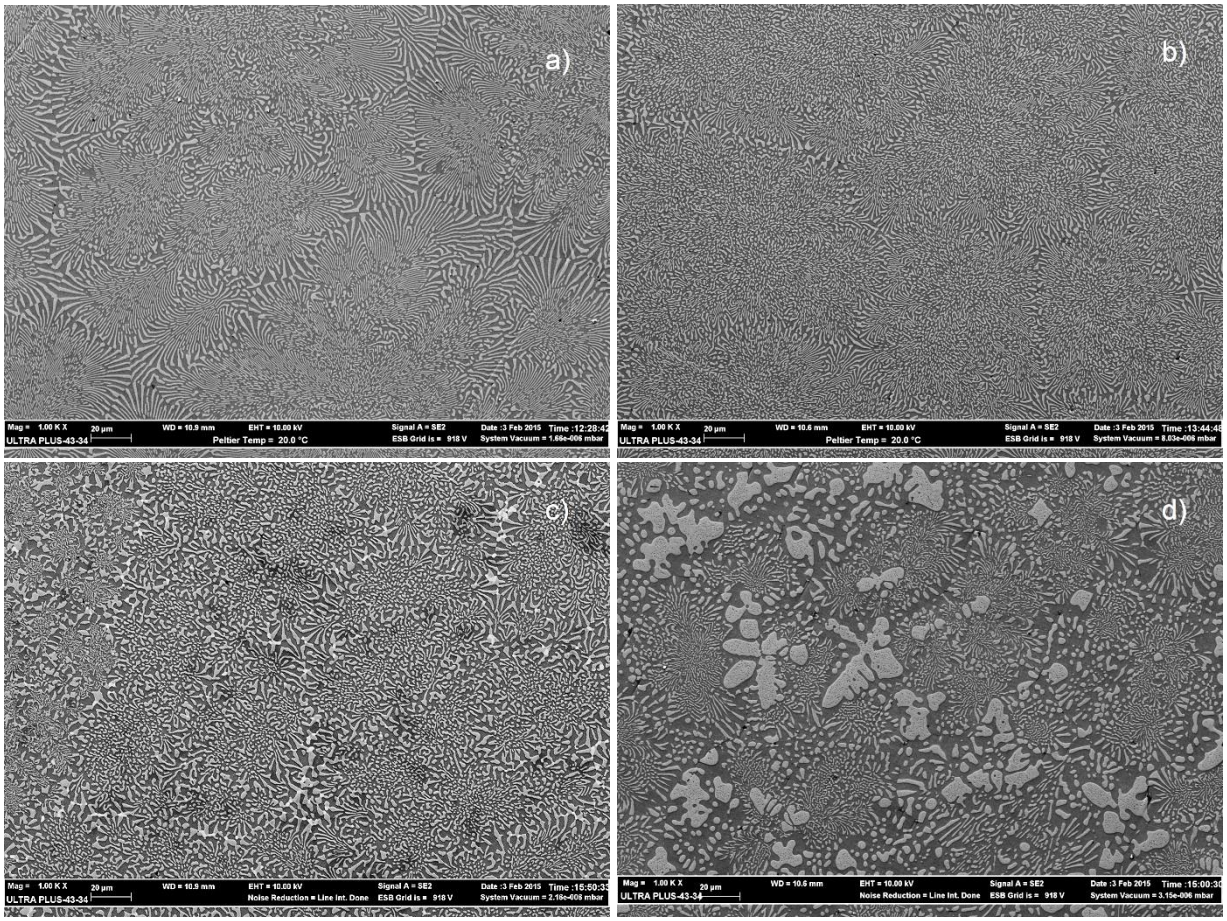
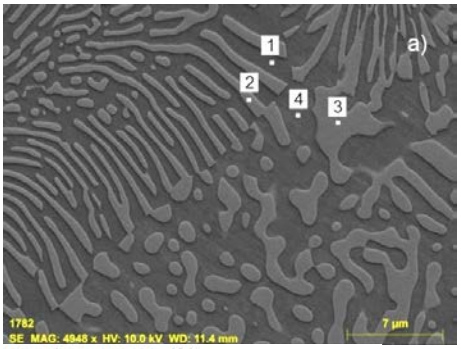


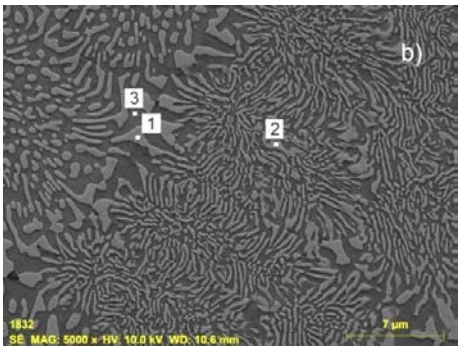

***Fig. 1*** *The microstructure of alloys; a) NiAl-Cr(Mo) b) NiAl-Cr(Mo)-0.1Fe c) NiAl-Cr(Mo)-1Nb and d) NiAl-Cr(Mo)-4Ti.*

phase [19,20]. The fact that chemical composition of the Cr(Mo) and NiAl phases in near eutectic cell center and interdendritic region are very similar indicates that the alloys are homogeneous. As it is seen from the point analyses, Fe partitions both Cr(Mo) and NiAl phases. However, Fe participates into the Cr(Mo) phase slightly more than the NiAl phase as it is given from the Fig.1b. It can be seen from Fig. 2c, the microstructure is composed of NiAl, Cr(Mo) and $Cr_2Nb$ phases. The $Cr_2Nb$ Laves phase formation in the Nb content alloy breaks down the cellular eutectic structure formation. The Fig.2d EDX spectra revealed that dark phase (matrix) enriched in Ni, Al, Ti and grey phase in Cr, Mo. However, both phases have small quantities of other elements.



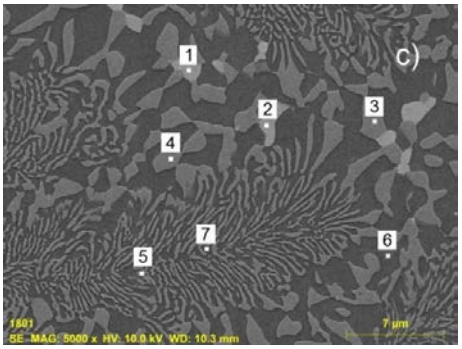

Atomic percent (%)

| Spectrum | Al | Cr | Ni | Mo |
|---|---|---|---|---|
| 1 | 50.02 | 2.40 | 47.53 | 0.04 |
| 2 | 4.85 | 78.94 | 2.22 | 13.99 |
| 3 | 4.75 | 79.23 | 2.16 | 13.86 |
| 4 | 49.91 | 2.10 | 47.85 | 0.14 |



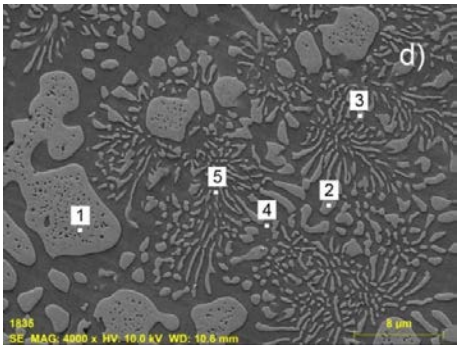

Atomic percent (%)

| Spectrum | Al | Cr | Fe | Ni | Mo |
|---|---|---|---|---|---|
| 1 | 5.68 | 75.75 | 0.46 | 2.37 | 15.74 |
| 2 | 6.14 | 75.85 | 0.37 | 2.61 | 15.04 |
| 3 | 50.24 | 2.29 | 0.30 | 47.11 | 0.06 |



Atomic percent (%)

| Spectrum | Al | Cr | Ni | Nb | Mo |
|---|---|---|---|---|---|
| 1 | 21.36 | 15.03 | 15.39 | 41.14 | 7.09 |
| 2 | 20.29 | 16.46 | 16.18 | 40.05 | 7.02 |
| 3 | 4.42 | 76.85 | 2.05 | 1.28 | 15.40 |
| 4 | 4.17 | 76.73 | 2.31 | 1.51 | 15.29 |
| 5 | 6.02 | 74.78 | 4.11 | 1.21 | 13.89 |
| 6 | 49.34 | 2.47 | 47.91 | 0.19 | 0.09 |
| 7 | 49.51 | 2.64 | 47.52 | 0.25 | 0.07 |

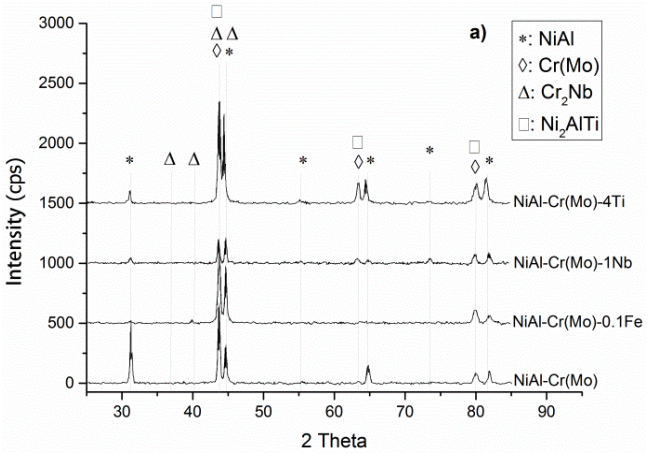



Atomic percent (%)

| Spectrum | Al | Ti | Cr | Ni | Mo |
|---|---|---|---|---|---|
| 1 | 5.04 | 0.81 | 76.30 | 2.34 | 15.50 |
| 2 | 5.16 | 1.00 | 75.18 | 2.87 | 15.79 |
| 3 | 4.33 | 0.78 | 76.25 | 2.66 | 15.98 |
| 4 | 43.64 | 5.76 | 2.68 | 47.73 | 0.18 |
| 5 | 43.89 | 5.58 | 2.44 | 48.03 | 0.06 |

***Fig. 2*** *The EDX points of alloys; a) NiAl-Cr(Mo), b) NiAl-Cr(Mo)-0.1Fe, c) NiAl-Cr(Mo)-1Nb and d) NiAl-Cr(Mo)-4Ti.*

Phase analyses of the alloys were performed at room temperature and 1000°C. The XRD patterns of the alloys are given in Fig. 3. The room temperature x-ray patterns of the alloys show that the all alloys have NiAl and Cr(Mo) phase structure. These phases were also observed by other researchers in NiAl-Cr(Mo) eutectic alloys containing Ti, Hf, Nb alloying elements [20–22]. In addition to these phases, the Nb containing alloy has $Cr_2Nb$, Laves phase and Ti containing alloy has $Ni_2AlTi$, Heusler phase. At 1000°C, the peaks slightly shift to lower Bragg angles indicating that lattice parameters of the phases increase. Increase in lattice parameters may be a result of increase in the separation of planes at high temperatures. In addition, at high temperature XRD patterns of NiAl-Cr(Mo) and 4Ti containing alloys, a peak does not belong to NiAl and Cr(Mo) phases is observed at 2-Theta 33.7°. Since high temperature x-ray data base is not available, phase diagrams were used to interpret the anomalous peak. First of all, the peak is not due to Ti addition because the peak is also present in NiAl-Cr(Mo). Based on the phases in Ni-Al-Cr-Mo systems at 1000°C, it is possible that beta-NiMo is formed at 1000°C.



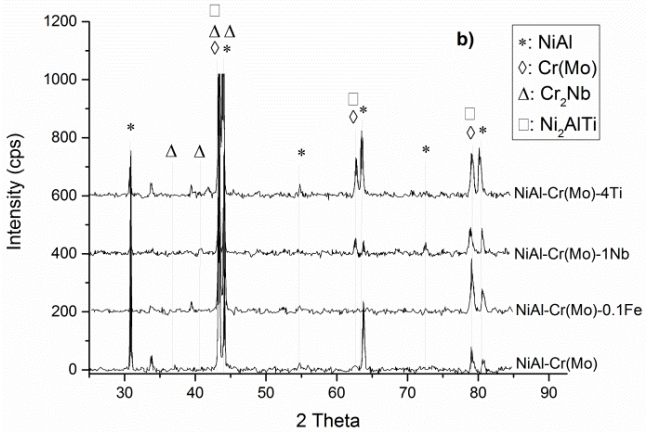




***Fig. 3*** *XRD patterns of the alloys a) at room temperature and b) at high temperature.*

## *3.2. Hardness properties*

Macro hardness test was used instead of micro hardness since penetration depth and area are small due to small applied loads in micro hardness tests. Therefore, it is not possible to obtain a representative hardness value of the alloys with micro hardness measurements. As a result, Brinell hardness of the homogenized alloys was measured by applying 31.5 kg load for 10 s on 2.5 mm steel ball (HB2.5/31.25/10). The hardness values of the alloys are given in Table 1.

As it is seen from the Table 1, Ti added alloy has the highest hardness. Nb containing alloy has similar hardness with the NiAl-Cr(Mo) base alloy but the hardness of Fe containing alloy is lower than that. Based on the hardness of the alloys, the average diameter of the indentations is 380 µm for NiAl-Cr(Mo).

***Table 1:*** *Brinell Hardness of the eutectic alloys.*

| Alloy | HB Measurements | | | **Average HB** |
|---|---|---|---|---|
| NiAl-Cr(Mo) | 283 | 270 | 269 | **274** |
| NiAl-Cr(Mo)-0.1Fe | 259 | 258 | 255 | **257** |
| NiAl-Cr(Mo)-1Nb | 286 | 276 | 266 | **276** |
| NiAl-Cr(Mo)-4Ti | 402 | 398 | 402 | **401** |

The Brinell hardness measurement also provided a valuable information on the deformation behaviour of the phases, ductility and toughness of the alloys. After Brinell hardness measurements, the surface of the alloys was analysed using SEM in order to determine presence of surface cracks. As it can be seen from the SEM images given in Fig. 4, plastic deformation occurs during indentation and any big surface cracks are not observed. Therefore, it can be said that all alloy have enough ductility and toughness. However, in a closer look, micro cracks formed during indentation in 0.1 Fe containing eutectic alloy. From microscopic analyses, it can be said that the Cr(Mo) phase behaves as barrier to crack propagation. As a result, the Cr(Mo) phase contributes to the fracture strength of the alloys by absorbing crack energy and slowing down the crack growth rate. Crack formation in the alloys can be explained with the ductility and toughness of the alloys. When a force is applied on the hard metallic phase, it transfers the applied load to the ductile matrix. The metal matrix absorbs the energy by going through plastic deformation. If the stress is larger than the fracture strength of the matrix, crack initiation in the matrix occurs.

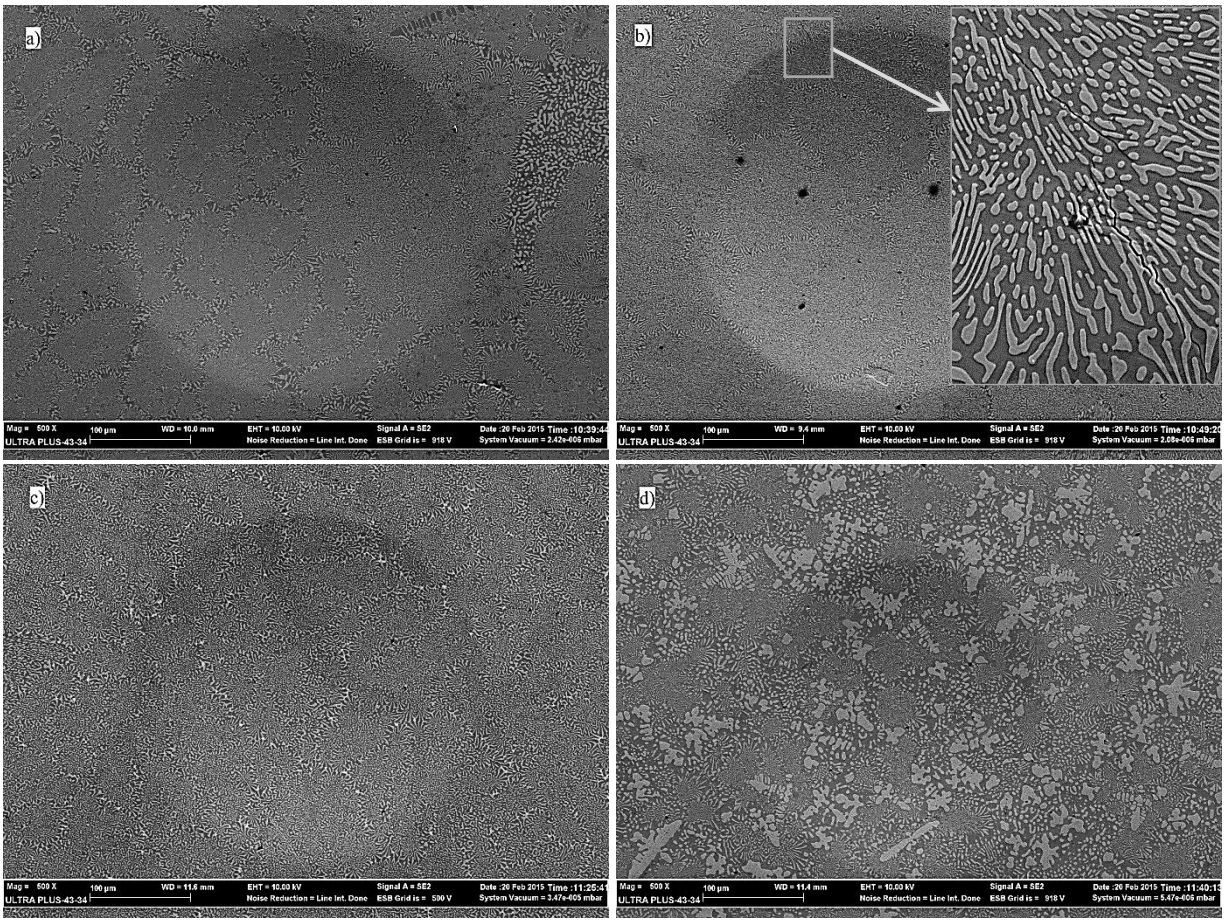



***Fig. 4*** *Deformations on the indentation for; a) NiAl-Cr(Mo), b) NiAl-Cr(Mo)-0.1Fe, c) NiAl-Cr(Mo)-1Nb and d) NiAl-Cr(Mo)-4Ti.*

### *3.3. Compressive properties*

Mechanical properties of the alloys were determined by compression tests at room temperature and 1000°C. The stress-strain curves are given in Fig. 5 and mechanical properties of the alloys are given in Table 2.

The modulus of elasticity of the alloys given in this table is taken from the slope of the stress-strain curves. As it is seen from the room temperature data, Ti bearing alloy shows very high ductility, yield strength and ultimate compression strength. The strength of the NiAl-Cr(Mo) eutectic alloy increases with Ti addition dramatically. However, the Fe addition slightly decreases the ultimate compression strength and strain, moreover Nb added alloy shows the lowest strain. Increasing the test temperature to 1000°C results in much lower mechanical properties. Among the alloys, Nb containing alloy shows the highest yield strength and ultimate compression strength. The increase in strength can be attributed to the formation of $Cr_2Nb$ Laves phases.

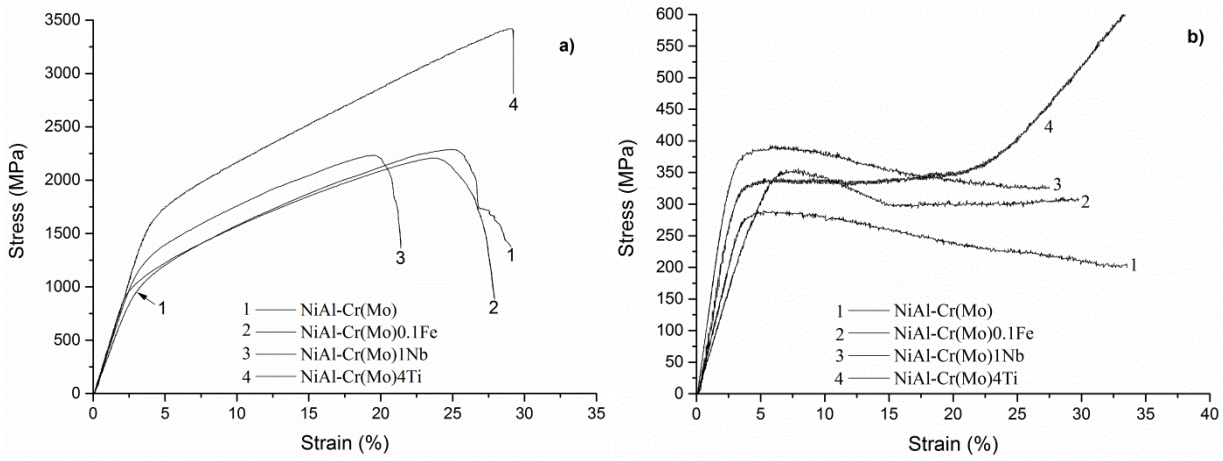



***Fig. 5****. Compression stress-strain curves, a) at room temperature and b) at 1000°C.*

***Table 2.*** *The room temperature and high temperature compressive properties of the alloys.*

| Alloy | | E (GPa) | $\sigma_y$ (MPa) | $\varepsilon_y$ (%) | $\sigma_u$ (MPa) | $\varepsilon_u$ (%) |
|---|---|---|---|---|---|---|
| NiAl-Cr(Mo) | RT | 36.58 | 902 | 2.68 | 2285 | 24.33 |
| | 1000°C | 8.95 | 268 | 3.17 | 292 | 5.6 |
| NiAl-Cr(Mo)-0.1Fe | RT | 43.82 | 949.9 | 2.36 | 2206.1 | 23.38 |
| | 1000°C | 7.48 | 261.9 | 3.71 | 357 | 6.80 |
| NiAl-Cr(Mo)-1Nb | RT | 41.16 | 1120 | 2.91 | 2231 | 19.06 |
| | 1000°C | 14.96 | 325 | 2.39 | 398 | 5.9 |
| NiAl-Cr(Mo)-4Ti | RT | 46.15 | 1548.5 | 3.6 | 3430.3 | 27.71 |
| | 1000°C | 12.09 | 293.2 | 2.6 | 340 | - |

## *4. Conclusions*

The room temperature and high temperature microstructure and mechanical properties of arc melted NiAl-Cr(Mo) eutectic and 65.99(NiAl)-28Cr-6Mo-0.1Fe, Ni(33-X)Al-28Cr-6Mo-X (X=1 at % Nb, 4 at % Ti) alloys are studied. NiAl-Cr(Mo) eutectic alloys have fully lamellar eutectic structure. The Fe addition results in coarser interdendritic regions and lower volume fraction of fine eutectic cells. The eutectic structure changed effectively with the addition of Nb and Ti. Both of them reduce the cellular eutectic structure formation. The EDX analyses reveal that Fe partitions both the NiAl and Cr(Mo) phases, Nb partition mainly to the Cr(Mo) and Ti partition to the NiAl. The room temperature and high temperature XRD measurements show that NiAl-Cr(Mo) and Fe added alloys have two-phase structure, NiAl and Cr(Mo). A third phase as $Cr_2Nb$ and AlTi were seen at Nb and Ti added alloys respectively. In addition, high temperature XRD patterns show that peaks shifted to the left indicating that lattice parameters of the phases increase and there is a possibility of beta-NiMo formation at $1^0$00°C.

All alloys exhibit very high yield strength and total strain at the room temperature. At high temperature, mechanical properties of the alloys decrease significantly. Addition of Fe does not have important effect on the room and high temperature yield strength of alloy while the Nb and Ti increase the yield strength of the alloys at both temperature. Among the alloys, Nb containing alloy has the highest high temperature yield strength, while Ti containing alloy has the highest room temperature yield strength.

***Acknowledgments***

The authors gratefully acknowledge the Tubitak for their financial support under Contract no. 213M247.

## *References*

[1] Noebe R, Bowman R, Nathal M. Physical and mechanical properties of the B2 compound NiAl. Int Mater Rev 1993;38:193–232.

[2] Miracle D. Overview No. 104 The physical and mechanical properties of NiAl. Acta Metall Mater 1993;41:649–84.

[3] George E, Liu C. Brittle fracture and grain boundary chemistry of microalloyed NiAl. J Mater Res 1990;5:754–62.

[4] Assadi H, Barth M, Greer A, Herlach D. Kinetics of solidification of intermetallic compounds in the Ni–Al system. Acta Mater 1998;46:491–500.

[5] Devred F, Reinhart G, Iles G, Van der Klugt B, Adkins N, Bakker J, et al. Synchrotron X-ray microtomography of Raney-type nickel catalysts prepared by gas atomisation: Effect of microstructure on catalytic performance. Catal Today 2011;163:13–9.

[6] Darolia R. NiAl alloys for high-temperature structural applications. JoM 1991;43:44–9.

[7] George E, Yamaguchi M, Kumar K, Liu C. Ordered intermetallics. Annu Rev Mater Sci 1994;24:409–51.

[8] Xie Y, Guo J, Liang Y, Zhou L, Ye H. Modification of NiAl–Cr (Mo)–0.15 Hf alloy by Sc addition. Intermetallics 2009;17:400–3.

[9] Chen Y, Wang H. Laser melted TiC reinforced nickel aluminide matrix in situ composites. J Alloys Compd 2005;391:49–54.

[10] Darolia R, Walston W, Noebe R, Garg A, Oliver B. Mechanical properties of high purity single crystal NiAl. Intermetallics 1999;7:1195–202.

[11] Liu E, Gao Y, Jia J, Bai Y, Wang W. Microstructure and mechanical properties of in situ NiAl–Mo 2 C nanocomposites prepared by hot-pressing sintering. Mater Sci Eng A 2014;592:201–6.

[12] Frommeyer G, Rablbauer R, Schäfer H. Elastic properties of B2-ordered NiAl and NiAl–X (Cr, Mo, W) alloys. Intermetallics 2010;18:299–305.

[13] Walter JL, Cline HE. The effect of solidification rate on structure and high-temperature strength of the eutectic NiAl-Cr. Metall Mater Trans 1970;1:1221–9.

[14] Sheng L, Yang F, Xi T, Zheng Y, Guo J. Improvement of compressive strength and ductility in NiAl–Cr (Nb)/Dy alloy by rapid solidification and HIP treatment. Intermetallics 2012;27:14–20.

[15] Sheng L, Guo J, Zhou L, Ye H. Microstructure and compressive properties of NiAl–Cr (Mo)–Dy near eutectic alloy prepared by suction casting. Mater Sci Technol 2010;26:164–8.

[16] Cline HE, Walter JL. The effect of alloy additions on the rod-plate transition in the eutectic NiAl− Cr. Metall Trans 1970;1:2907–17.

[17] Cline H, Walter J, Lifshin E, Russell R. Structures, faults, and the rod-plate transition in eutectics. Metall Trans 1971;2:189–94.

[18] Bei H, George E. Microstructures and mechanical properties of a directionally solidified NiAl–Mo eutectic alloy. Acta Mater 2005;53:69–77.

[19] Sheng L, Wang L, Xi T, Zheng Y, Ye H. Microstructure, precipitates and compressive properties of various holmium doped NiAl/Cr (Mo, Hf) eutectic alloys. Mater Des 2011;32:4810–7.

[20] Sheng L, Guo J, Ye H. Microstructure and mechanical properties of NiAl–Cr (Mo)/Nb eutectic alloy prepared by injection-casting. Mater Des 2009;30:964–9.

[21] Huai K, Guo J, Ren Z, Gao Q, Yang R. Effect of Nb on the microstructure and mechanical properties of cast NiAl-Cr (Mo) eutectic alloy. J Mater Sci Technol 2006;22:164–8.

[22] Tang L-Z, Zhang Z-G, Li S-S, Gong S-K. Mechanical behaviors of NiAl-Cr (Mo)-based near eutectic alloy with Ti, Hf, Nb and W additions. Trans Nonferrous Met Soc China 2010;212–6.

# INVESTIGATIONS ON MAGNETRON SPUTTERED TANTALUM OXYNITRIDE THIN FILMS

D. Cristea[1*], L. Cunha[2], M. Pătru[1], D. Munteanu[1]
Faculty of Materials Science and Engineering – Transilvania University, Romania [1]
Center of Physics, University of Minho, Campus de Gualtar, 4710-057 Braga, Portugal [2]

daniel.cristea@unitbv.ro

***Abstract:*** *Tantalum oxynitride thin solid films have been deposited by reactive magnetron sputtering, using a fixed proportion reactive gas mixture (85% $N_2$ + 15% $O_2$) but with varying partial pressures, onto silicon (100) wafer substrates. The physical integrity was observed after vacuum thermal annealing at temperatures from 100 °C to 800 °C. The structural evolution on the as deposited and annealed samples was obtained by X-ray Diffraction. For the lowest partial pressure, the crystalline structure is that of tetragonal β-Ta. Increasing the reactive gas partial pressure leads to the formation of fcc-Ta(O,N) crystals, with various orientations (111, 200, 220).The higher partial pressure films are amorphous. The thermal annealing induces a phase transformation, from tetragonal β-Ta to hexagonal $TaN_x$ (x<1). AFM measurements resulted in low RMS roughness values, regardless of the partial pressure or the annealing temperature.*

**Keywords**: TANTALUM OXYNITRIDE, THIN FILM, SPUTTERING, MICROSTRUCTURE

## *1. Introduction*

Transitional metal oxynitride thin solid films have found a wide application in industrial environments, due to interesting electrical, optical, mechanical or other properties in association with a relatively low cost and ease of manufacturing. Films from this class of compounds (oxynitrides) are promising candidates to be implemented in practical applications, due to their main feature, which is the possibility to tune firstly the metallic/non-metallic ratio and secondly the non-metallic content ratio ($O_2/N_2$), by closely controlling the deposition parameters. Tantalum oxynitride thin films have been already studied for their potential in tribological and/or mechanical applications [1, 2], electrical applications [3-8], or optical applications [9, 10].

This work presents our results concerning magnetron sputtered tantalum oxynitride thin films. In particular, some key information regarding the structural evolution and morphology, as a function of the deposition parameters and annealing temperature will be presented.

## *2. Experimental details*

$TaO_xN_y$ thin films were deposited onto silicon (100) wafers substrates by DC reactive magnetron sputtering, using a laboratory-size deposition chamber, containing a tantalum target (99.6% purity), with the following dimensions: (200 × 100 × 6) mm, positioned at 70mm relative to the substrate holder. The schematic for the deposition equipment used for the experimental part of this work is presented in Figure 1.

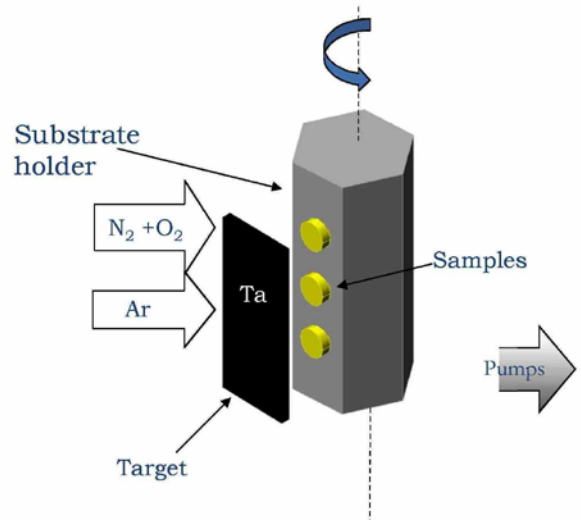



***Fig. 1*** *Schematic of the laboratory chamber used for the deposition of the tantalum oxynitride films.*

The gas atmosphere during deposition was composed of argon as working gas and a mixture of nitrogen and oxygen (fixed proportion of 15 % $O_2$ + 85 % $N_2$) as reactive gases. The argon flow during deposition (70 sccm) was kept constant during all depositions, while the overall $N_2$+$O_2$ gas mixture flow was varied between 2.5 and 30 sccm, corresponding to partial pressures ranging from 0.02 Pa to 0.24 Pa. The partial pressure values were registered before the plasma ignition. The substrate holder was grounded (GND), and the temperature was maintained at 100 °C for all depositions. A more detailed presentation for the deposition protocol for the samples included in this work is presented elsewhere [11]. Table 1 contains information regarding the deposition parameters for the samples presented in this paper.

***Table 1:*** *Deposition parameters for the tantalum oxynitride films.*

| Sample | Reactive gas flow (sccm) | Partial pressure $N_2$+$O_2$ (Pa) |
|---|---|---|
| B2 – $TaN_{0.07}O_{0.03}$ | 2.5 | 0.02 |
| B3 – $TaN_{0.27}O_{0.20}$ | 5 | 0.04 |
| B4 – $TaN_{0.55}O_{0.45}$ | 10 | 0.08 |
| B5 – $TaN_{0.54}O_{0.49}$ | 15 | 0.13 |
| B6 – $TaN_{0.47}O_{0.67}$ | 20 | 0.17 |
| B7 – $TaN_{0.41}O_{0.91}$ | 22.5 | 0.20 |
| B8 – $TaN_{0.39}O_{0.91}$ | 25 | 0.22 |
| B9 – $TaN_{0.32}$ $O_{1.24}$ | 30 | 0.24 |

In order to test the physical integrity of the films as a function of the temperature, the films were annealed in vacuum, with the following protocol: a base pressure of $10^{-4}$ Pa, with a thermal cycle in three steps:

i) an increase of the furnace temperature with an increment of 5 °C/min up to the desired temperature;
ii) a period of 1 h annealing at the desired temperature;
iii) free cooling until reaching ambient temperature.

The samples were annealed at temperatures ranging from 300 °C up to 800 °C. The physical integrity was observed with an optical microscope.

The structural evolution and stability as function of the annealing temperature was observed by X-ray diffraction investigations performed using a Philips PW diffractometer (Cu-Kα radiation) in a Bragg–Brentano geometry configuration. The

resulting patterns were processed with a Pearson VII function and the peak characteristics (position, intensity, width) were obtained.

Atomic force microscopy (AFM) measurements were performed on both coated and uncoated samples, with the following equipment:

i) on selected samples using a Park XE-100 atomic force microscope, at room temperature, on areas of 20 × 20 μm, the surface characteristics being captured with a 200× magnification video microscope;
ii) on selected samples using a Park NX-10, in True Non-Contact Mode, at room temperature, 100 °C, 300 °C and 600 °C, on areas of 2 × 2 μm and 500 × 500nm, respectively. For all the AFM measurements, the RMS (root mean square) roughness was measured.

## *3. Results and discussions*

### *3.1. Structural evolution and stability*

A more in depth discussion regarding the structural evolution of the as deposited (non-annealed) tantalum oxynitride thin films presented in this paper, as a function of the reactive gas partial pressure, can be found elsewhere [11]. However, considering that a number of references to the type of structure will be made in the following sections, a short overview will be presented hereinafter. Figure 2 exhibits the structure variation for the tantalum oxynitride samples, as function of the reactive gas partial pressure. Observing Figure 2, the samples can be divided in two sets: the samples obtained with partial pressures equal or greater than 0.13 Pa are essentially amorphous, while the samples obtained with $P(N_2+O_2)$ < 0.13 Pa exhibit diffraction peaks evidencing the presence of crystallites. The diffraction pattern for the sample produced with the lowest partial pressure ($TaN_{0.07}O_{0.03}$) reveals a broad peak containing several diffraction peaks attributed to the tetragonal β-Ta phase (00-025-1280). Upon rising the partial pressure (samples $TaN_{0.27}O_{0.20}$ and $TaN_{0.55}O_{0.45}$), the diffraction patterns contain peaks attributed to a fcc-Ta(O,N) type of structure, which signify either a face centered cubic fcc-TaN (00-049-1283) or a fcc-γ-TaO (03-065-6750) structure, containing O and/or N atoms, either substitutionally or interstitially, discussed in greater detail elsewhere [11, 12].

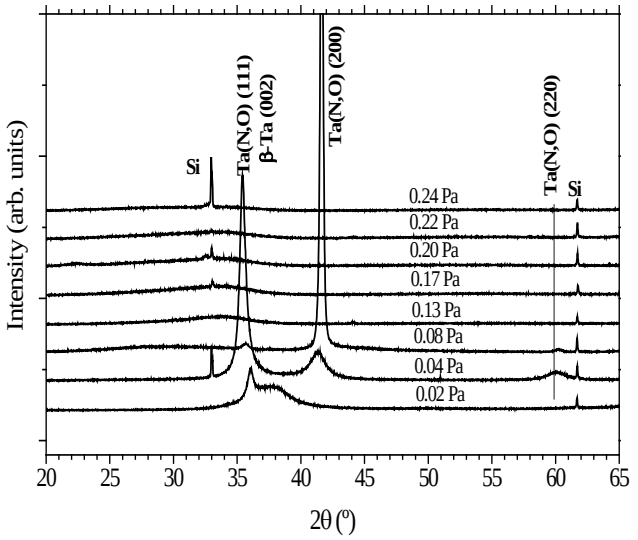



***Fig. 2** X-Ray diffraction patterns, as a function of the reactive gas partial pressure, for the tantalum oxynitride films (Si – substrate, silicon).*

The structural stability was assessed by XRD, on the samples that were subjected to thermal annealing. Previous results concerning the thermal stability of films from the TaON system, published by the authors of this paper elsewhere [12], show that apart from the lower partial pressure samples, no significant changes occur, the films maintaining their structure throughout the entire temperature range that was studied (100 °C – 800 °C). The main difference between the already reported results and the information regarding the samples presented in this paper is the fact that the samples presented here were deposited with a grounded substrate GND, as opposed to a polarization bias of -50V for the samples presented in reference [12]. Some key differences between the two sets of samples appear, as a result of the thermal annealing, which will be presented in the following section.

Following the XRD pattern analysis obtained from the thermally treated samples, three observations can be made:

i) the film deposited with $P(N_2 + O_2)$ = 0.02 Pa exhibits the most interesting evolution, due to new diffraction peaks, observed on the pattern for the 600 °C annealed sample;
ii) the films deposited with intermediate partial pressures exhibit structural stability, regardless of the annealing temperature, accompanied by an increase in crystallinity;
iii) the samples obtained with higher partial pressures maintain their amorphous structure, throughout the annealing temperature regime.

Figure 3 contains the diffraction patterns for the sample obtained with 0.02 Pa partial pressure ($TaN_{0.07}O_{0.03}$), in the following conditions: as deposited, and annealed at 400 °C, 600 °C and 800 °C. The first two conditions presented in Figure 3 (As deposited and 400 °C) exhibit peaks which were attributed to the tetragonal β-Ta structure, albeit with a higher degree of amorphization, deduced from the presence of the broad peak located in the range 36.6° < 2θ < 41.3°. With an increase in temperature, new diffraction peaks can be observed, starting with the diffraction pattern for 600 °C. This means that somewhere between 400 °C (where no new peaks can be observed) and 600 °C (where the new peaks are clearly distinguished), a phase transformation occurs. One key observation needs to be mentioned: this structural change was reported previously, however the temperature interval where it occurs, for the GND sample, is significantly lower (400 °C ÷ 600 °C), compared to the samples produced with the polarized substrate holder (-50V bias) (600 °C ÷ 700 °C) [12]. These new peaks have been attributed to a $TaN_x$ hexagonal structure, where x < 1 (due to the stoichiometry of this sample [11]). None of the peaks for the tantalum phases (α-Ta or β-Ta) coincide with the peaks found on the diffraction patterns presented in Figure 3. Accordingly, considering the stoichiometry of the sample and the peak positions, the following hexagonal phases are equal candidates: β-$TaN_{0.43}$ (01-071-0265), $Ta_2N$ (00-026-0985), $TaN_{0.5}$ (01-089-4764), $Ta_2N_{0.86}$ (01-089-5199).

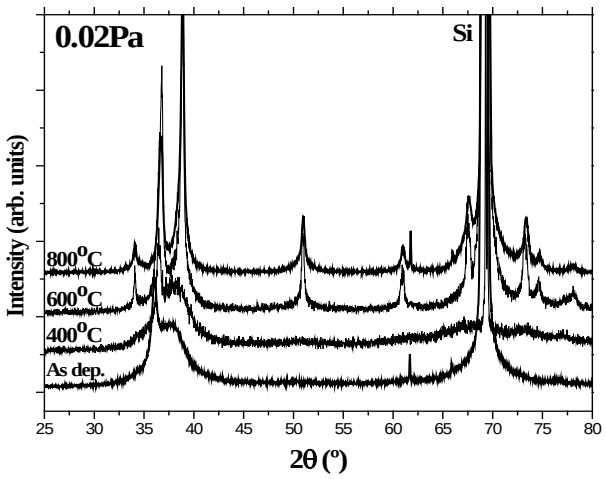



***Fig. 3** The diffraction patterns for the sample deposited with $P(N_2 + O_2)$ = 0.02 Pa, obtained for the as deposited film, and for the 400 °C, 600 °C and 800 °C annealed films.*

It would seem that the annealing treatment promotes the transformation from the tetragonal β-Ta phase to the hexagonal phase of tantalum nitride. This transformation is due to the

migration of the N atoms from grain boundaries and interstitial positions. Taking into account that oxygen is present in the sample, it is possible that these hexagonal crystals contain some O atoms, as it was referred previously [12].

The annealed samples have been also subjected to an optical analysis. Apart from the samples deposited with $P(N_2 + O_2)$ = 0.02 Pa and $P(N_2 + O_2)$ = 0.08 Pa, all the films keep their physical integrity, regardless of the annealing temperature, meaning that no visible cracks and/or delaminations have been observed on the surface. The observed defects, which were noticed starting with the 700 °C temperature, for the $P(N_2 + O_2)$ = 0.02 Pa and $P(N_2 + O_2)$ = 0.08 Pa samples, are presented in Figure 4a and 4b, respectively.

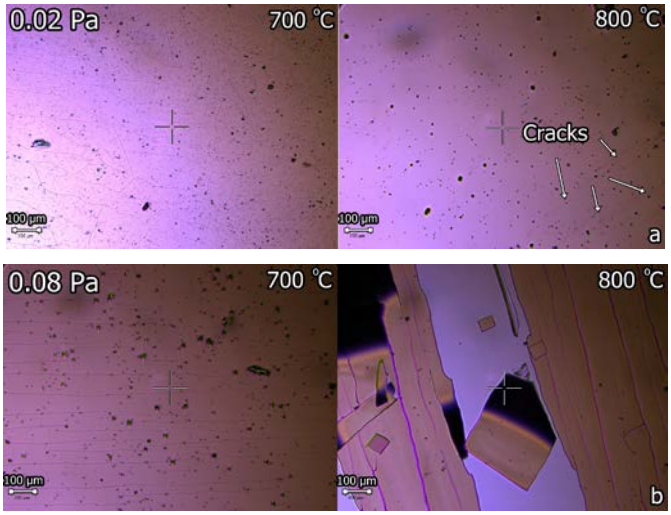



***Fig. 4*** *Failure features observed on the surface of the annealed samples, deposited with $P(N_2 + O_2)$ = 0.02 Pa (a) and $P(N_2 + O_2)$ = 0.08 Pa (b).*

The cracks and delamination observed in Figure 4 could be explained either by a change in dimension for the lattice parameters, considering that this sample exhibits the phase transformation from tetragonal to hexagonal, in the case of the sample deposited with $P(N_2 + O_2)$ = 0.02 Pa, or by a thermal expansion coefficient mismatch between the film and the substrate, for both samples.

### *3.2. Surface morphology*

Several applications necessitate a much larger effective surface area than the apparent surface area (ex. solar cells, photocatalytic materials, etc). The thin film should, therefore, have a high effective surface area, thus an increased surface roughness. An increased surface roughness can be obtained by generating loosely packed small grains. Quantitative measurements of roughness and surface area, obtained using AFM, suggest that nor the deposition parameters (for the as deposited films), neither an increase in temperature (after potential thermal annealing processes) influence significantly the surface roughness of the TaON thin films presented in this paper.

Figure 5 presents the RMS roughness values for some of the as deposited samples and uncoated substrates. The samples were analyzed on a 20 × 20 μm area. From the RMS roughness values and also considering the surface features inherited from the substrate, shown in figure 5, one can conclude that the deposition process variable parameter (the reactive gas partial pressure) does not have a significant influence on the surface roughness, and, furthermore, that the preparation stage of the substrate could be used, at least in this particular case, to increase the effective surface area of the TaON films, due to the fact that the films follow the irregularities of the substrate surface.

Figure 6 shows the variation of the RMS roughness as a function of temperature, for the lowest partial pressure sample. The roughness at 100 °C, 300 °C and 600 °C was measured in-situ, the AFM equipment having the capacity to heat the sample at the desired temperature, up to 600 °C, which was the maximum capability of the microscope. A slight increase in surface roughness can be observed after the phase transformation, from tetragonal to hexagonal structures, which occurs somewhere in the 400 °C – 600 °C temperature domain. However, all the RMS roughness values can be considered to be very low, which translates into a relatively small effective surface area of the material. Higher surface roughness values would allow for a better adsorption of dye molecules on the surface of the films and subsequent rapid degradation of the molecules (for photocatalytic materials), thus the surface roughness would be one of the first parameters to be improved in order to obtain a higher effective area.

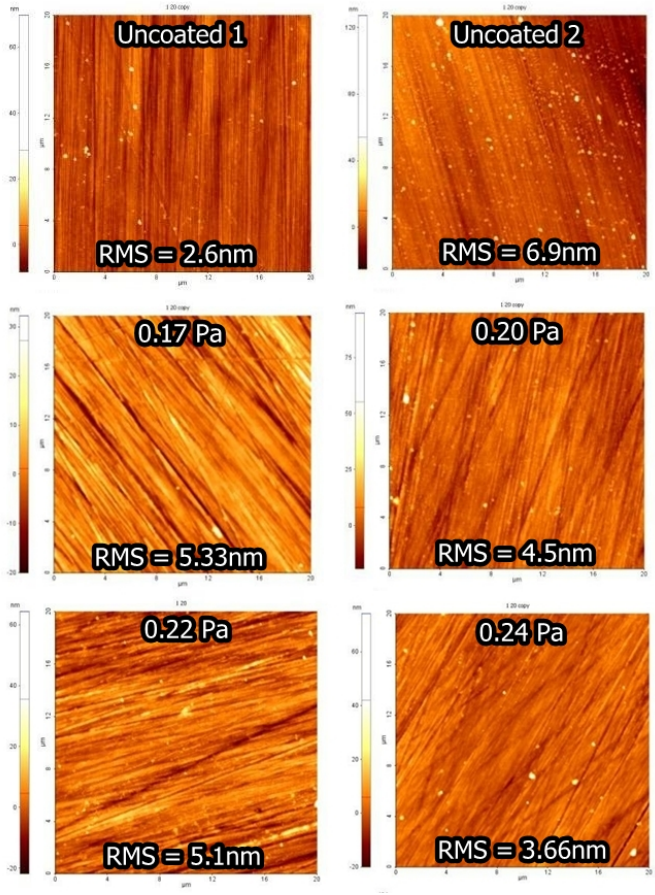



***Fig. 5*** *AFM micrographs obtained from uncoated substrates and from the intermediate and high partial pressure samples (a,b – uncoated, c – $P(N_2 + O_2)$ = 0.17 Pa, d - $P(N_2 + O_2)$ = 0.20 Pa, e - $P(N_2 + O_2)$ = 0.22 Pa, f - $P(N_2 + O_2)$ = 0.24 Pa).*

## *4.Conclusions*

1. A set of tantalum oxynitride thin films were produced by DC reactive magnetron sputtering. Several configurations have been obtained by modifying the partial pressure of the reactive gases mixture (15% $O_2$ + 85% $N_2$) between 0.02 Pa and 0.24 Pa, while keeping the other deposition parameters identical (GND substrate, 100°C substrate temperature, 1A target current, 1h deposition time).

2. The structures exhibited by the as-deposited films are as follows: for the lowest partial pressure – tetragonal β-Ta; intermediate partial pressures – fcc Ta(O,N) structure; high partial pressures – amorphous.

3. After deposition, the films were subjected to vacuum annealing treatments from temperatures ranging from 300 ºC up to 800 ºC,

in order to assess their physical integrity (cracks, delaminations) and their structural stability (phase transformations), as function of the temperature. The lowest partial pressure sample presents a phase transformation somewhere in the 400 °C – 600 °C temperature domain, from tetragonal to hexagonal.

4. Further investigations would be needed in order to pinpoint the temperature or temperature domain where this phase transformation occurs.

5. No delamination or cracks were detected after the annealing at all the temperatures, with the exception of the samples produced with $P(N_2 + O_2) = 0.02$ Pa and $P(N_2 + O_2) = 0.08$ Pa, which after the annealings done at 700 °C and 800 °C exhibit fissures and/or severe delamination.

6. AFM measurements showed very low RMS roughness values, regardless of the deposition parameters, for the as deposited samples, and also when subjected to heating up to 600 °C.

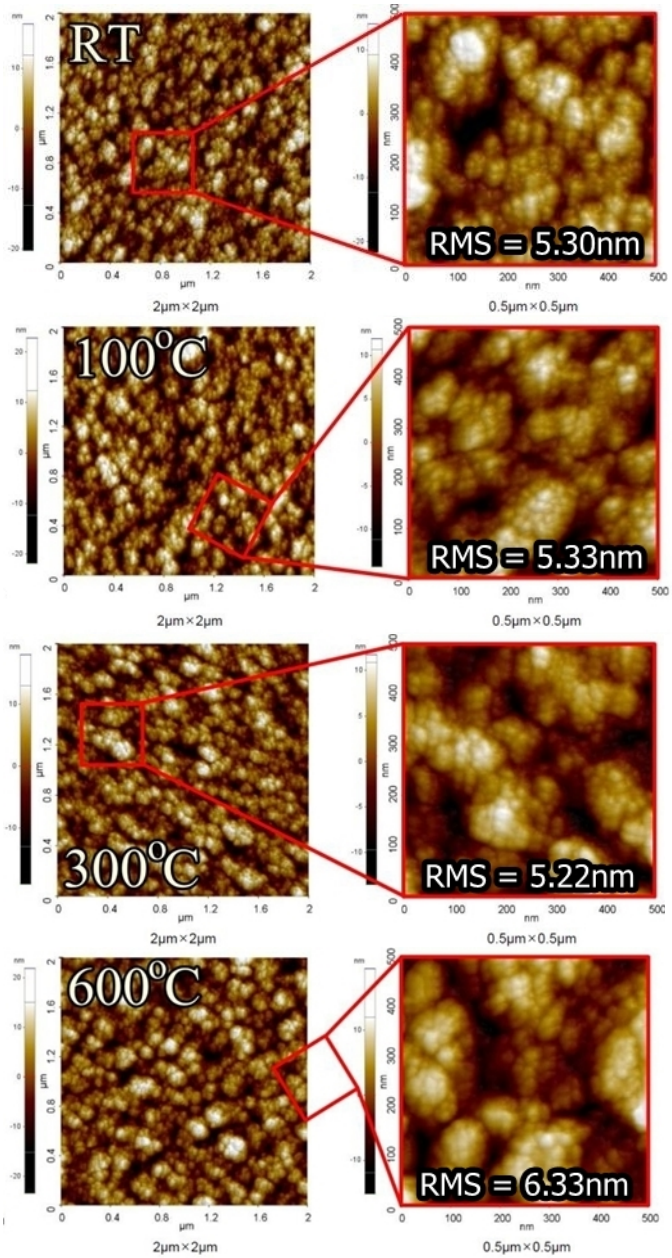



***Fig. 5*** *The influence of temperature on the surface roughness, for the sample obtained with $P(N_2 + O_2) = 0.02$ Pa.*


## *Acknowledgement*

This work was supported by FEDER through the COMPETE Program and by the Portuguese Foundation for Science and Technology (FCT) in the framework of the Strategic Project PEST-C/FIS/UI607/2011 and by the Sectoral Operational Programme Human Resources Development (SOP HRD), financed from the European Social Fund and by the Romanian Government under the project number POSDRU/159/1.5/S/134378.


### *References*


1. O. Banakh, C. Csefalvay, P.-A. Steinmann, M. Fenker, H. Kappl. Surface & Coatings Technology 200 (2006) 6500–6504
2. O. Banakh, P.-A. Steinmann, L. Dumitrescu-Buforn. Thin Solid Films 513 (2006) 136–141
3. Koji Kato, Hiroshi Toyota, Yoshito Jin, Toshiro Ono. Vacuum 83 (2009) 592–595
4. C.K. Chung, T.S. Chen, N.W. Chang. Thin Solid Films 519 (2011) 5099–5102
5. E. Misra, Y. Wang, N.D. Theodore, T.L. Alford. Thin Solid Films 457 (2004) 338–345
6. M. Verchiani, E. Bouyssou, G. Fiannaca, F. Cantin, C. Anceau, P. Ranson. Microelectronics Reliability 48 (2008) 1412–1416
7. Akimitsu Ishihara, Shotaro Doi, Shigenori Mitsushima, Ken-ichiro Ota. Electrochimica Acta 53 (2008) 5442–5450
8. Min-Chen Chen, Ting-Chang Chang, Yi-Chieh Chiu, Shih-Cheng Chen, Sheng-Yao Huang, Kuan-Chang Chang, Tsung-Ming Tsai, Kai-Hsiang Yang, Simon M. Sze, Ming-Jinn Tsai. Thin Solid Films 528 (2013) 224-228
9. S. Venkataraj, H. Kittur, R. Drese, M. Wuttig. Thin Solid Films 514 (2006) 1 – 9
10. Chao-An Jong, Tsung Shune Chin. Materials Chemistry and Physics 74 (2002) 201–209
11. D. Cristea, D. Constantin, A. Crisan, C.S. Abreu, J. R. Gomes, N. P. Barradas, E. Alves, F. Vaz, L. Cunha, Vacuum 98, 63 (2013).
12. D. Cristea, A. Crisan, N. P. Barradas, E. Alves, C. Moura, F. Vaz, L. Cunha, Appl Surf Sci 258P (2013) 19-26.

# INVESTIGATION OF PLASTIC DEFORMATIONS OF CARBURIZED ALLOY STEEL DURING HEAT TREATMENT

Assoc. Prof. Dr. Kandrotaitė Janutienė R.
Kaunas University of Technology, Lithuania
E-mail: raskand@ktu.lt

***Abstract :*** *The article deals with the investigation of plastic deformations of carburized medium carbon stainless steel after quenching and tempering. After carburization the specimens were heated at 1020 °C temperature and then air quenched. At the process of air quenching the specimens were bent within the temperature dropping interval approximately from 550 °C to room temperature. The bending caused tension or compression in different parts of the specimen, so interstitial distortion was formed. As the bending stress was much lower than the yield stress, the specimen didn't bend during the first minutes of experiment, and then started bending during the martensitic transformation (transformation plasticity effect). The curved quenched specimens then were tempered at temperatures 200, 300, 400, 500, 600 and 700 °C for 1 hour and the deflection of specimen after each tempering was measured.*
*The results showed different influence of tension and compression on transformations occurring in steel during quenching and tempering. The tempering temperature effect on self-deformation of curved specimen was revealed.*

*KEYWORDS: STEEL, TRANSFORMATION PLASTICITY, DEFORMATION, QUENCHING, TEMPERING, MICROSTRUCTURE*

## *1. Introduction*

Steel 40X13 (GOST 5632-72) containing 0.4 % carbon and 13 % chromium is medium carbon stainless steel of martensitic class and is often used as corrosion resistant steel in production of plastic injection moulds, springs, bearings and other products that work under the fatigue conditions [1, 2]. On purpose to reach the best mechanical properties of this steel it has to be hardened and double or triple-tempered as during tempering large volumes of secondary carbides precipitate [3]. The resistance to fatigue and wear of steel 40X13 can be increased by thermo-chemical treatment, i. e. by carburizing or nitriding [4-6].

Surface carburizing of specimens gives rather multiplex microstructure: at the very surface the microstructure composes of matrix (pearlite and ferrite) and different amount of surplus carbides dependent on the degree of carbon saturation. During quenching of the carburized specimens, the martensite transformation at the lower carbon core begins considerably earlier ($M_s$ = 270°C) comparing to the transformation inside the carburized surface ($M_s$ < 200°C) [7]. When austenite transforms into martensite, the relative volume increases less at the lower carbon core and signally more at the carburized surface. These transformations proceed great internal stress causing distortions of carburized steel parts due to thermal stresses, volume changes, transformation plasticity, etc. [8-10]. Usually, the steel 40X13 is called as "not much inclined to deformation" during heat treatment [11], however, such precise products as moulds or tools have to maintain especially high precision of the form and parameters. Since the working temperature of some parts can be elevated (tools, moulds), it is important for them to maintain the stable parameters during exploitation. Increased temperature may stimulate such processes as diffusion of carbon and alloying elements, self-tempering of martensite, dissociation of retained austenite, precipitation of carbides and other transformations causing the self-deformation and loss of a stable form [12].

This work was mainly focused on the investigation of plastic properties of carburized specimens of steel 40X13 during air quenching and tempering. The plastic deformation due to transformation plasticity occurred during air quenching was analysed and the phenomenon of self-deformation of the curved specimens after tempering was investigated. This article is the continuous work of the further research based on carburized steel plastic behaviour during heat treatment [13, 14].

## *2. Material and methodology*

Material used for the experimentation was steel 40X13 (GOST 5632-72) with chemical composition listed in Table 1. The critical temperatures of steel 40X13 are presented in Table 2. Table 3 shows the dependence of mechanical properties of steel at elevated temperatures.

***Table 1****. Chemical composition of steel 40X13 according certification of producer No. 747, 2001 09*

| Element, wt.% | | | | | | |
|---|---|---|---|---|---|---|
| C | Si | Mn | Cr | P | S | Fe |
| 0.38 | 0.32 | 0.35 | 12.89 | 0.020 | 0.010 | Rem |

***Table 2.*** *Critical temperatures of steel 40X13* [7]

| $A_{c1}$, °C | $A_{c3}$, °C | $A_{r1}$, °C | $M_s$, °C |
|---|---|---|---|
| 820 | 870 | 780 | 270 |

***Table 3.*** *Mechanical properties of steel 40X13 at elevated temperatures* [7]

| Test temperature, °C | $R_{p0.2}$, MPa | $R_m$, MPa |
|---|---|---|
| *1030-1050 °C, air quenching, tempering 530 °C, 2 h* | | |
| 20 | 1420 | 1670 |
| 410 | 1310 | 1360 |
| 470 | 960 | 1130 |
| 510 | 980 | 1070 |
| *1050 °C, air quenching, tempering 600 °C, 3 h* | | |
| 20 | 890 | 1120 |
| 200 | 810 | 940 |
| 300 | 710 | 900 |
| 400 | 670 | 780 |
| 500 | 470 | 520 |
| 600 | 255 | 300 |

The steel rods were used for manufacturing of the specimens of rectangular cross-section and measurement of 100 × 8 × 6 mm$^3$. The specimens were carburized at 930°C temperature 6 hours placed in the hard carburizer for the purpose to get approximately 1 mm of carburized surface depth. Three schema of carburizing were chosen that are presented in the Table 4. Not carburized surfaces were protected by silicate glue film.

***Table 4.*** *Schematic view of carburized specimens*

| Marking of carburized specimen type | A | B |
|---|---|---|
| Schematic view |  |  |
| Comment | One carburized surface | Three carburized surfaces |

The specimens were austenized for air quenching at 1020 °C temperature in an environment of protective gas of $N_2$ + CO + $CO_2$. For the investigation of steel plasticity during transformations, the austenized specimen was placed in the special testing device for bending [14] and air quenched. At the set temperature the specimen was loaded by bending load generated bending stress of 100 MPa and not exceeded yield strength $R_{p0.2}$ of steel at the certain

temperature (table 3) then, the plastic deflection of specimen was measured with accuracy of 0.01 mm until the temperature of specimen reached room temperature (RT). The range of bending temperatures was from 550 °C to RT. The temperature 550 °C is an approximate temperature at which the specimen is placed in testing device and bending starts. This temperature was indicated by chromel-alumel thermocouple.

The influence of stress type on transformations proceeding inside the material was investigated as well. The position of specimens was varying as table 5 presents. The purpose of this was either to compress, or to stretch the carburized part of specimen.

*Table 5. Schematic view of bending of carburized specimens*

| Marking of bending schema | A1 | A2 | B1 | B2 |
|---|---|---|---|---|
| Schematic view (arrow shows the direction of bending) |  |  |  |  |

After air quenching and bending the specimens were tempered at different temperatures for 1 hour: 200, 300, 400, 500, 600 and 700 °C. Then the change in deflection of specimen was measured observing the effect of self-deformation as well.

After quenching and tempering the samples were tested for heat treatment quality. Universal hardness meter VERZUS 750CCD for Rockwell hardness measurement was used.

The microstructure of specimens was investigated by monitoring with the laser analyzer LMA Carl Zeiss using a video camera YCH15. Following thermal or thermo-mechanical treatment, the samples for optical analysis were carefully cut off by METKON MICRAcut125 low speed precision cutter, then ground and polished by Lam Plan machine using diamond suspension of 1μm grain size, and finally etched in 3% Nital solution.

## 3. Results and discussion

### 3.1. Evaluation of structure of steel 40X13 after carburizing

The microstructures of the carburized specimens exhibit different phase composition at the core and at the surface. The microstructure of the core consists of ferrite, pearlite and here and there hardly visible carbides (Fig. 1). The carburized surface of about 1 mm in depth was found to be rich of iron-chromium carbides that possibly are $M_{23}C_6$ [2, 15] or $M_7C_3$ as the surface contain higher carbon content than the core [16] (Fig. 2).

At the temperature of quenching – 1020 °C, the microstructure of the specimen was austenite with not dissolved carbides as its temperature $A_{c3}$ is 870 °C (table 2).

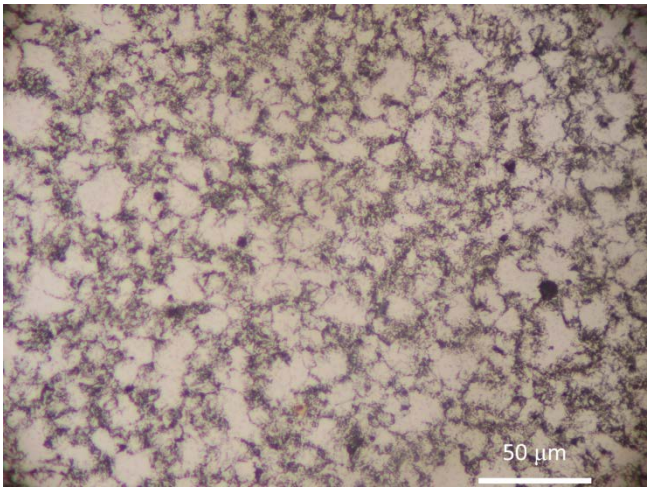



***Fig. 1.*** *Core of carburized specimen of 40X13 steel*

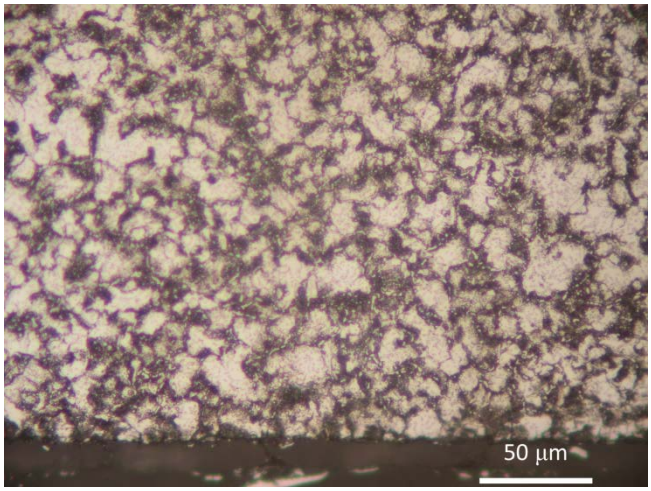



***Fig. 2.*** *Carburized surface of steel 40X13 specimen*

### 3.2. Investigation of transformation plasticity of steel 40X13 specimens during air quenching

Carburized steel specimens were austenized in the furnace at 1020 °C temperature in an environment of protective gas of $N_2 + CO + CO_2$. Then the specimen was withdrawn from the furnace and placed into bending device. The specimen was loaded after 45 seconds starting from the very beginning of air quenching and the temperature of the specimen was 590-595 °C. The bending stress was 100 MPa and it was clear, that this value was much lower than the yield stress of austenite of steel as it caused just elastic deflection which was not increasing until the martensitic transformation started (Fig. 3). The Fig. 3 shows that the martensitic transformation of bent specimens started approximately after 2-3 min of cooling and when temperature dropped until 310-320 °C. As $M_s$ of steel 40X13 is 270 °C, the higher temperature of martensitic transformation start could be related with stresses occurred inside the specimen and the formed martensite could be named as "stress-assisted martensite" [17, 18]. So, in generally, the stresses, even low, stimulate martensitic transformation of steel.

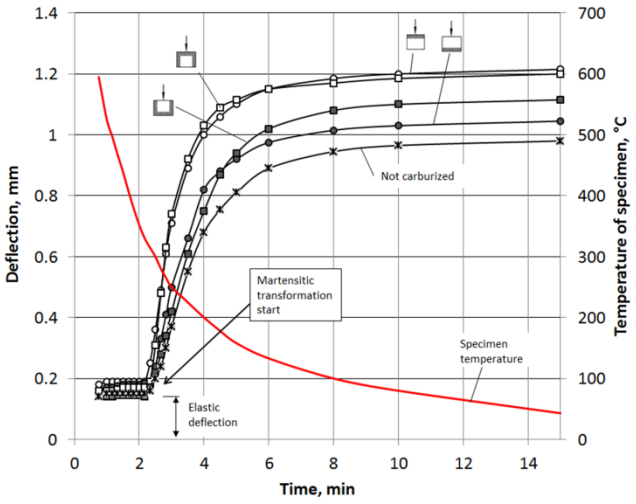



***Fig. 3.*** *Plastic deformation of specimens of steel 40X13 during air quenching due to transformation plasticity caused by martensitic transformation*

Bending of specimens as the mode of stress type was chosen for the purpose. During bending a half of specimen's volume is compressed and another part is stretched (Fig.4). We can investigate the influence of stress mode on martensite transformation. So, at the same experiment there are several variables: stress mode and carbon content causing the difference in martensite start temperature.

Compression and tension act differently on martensite transformation and its start. Stresses, in generally, stimulate martensitic transformation, but tension induces it more intensively. That was found in some references [19, 20] and this is also visible in Fig. 3: the plastic deflection of schema A1 is approximately 15 % bigger than the one of schema A2. In the case of schema A1, the austenite of the stretched part has lower carbon content and it transforms to martensite first. During transformation the volume of stretched part increases and elongates. The stresses caused by volume changes summarize with external stresses and exceed the yield strength of material. The result is big plastic deflection. In the case of schema A2, the martensitic transformation starts at first in compressed part and we can see a result: the plastic deflection is less.

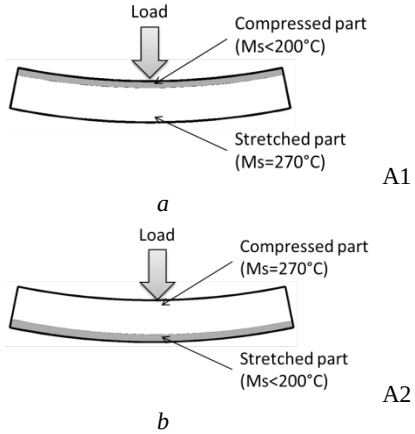



***Fig. 4.*** *Deformation of the specimens according schema A1 and A2 and the position of carburized surface*

The total plasticity due to martensitic transformation is directly related with carbon content. It is seen clearly comparing the total deflection of not carburized specimens and the carburized ones (Fig. 3). Not carburized specimens have the lowest plastic deflection. The reason of that is not sufficiently revealed yet. Maybe the bigger plasticity of carburized steel could be related with higher carbon content in austenite causing bigger distortion of transformed martensite lattice [21] and, thus, higher stresses that summarize with external ones. However, this assumption requires more experiments and investigation methods.

## *3.3. Investigation of self-deformation of steel 40X13 specimens during tempering*

After bending during air quenching, the curved specimens were tempered at temperatures of 200, 300, 400, 500, 600 and 700 °C for 1 hour. After each tempering the deflection of specimens was measured and the change of deflection comparing with the initial one was calculated. Fig. 5 presents the change of deflection, %.

The steel 40X13 is presented as material not much inclined to deformation [11], however some factors may cause self-deformations of quenched parts during tempering, especially if they have heterogeneous phase structure: different content of retained austenite in carburized and not carburized parts that could be from 6 % to 10 % [22]. The retained austenite transforms into martensite at tempering temperatures of 450-500 °C [2, 11], that may decrease the dimension stability on account of 4 % vol. expansion [8, 10]. Also, the carbide precipitation proceeds during tempering. When tempering temperature increases to 500 °C a large amount of dispersive carbides, mainly $M_{23}C_6$ are precipitated within the steel [2, 10].

The biggest self-deformation of specimens was found at the temperatures started from 400 °C (Fig. 5) that is in a good agreement with the changes of material structure mentioned above. Significant decrease of deflection was determined for all modes of carburizing and bending when temperature was higher than 600 °C. Total self-deformation of specimens was in the range of 1-3 %.

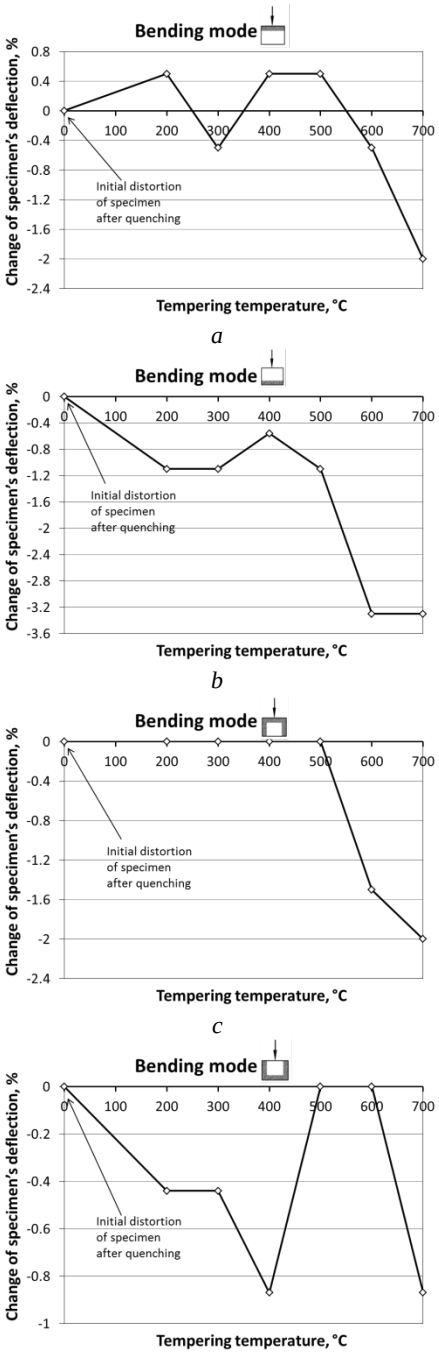



***Fig. 5.*** *Self-deformation of specimens of steel 40X13 influenced by tempering temperature*

## *3.4. Investigation of hardness of steel 40X13 specimens during tempering*

The Rockwell hardness of specimens was measured at the carburized and not carburized surfaces after quenching and each tempering. A big difference between hardness of carburized and not carburized surfaces was not determined, just slightly bigger values of hardness were showed by carburized ones (Fig. 6). The hardness after quenching was obtained 55-60 HRC for carburized surfaces and 54-59 HRC for not carburized ones.

The secondary hardening due to precipitation of chromium rich $M_{23}C_6$ carbides was determined at 400-500 °C temperatures. As some references stated that the temperature of peak of carbides precipitation was 500 °C [2], hardness increase at 400 °C showed the possible stress effect on stimulation of the carbide precipitation process. The bending stresses increase the content of dislocations

and other defects of the material. During the tempering treatment, the diffusion of carbon and alloying elements proceeds to the nearby defects. These segregated areas are preferable sites for small secondary carbide nucleation [3]. Hence, a larger volume of defects provided more driving force for carbide nucleation at lower temperature.

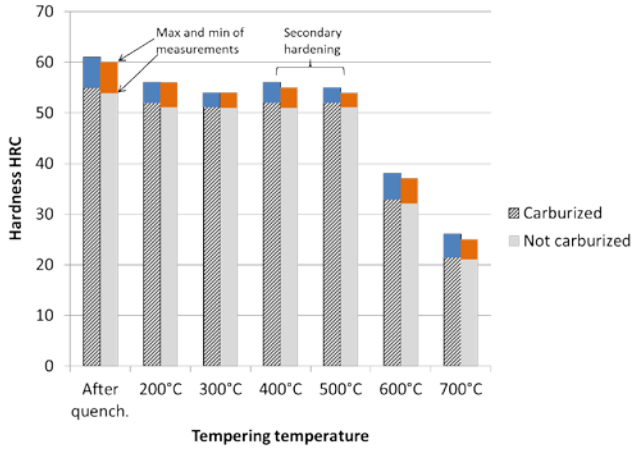



***Fig. 6.*** *Rockwell hardness of specimens of steel 40X13 influenced by tempering temperature*

## *4. Conclusions*

1. It was revealed that external stresses stimulated martensitic transformation, but tension induced it more intensively comparing to compression. The result obtained was the bigger transformation plasticity of specimens of steel 40X13.
2. The total plasticity due to martensitic transformation is directly related with carbon content. Not carburized specimens have the lowest plastic deflection comparing to carburized ones.
3. Self-deformations of bent specimens occur during tempering because of many factors: phase transformations, volume changes, residual stresses, thermal expansion, etc. The highest self-deformations were obtained above 400 °C tempering temperature and were determined of 1-3 %.
4. Secondary hardening of steel 40X13 was determined at 400-500 °C tempering temperatures, i.e. at a little bit higher than found in scientific data, possibly because of the stress effect.

## *5. Literature*


1. Houdremont, E. Special steels. Vol.1.-Moscow: Metallurgy, 1966, 736 p. (in Russian).
2. Si-Yuan, L., Ke-Fu, Y., Yun-Bo, Ch., Miao-Hui, W., Xue, L., Xueyun, G. The effect of tempering temperature on the microstructure and electrochemical properties of a 13 wt.% Cr-type martensitic stainless steel.-Electrochimica Acta, Vol. 165, 2015, p. 45-55.
3. Torkamani, H., Raygan, Sh., Rassizadehghani, J. Comparing microstructure and mechanical properties of AISI D2 steel after bright hardening and oil quenching.-Materials and Design, Vol. 54, 2014, p. 1049-1055.
4. Romanenko, A. G. Development of exploitation properties of structural steel during thermos-chemical treatment by using paste carburizer. Summary of doctoral thesis.-Kursk, 2014, 17 p. (in Russian).
5. Jun, W., Yuanhua, L., Jing, J., Dezhi, Z., Qiang Zh., Runbo, H., Hongyuan, F. Influence of time on the microstructure of AISI 321 austenitic stainless steel in salt bath nitriding.-Surface & Coatings Technology, Vol. 206, 2012, p. 3399-3404.
6. Ulutan, M., Celik, O. N., Gasan, H., Er, U. Effect of different surface treatment methods on the friction and wear behaviour of AISI 4140 steel.-Material Science & Technology, Vol. 26, Iss. 3, 2010, p. 251-257.
7. Grade handbook of steels and alloys. Ed. By Sorokin V. G.-Moscow: Machines engineering, 1989, 639 p. (in Russian).
8. Amini, K., Akhbarizadeh, A., Javadpour, S. Investigating the effect of the quench environment on the final microstructure and wear behaviour of 1.2080 tool steel after deep cryogenic heat treatment.-Materials and Design, Vol. 45, 2013, p. 316-322.
9. Atraszkiewicz, R., Januszewicz, B., Kaczmarek, L., Stachurski, W., Dybowski, K., Rzepkowski, A. High pressure gas quenching: Distortion analysis in gears after heat treatment.-Materials Science & Engineering A, Vol. 558, 2012, p. 550-557.
10. Cho, J. R., Kang, W. J., Kim, M. G., Lee, J. H., Lee, Y. S., Bae, W. B. Distortions induced by heat treatment of automotive bevel gears.-Journal of Materials Processing Technology, Vol. 153-154, 2004, p. 476-481.
11. Adaskin, A. M., Sapronov, I., Yu. Corrosion-resistant steel for metal-shop tools.-Russian Engineering Research, Vol. 32, No. 3, 2012, p. 301-304.
12. Manual on structural materials. Ed. By Arzamasov, B. N., Solovjova, T. V.-Moscow: press MGTU of Bauman, 2005, 637 p. (in Russian).
13. Kandrotaitė Janutienė, R. Influence of carburized surface on plastic properties of steel during tempering.-Mechanika, Vol. 77, No. 3, 2009, p. 74-78.
14. Kandrotaitė Janutienė, R. Investigation of hardening and tempering deformations of carburized low alloy steel.-Mechanika, Vol. 19, No. 2, 2013, p. 236-242.
15. Kovalevskaya, Zh. G., Kukarenko, V. A. Investigation of the structure and phase composition of the nitrided layers of martensitic steel produced by ultrasonic burnishing and ion implantation.-Obrabotka metallov, Vol. 61, No. 4, 2013, p. 19-27. (in Russian).
16. Suchanek, J., Kuklik, V. Influence of heat and thermochemical treatment on abrasion resistance of structural and tool steels.-Wear, Vol. 267, 2009, p. 2100-2108.
17. Novikov., I.I. Theory of heat treatment of metals.-Moscow: Metallurgy, 1978, 392 p. (in Russian).
18. Yeddu, H. K., Borgenstam, A., Agren, J. Stress-assisted martensitic transformations in steels: A 3-D phase-field study.-Acta Materialia, Vol. 61, 2013, p. 2595-2606.
19. Kim, H., Lee, J., Barlat, F., Kim. D., Lee, M.-G. Experiment and modelling to investigate the effect of stress state, strain and temperature on martensitic phase transformation in TRIP-assisted steel.-Acta Materialia, 2015, article in press.
20. Fischlschweiger, M., Antretter, Th., Cailletaud, G. Transformation hardening and kinetics for stress assisted and temperature driven martensitic transformation in steels.-Mechanics Research Communications, Vol. 47, 2013, p. 84-88.
21. Krauss, G. Martensite in steel: strength and structure.-Materials Science and Engineering, Vol. A273-275, 1999, p. 40-57.
22. Kandrotaitė Janutienė, R., Žvinys, J. Investigation of kinetic plasticity of high chromium steel during tempering.-Materials Science (Medžiagotyra), Vol. 9, Iss. 3, 2003, p. 250-254.

# MECHANICAL PROPERTIES OF NANOSTRUCTURED $B_4C/C_{60}$ AND c-BN/$C_{60}$ COMPOSITES PREPARED BY HPHT METHOD

## МЕХАНИЧЕСКИЕ СВОЙСТВА НАНОСТРУКТУРИРОВАННЫХ $B_4C/C_{60}$ и c-BN/$C_{60}$ КОМПОЗИТОВ, ПОЛУЧЕННЫХ МЕТОДОМ ВДВТ

M.Sc. Prokhorov V. PhD.[1], Prof. Blank V.[1], M.Sc. Ovsyannikov D.[1], M.Sc. Popov M. Dr.[1,2], M.Sc. Levin V. PhD.[3], M.Sc. Morokov E.[3].
Technological Institute for Superhard and Novel Carbon Materials [1], Russia
National University of Science and Technology MISiS [2], Russia
Emmanuel's Institute of Biochemical Physics [3], Russia

pvm@tisnum.ru

***Abstract:*** *Nanostructured boron carbide/$C_{60}$ ($B_4C/C_{60}$) and cubic boron nitride/$C_{60}$ (c-BN/$C_{60}$) carbon-ceramic composites were prepared by a high-energy ball milled pre-treatment of the parent materials with the addition of a $CS_2$ solvent followed by a high-pressure/high-temperature (HPHT) treatment. Tthe elastic moduli were calculated based on the experimentally measured density and velocity values of the longitudinal and transverse bulk acoustic waves (BAW) in the specimens. The BAW velocities were measured with a pulse-echo method by laser optoacoustic excitation of ultrasonic pulses. Acoustic microscopy was used to visualize the bulk microstructure and internal defects and to measure the local values of BAW velocities of specimens on which the elastic moduli had been calculated and compared with the data defined by the pulse-echo method. The microhardness and flexural strength of the samples were measured also.*

**Keywords**: NANOSTRUCTURED COMPOSITES, HPHT TREATMENT, MECHANICAL PROPERTIES

## *1. Introduction*

One of the characteristics of a durable, lightweight, hard, and high-refractory material is a ratio of the tensile strength or bending strength (in units of MPa) and its density (in units of g/cm$^3$) $\sigma^*/\rho$. Thus, a B95 aluminum alloy has the highest value of $\sigma^*/\rho$ ($\sigma^*/\rho \approx 200$ MPa·cm$^3$·g$^{-1}$) [1,2], and so do the carbon fiber–reinforced polymers ($\sigma^*/\rho$ up to 400 MPa·cm$^3$·g$^{-1}$) [3]. In this case, both materials are neither high-hardness (hardness $\boldsymbol{H} \leq 1$ GPa), nor heat-resistant (operating temperature less than 200 $^0$C). The known carbon-carbon composite materials are durable and heat-resistant, but are not highly hard. (Tensile strength of Carbon glassy is 600–1000 MPa, $\rho$=1.5 g/cm$^3$, $\sigma^*/\rho$ from 400 to 600) [4].

Our goal was to develop a technique for commercial production of the carbon-based composite materials that are at the same time highly durable, lighter, highly rigid and heat-resistant. With this purpose, we took very hard materials as a basis and, with the help of nanocarbon, made them less brittle and more heat-resistant.

The cubic boron nitride c-BN hardness is inferior only to diamond, and its thermal and chemical stability exceeds the diamond parameters. Another well-known material, boron carbide $B_4C$, is light ($\rho$ = 2.52 g/cm3), high-hardness ($\boldsymbol{H} \approx 35$ GPa), and refractory (operating temperature up to 2000 $^0$C), but both of these materials are extremely fragile, which makes it almost impossible to determine their $\sigma^*/\rho$ parameter [5].

The strength characteristics include hardness, tensile strength, elastic modulus (Young's modulus), proportional limit, and yield strength. There is a close correlation between the modulus and strength of the ceramic materials, which is confirmed by numerous works [6-8].

It is known that the tensile strength of the materials at temperatures less than 0.5 $T_m$ (melting) is combined with hardness by the empirical relationship $\boldsymbol{H}/\boldsymbol{\sigma_t} \approx 3$. For nanostructured materials, the relation between tensile stress and grain size is described mathematically by the Hall–Petch equation [9-10]:

$$\boldsymbol{\sigma}(d) = \boldsymbol{\sigma_0} + k\boldsymbol{d}^{-1/2}$$

where $\boldsymbol{\sigma}$ is the tensile (yield) stress, $\boldsymbol{\sigma_0}$ is a material constant for the starting stress for dislocation movement (or the resistance of the lattice to the dislocation motion), k is the strengthening coefficient (a constant specific for each material), and $\boldsymbol{d}$ is the average grain diameter.

Therefore, to improve the strength of the material, it is necessary to carry out its nanostructuring.

Ultrasonic methods are among the basic and important methods for the diagnostics and nondestructive testing of materials, including the nanostructured ones. In this paper, we used the ultrasonic methods (laser ultrasound and acoustic microscopy) to investigate the elastic properties (Young's modulus, in particular) and microstructure of nanostructured carbon-composite ceramics, depending on the composition and preparation conditions.

Mechanical properties of $B_4C$ ceramics, prepared by a high-energy ball milled pre-treatment of the parent materials followed by a hot-pressing sintering were studied in [11].

## *2. Experimental procedure*

### *2.1. Materials and processing*

The $B_4C$ boron carbide powder (average grain size of 100 nm) is mixed with powdered molecular $C_{60}$ (average grain size of 1 μm) in a weight ratios in the range from 80/10 to 50/50 wt.% in a vibratory mill. Then, the nanostructured boron carbide/$C_{60}$ ($B_4C/C_{60}$) and boron nitride/$C_{60}$ (c-BN/$C_{60}$) carbon-ceramic composites were prepared from this mixture by a high-energy ball milled pre-treatment of the parent materials. Refinement and homogenization was carried out in a high-power and high-speed planetary mill AGO-3Y which provides the effective crushing of ingot and mixing of powders at impact of working bodies with acceleration up to 20g.

Sulfur compound, in this case carbon disulfide $CS_2$, dissolving the $C_{60}$ fullerene, was added to the resulting $B_4C/C_{60}$ powder composite in amounts from 0.1 to 3.0 wt.% in terms of sulfur. This additive serves to facilitate the phase transitions in the subsequent formation of a $C_{60}$ solid binder (matrix) in the nanocomposite at HPHT-treatment [12]. Then, the mixture of $B_4C/C_{60}/CS_2$ was triturated in an agate mortar to obtain a uniform consistency and was used for preparing the specimens. This mixture was charged into a pressure chamber, fixed to the load pressure between 1.0 and 5.0 GPa and heated to 1000 $^0$C with a holding time of 60–100 sec. The preparation method of boron nitride composite powders and dense samples was similar.

After unloading, the specimen was examined by X-ray diffraction, Raman spectroscopy, transmission electron microscopy, and thermogravimetric analysis, and its mechanical properties were studied, including elastic and ultrasonic properties.

### *2.2. Experimental*

#### *2.2.1. Ultrasonic measurements*

The BAW velocities were measured with a pulse-echo method in two ways: by laser optoacoustic excitation of ultrasonic pulses [13-14], and by acoustic microscopy [15-16]. For ultrasonic measurements, we used the specimens in the shape of parts of disks with a 15–17 mm diameter, 2.5–6.0 mm height and nonflatness of the opposite faces ±1 μm/cm (Fig.1). The specimens containing the $C_{60}$ component of 50wt.% (denoted S50) and 10wt.% (denoted S10) were taken for studies.




***Fig.1*** *Samples for ultrasonic measurements.*

The data on sound velocities of the longitudinal $V_L$ and transverse $V_T$ BAW were obtained with an accuracy of ~1%; elastic moduli ~2–3%.

The densities of $B_4C/C_{60}$ ceramics ranged from 2.125 to 2.301 (± 0.002) g/cm$^3$ for the specimens with 50wt.%$C_{60}$, and from 2.333 to 2.548 g/cm$^3$ for the specimens with 10wt.%$C_{60}$. The data on the elastic moduli of the HPHT-treated specimens were compared to the applicable data for the specimens prepared without the addition of carbon bisulfide.

Figure 2 shows the waveforms of ultrasonic pulses of the specimen S50-2 obtained by the laser optoacoustic method (a) and the acoustic microscopy method (b).

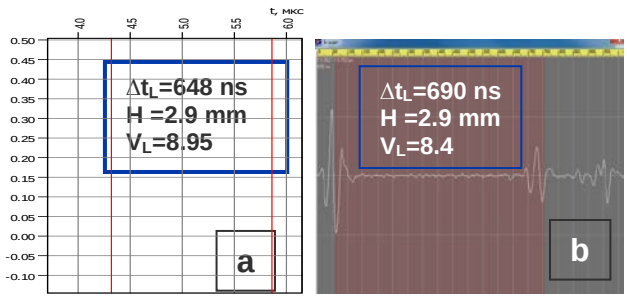



***Fig.2*** *The waveforms of ultrasonic pulses of the specimen S50-2 obtained by the laser optoacoustic method* (a) *and the acoustic microscopy method* (b). *(*$\Delta t_L$*- time-of-flight double thickness* H *of the specimen)*

The difference in the measured values of the BAW velocity is related to the fact that in the measurements by acoustic microscopy, the local velocity values are determined and the elasticity moduli are calculated from these local values. So, the local values can either exceed or be less than the integral values obtained by the laser optoacoustic method.

For some specimens, the data on BAW velocities, densities and elastic moduli of $B_4C/C_{60}$ carbon-ceramic composites are presented in Table 1. We found that the specimens with the addition of carbon disulfide have higher velocities and modules at almost the same density.

***Table 1*** *Bulk acoustic wave densities, velocities, and elastic moduli of* $B_4C/C_{60}$ *carbon-ceramic composites.*

| No | ρ (±0.002) g/cm$^3$ | $V_L$ km/c | $V_T$ km/c | E (±3) GPa | G (±1) GPa | σ |
|---|---|---|---|---|---|---|
| S50-1* | 2.125 | 8.15 | 4.42 | 117 | 41 | 0.291 |
| S50-1 | 2.125 | 8,62 | 4,44 | 111 | 42 | 0,319 |
| S50-2* | 2.293 | 8.42 | 5.27 | 150 | 63 | 0.178 |
| S50-2 | 2.301 | 8.95 | 5.06 | 149 | 59 | 0.265 |
| S50-3H1 | 2.238 | 8.30 | 5.03 | 136 | 56 | 0.214 |
| S50-3H2 | 2.238 | 8.05 | 4.66 | 121 | 48 | 0.245 |
| S10-1* | 2.333 | 6.72 | 4.00 | 92 | 37 | 0.229 |
| S10-1 | 2.333 | 7.42 | 4.05 | 97 | 37 | 0.293 |
| S10-3 | 2.342 | 8.16 | 4.33 | 114 | 43 | 0.309 |
| S10-4 | 2.391 | 7.97 | 4.70 | 133 | 54 | 0.225 |
| S10-5 | 2.548 | 11.3 | 6.32 | 260 | 102 | 0.272 |
| S10-5** | 2.548 | 11.6 | 7.27 | 307 | 130 | 0.181 |

* -without $CS_2$ additives

** - acoustic microscopy data

Specimen S10-5 demonstrated exceptionally high values of the sound velocities and elastic moduli. Its density is also by 6% higher as compared to the density of the specimens S10-3 and S10-4. The velocity of longitudinal waves is equal to 11.3 km/s, which coincides with the measurements of the acoustic microscopy method. The local method of acoustic microscopy in some parts of the specimen obtained even higher values of the moduli (Young's modulus exceeding 300 GPa). The hardness of this material is up to 70 GPa; the material is highly rigid.

In the specimens of the composite based on the boron nitride (c-BN/$C_{60}$) we were not able to get any good results when used the above-mentioned values of the HPHT-treatment parameters. The elastic moduli of the specimens are as follows: Young's modulus E = 55–80 GPa, the bulk modulus K = 37–58 GPa, shear modulus G = 22–33 GPa. Low elastic moduli indicate the absence of the chemical bond between the c-BN and the resulting HPHT-treatment $C_{60}$ phase. Thus, the resulting composite material is not durable. The hardness of the material obtained by us is within 10–70 GPa, and the material is highly rigid

#### *2.2.2. Acoustic microscopy*

The principle of the acoustic microscopy is well known [15-17]. Acoustic microscopy is used to measure the local values of ultrasonic velocities (microacoustic technique) and to visualize the bulk microstructure of a sample (scanning acoustic microscopy). The waveform of the reflected signal is an ultrasonic A-scan. 1D- or 2D- scanning of the probe beam over the specimen surface results in the raster-formation acoustic images (B- and C-scans, respectively).

A SIAM Scanning impulse acoustic microscope (50 ÷ 200 MHz), designed and fabricated in the AM-laboratory of Emmanuel's Institute of Biochemical Physics, Russian Academy of Science, was used to make the measurements. Ultrashort probing ultrasonic 30-40 ns pulses were used for the measurements.

Figures below represent the A- and C-scans.

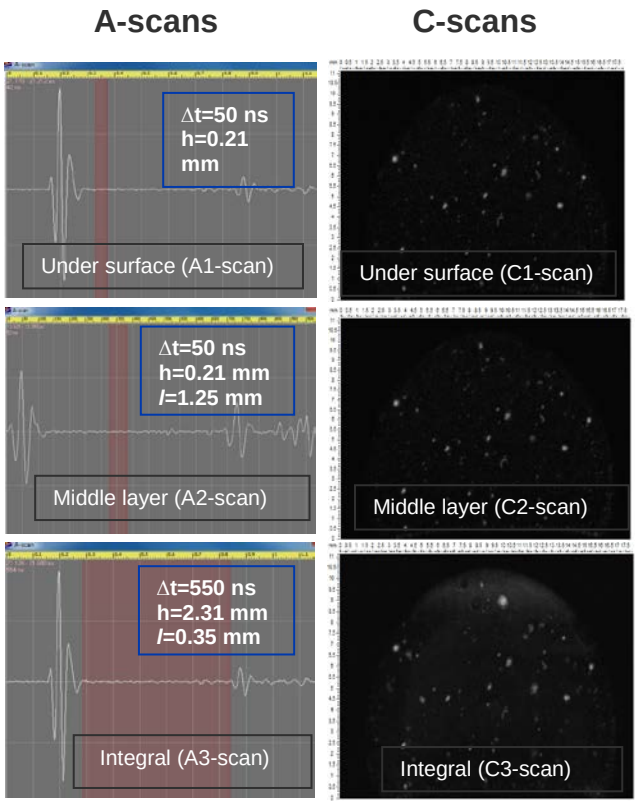



***Fig.3*** *Acoustic waveforms (A-scans) and images (C-scans) of the specimen S50-2.*

The C1-scan is obtained using parts of the A-scans array representing the reflected acoustic signals (echoes) from the subsurface layer of the specimen. The C2-scan represents the echoes from the medial layer of the specimen, and the C3-scan is formed using parts of the A-scans array representing the echoes from all of the specimen volume.

Using parts of the A-scans array lying in a predetermined time slot, we can construct an acoustic image (a C-scan) of a certain layer in the specimen volume. The thickness of this layer (h) and its location in the specimen (***l***) is given by time interval Δt and its position to be installed on an array of A-scans.

Figure 3 illustrated the acoustic waveforms (A-scans) and internal microstructure images (C-scans) of the specimen S50-2. The thickness of the imaging at the C-scan layer is defined by the time interval marked on the A-scan highlighted by a pink stripe.

The spots on the C-scans represent voids or pores in the specimen. Their size reaches 500 microns.

Figure 4 shows an A-scan and an integral acoustic image (C-scan) of the specimen S10-5.

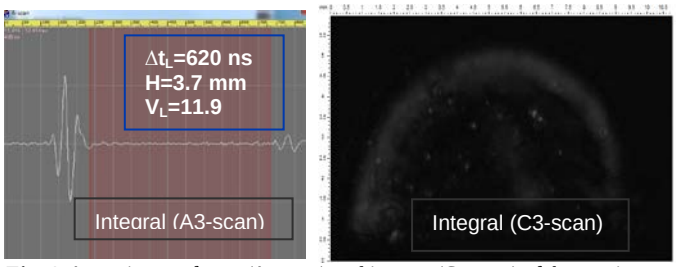



***Fig. 4*** *Acoustic waveforms (A-scans) and images (C-scans) of the specimen S10-5.*

The concentration of pores in this sample is considerably smaller than in the others, and accordingly, the density is higher.

The local velocity of longitudinal waves is equal to 11.9 km/s, which exceeds the integral values obtained by optoacoustic method. The corresponding value of the Young's modulus is greater than the integral values of the moduli (Young's modulus exceeding 300 GPa, integral value is 260 GPa).

Figure 5 shows the acoustic images of a c-BN/$C_{60}$ composite sample microstructure. The data illustrate the possibilities of the acoustic microscopic inspection. We see quite a large defect/pore, and we can determine its position in the sample volume with sufficient accuracy.

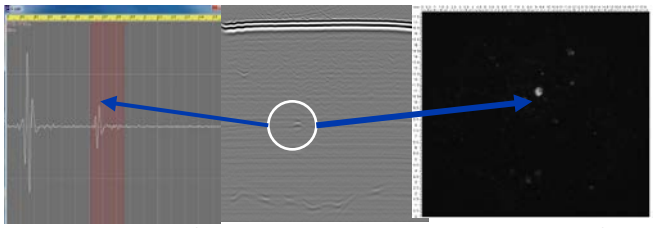


***Fig. 5*** *Acoustic waveforms (A-scans) and images (B- and C-scans) of a sample of c-BN/$C_{60}$. The kind of reflection from the bottom of the sample on the B-scan indicates its great heterogeneity.*

## *4. Conclusion*

The possibilities of acoustic microscopy for the study of elastic properties and microstructure in the bulk nanostructured carbon-composite ceramics are demonstrated.

Nanostructured boron carbide/$C_{60}$ ($B_4C/C_{60}$) and cubic boron nitride/$C_{60}$ (c-BN/$C_{60}$) carbon-ceramic composites were studied to obtain high values of the parameter σ*/ρ and reduce porosity by adjusting the parameters of the composite synthesis and sintering.

Elastic moduli were calculated based on the experimentally measured density and velocity values of longitudinal and transverse BAW in the specimens. The sound velocities were measured with a pulse-echo method by laser optoacoustic excitation of ultrasonic pulses.

Several nanostructured $B_4C/C_{60}$ composite specimens prepared with the addition of carbon bisulfide demonstrated sufficiently high values of the sound velocities and elastic moduli. The elastic moduli of the specimens were as follows: Young's modulus E = 140–150 GPa, bulk modulus K = 80–105 GPa, shear modulus G = 58–63 GPa. A certain $B_4C/C_{60}$ ceramic composite demonstrated exceptionally high values of the BAW velocities and elastic moduli (Young's modulus exceeding 300 GPa). The hardness of this material is up to 70 GPa, i.e. the material is highly rigid.

The elastic moduli of the c-BN/$C_{60}$ specimens are not high. Thus the resulting composite material is not durable. Its hardness is within 10–30 GPa, and the material is sufficiently highly rigid.

## *5. References*

[1] http://www.alueurope.eu/talat. TALAT, Lecture 1501.

[2] Prokhorov V., et al. Preparation and microstructure, elasticity and hardness investigation of Al-alloy/Nanodiamond composite. Machines, Tecnologies, Materials. 11/2011. pp.40-42. ISSN 1313-0226.

[3] Kopeliovich D. Carbon Fiber Reinforced Polymer Composites. http://www.e-plastic.ru

[4] Corum J.M., et al. Basic Properties of Reference Crossply Carbon-Fiber Composite. ORNL/TM-2000/29. February 2000. http://web.ornl.gov/~webworks/cpr/v823/rpt/106099.pdf.

[5] Stubna I. et al. Relationship between mechanical strength and Young's modulus in traditional ceramics. Materials and technology, **45,** 2011, 375–8.

[6] Prokhorov V. et al. Determination with integral ultrasonic method and local force microscopy method of elastic properties of $B_4C$ ceramics prepared by hot pressing.

Machines, Tecnologies, Materials. 12/2013. pp.21-23. ISSN 1313-0226.

[7] Gong J. Correlation between Weibull moduli for tensile and bending strength of brittle ceramics: a numerical simulation analysis based on a three-parameter Weibull distribution. J. Mater. Sci., **38,** 2003, 2541-5.

[8] Zhou Y., Yang L., Huang Y. Micro- and Macromechanical Properties of Materials. Science, Series: Advances in Materials Science and Engineering. Published by CRC Press; 2013.

[9] Hall E.O. The Deformation and Ageing of Mild Steel: III Discussion of Results. Proc. Phys. Soc. London, **64,** 1951, 747-753.

[10] Petch N.J. The Cleavage Strength of Polycrystals. J. Iron Steel Inst. London, **173,** 1953, 25-8.

[11] Blank V. et al. Second-Order and Third-Order Elastic Constants of $B_4C$ Ceramics. Physics of Solid State, **56**, 2014, 1574-1578

[12] Popov M. et al. Unique mechanical properties of fullerite derivatives synthesized with a catalytic polymerization reaction. MRS Communications, **5**, 2015, 71-75.

[13] Gusev V.E., Karabutov A.A. Laser optoacoustic. M.; Nauka. 1991. 304 p.

[14] Karabutov A.A. et al. Laser optoacoustic method for local elastic moduli measurement of particle reinforced metal matrix. Electronic Journal "Technical acoustics", **19,** 2008, ISSN 1819-2408.

[15] Briggs G.A.D., Kolosov O.V. Acoustic Microscopy. New York: Oxford University Press; 2010.

[16] Prokhorov V.M., Pivovarov G.I. Detection of internal cracks and ultrasound characterization of nanostructured $Bi_2Te_3$-based thermoelectrics via acoustic microscopy. Ultrasonics, **51,** 2011, 715-718.

[17] Prokhorov V.M., Ovsyannikov D., Levin V.M., Morokov E. Acoustic microscopy characterization of nanostructured carbon-ceramic composites. Testing and measurement: Techniques and applications. Proceedings of the 2015 International conference on testing and measurement: Techniques and applications (TMTA 2015). January 16-17, 2015, Phuket Island, Tailand. Ed. Kennis Chan, CRC Press/Balkema, Taylor&Francis Group, London, UK. 2015, p.65-68.

## *6. Acknowledgments*

This work was supported by the Ministry of Education and Science of the Russian Federation, grant 14.577.21.0090 (project ID RFMEFI57714X0090); the work was done using the Shared-Use Equipment Center “Research of Nanostructured, Carbon and Superhard Materials” FSBI TISNCM. The authors acknowledge Lomakin R., Perfilov S. for many assistance in samples preparation and useful discussions.

# MICROSTRUCTURE AND THERMAL STABILITY OF 0.08%C-17.0%Cr-0.8%Ti STEEL AFTER HIGH-TEMPERATURE NITRIDING AND HIGH PRESSURE TORSION

## МИКРОСТРУКТУРА И ТЕРМИЧЕСКАЯ СТАБИЛЬНОСТЬ СТАЛИ 08Х17Т ПОСЛЕ ВЫСОКОТЕМПЕРАТУРНОГО АЗОТИРОВАНИЯ И КРУЧЕНИЯ ПОД ВЫСОКИМ ДАВЛЕНИЕМ

Ph.D. Rogachev S.O.[1], Khatkevich V.M.[1], Dr. Sci. Kaibyshev R.O.[2], Ph.D. Tikhonova M.S.[2], Dr. Sci. Dobatkin S.V.[1,3]
[1]The National University of Science and Technology "MISIS", Leninsky pr. 4, 119049, Moscow, Russia
[2]Belgorod State National Research Univetsity, Pobedy St. 85, Belgorod, 308015, Russia
[3]A.A.Baikov Institute of Metallurgy and Materials Science of RAS, Leninskiy pr. 49, 119991 Moscow, Russia
csaap@mail.ru

**Abstract:** *The influence of high pressure torsion (HPT) on structure, phase composition, microhardness and thermal stability of 0.08%C-17.0%Cr-0.8%Ti steel subjected to volume high-temperature nitriding were investigated. HPT results in the formation of the nanostructure with structural elements size of 55-85 nm. Microhardness of nitrided steel after HPT increases by 2.2-2.7 times. Hardening is retained when heated to 450 °C.*
**KEY WORDS**: HIGH PRESSURE TORSION, HIGH-TEMPERATURE NITRIDING, FERRITIC STEEL, NANOSTRUCTURE

### *1. Introduction*

The possibility of significant refinement of grain structure and improve the complex properties by severe plastic deformation was shown for many materials, including to low-carbon low-alloy steel [1-5], and corrosion-resistant austenitic steels [6-9]. The nature and morphology of the second phase play an important role in the refinement of the structure of multi-phase alloys.

In present study, we analyze the influence of high pressure torsion (HPT) on structure, phase composition, microhardness and thermal stability of 0.08%C-17.0%Cr-0.8%Ti steel subjected to volume high-temperature nitriding. In [10] the high-temperature volume nitriding with subsequent annealing, provides a uniform hardening of thin-walled 0.08%C-17.0%Cr-0.8%Ti steel products, with the structure of the material consists of a nitrogen ferrite and second phase particles such as $Cr_2N$ with different morphology.

### *2. Experimental procedure*

Nitriding of flat samples 0.5 mm thick in the recrystallized state were carried out in pure nitrogen at 1075 °C. The samples were processed under two conditions: nitriding for 4 hours and annealing in vacuum at 700 °C for 1.5 hours (condition 1); nitriding for 1 hours and annealing in vacuum at 900 °C for 5 hours (condition 2). After this treatment, the nitrogen ferrite structure with second phase particles such as $Cr_2N$ (lamellar form in condition 1 and oval form in condition 2) were observed over the entire cross section of samples (Fig. 1).

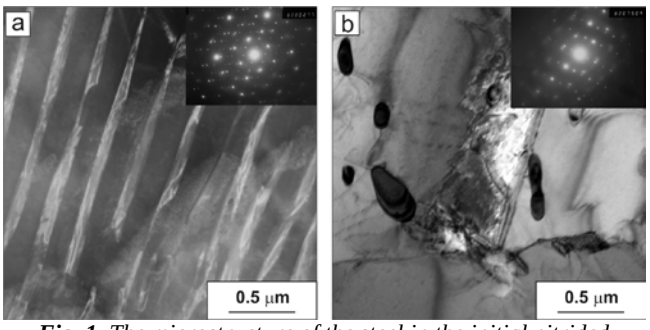


***Fig. 1.*** *The microstructure of the steel in the initial nitrided state (TEM): a - condition 1; b - condition 2*

The nitrogen mass fraction in samples after nitriding for 1 and 4 hours was 0.46 and 0.79 %, respectively.

High pressure torsion (HPT) after nitriding was performed on the discs with a diameter of 10 mm at room temperature with number of revolutions N=5 using the pressure of 4 GPa (the degree of deformation of 5.7).

### *3. Results and discussion*

HPT results in the formation of the nanostructure with structural elements size of 55-85 nm (Fig. 2).

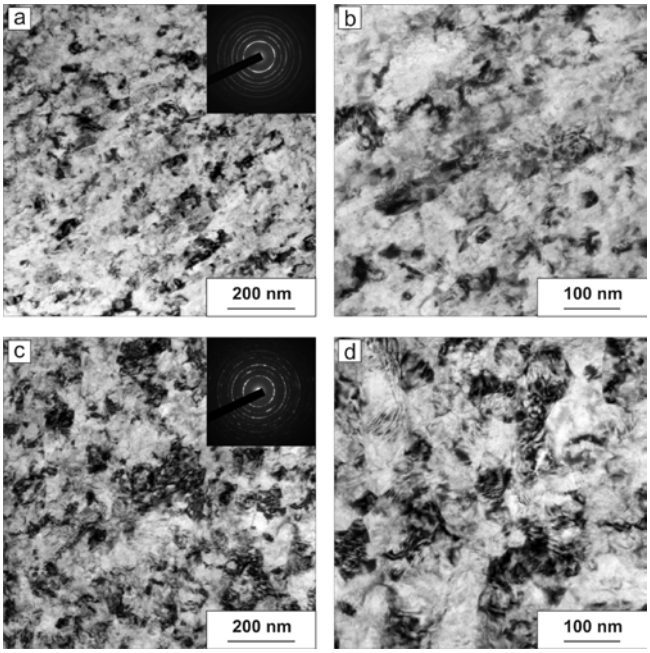


***Fig. 2.*** *The microstructure of the steel after HPT (TEM): a, b - condition 1; c, d - condition 2*

The results of TEM and electron microprobe analysis of replicas showed that oval $Cr_2N$ particles with size of 50-300 nm were observed in the steel structure after HPT. Microhardness of nitrided steel after HPT (measured at the middle radius of the sample) increases with 320±8 HV to 860±20 HV and with

350±38 HV to 780±20 HV, for conditions 1 and 2, respectively (Fig. 3). Hardening is retained when heated to 450 °C.

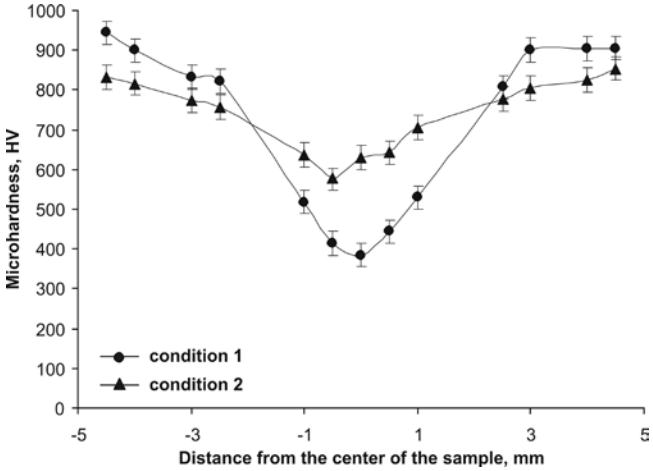



***Fig. 3.*** *The distribution of the microhardness of the diameter of the sample after the HPT*

X-ray phase analysis of steels prior HPT showed the presence of solid solution of chromium in the α-iron and $Cr_2N$ nitrides with a volume fraction of 6.1 and 2.2 % for the conditions 1 and 2, respectively. After HPT the volume fraction of the $Cr_2N$ nitrides in the steel of conditions 1 and 2 was 3.3 and 3.7 %, respectively. The heating of the steel after the HPT to 450 °C leads to the formation of predominantly equiaxed grain structure (Fig. 4).

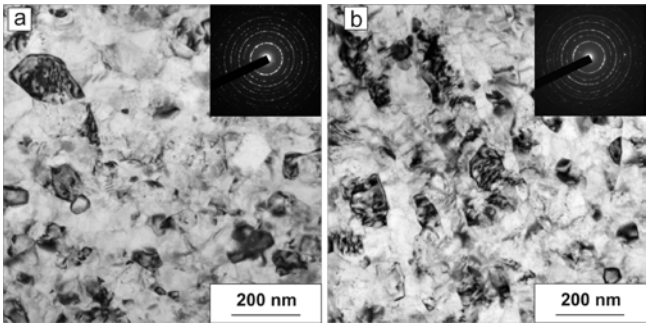



***Fig. 4.*** *The microstructure of the steel after HPT and annealing at 450 °C (TEM): a - condition 1; b - condition 2*

The volume fraction of $Cr_2N$ particles is increased up to 8-10 %.

## *4. Conclusion*

High pressure torsion (HPT) of 0.08%C-17.0%Cr-0.8%Ti steel subjected to volume high-temperature nitriding results in the formation of the nanostructure with structural elements size of 55-85 nm. HPT leads both fragmentation and dissolution of nitrides and their precipitate in the steel structure (depending on the volume fraction and morphology of the nitrides present in the steel structure before HPT). Microhardness of nitrided steel after HPT increases by 2.2-2.7 times (to 9 GPa). Hardening is retained when heated to 450 °C.

*This work was funding from Russian Federal Ministry for Education and Science (grant 14.A12.31.0001).*

## *4. Literature*

1. D.M. Marulanda, J. Wongsa-Ngam, T.G. Langdon. Microstructural evolution and microhardness in a low carbon steel processed by high-pressure torsion // Journal of Materials Research and Technology.–2014.–V. 3.–N 4.–P. 344-348.
2. G.G. Zakharova, E.G. Astafurova, E.V. Naydenkin, G.I. Raab, S.V. Dobatkin. The evolution of structure and mechanical properties of Fe-Mn-V-Ti-0,1C low-carbon steel subjected to severe plastic deformation and subsequent annealing // Materials Science Forum.–2012.–V. 715-716.–P. 994-999.
3. Zrník J., Dobatkin S.V., Raab, G.I., Kraus, L. Effect of initial treatment on the structure and mechanical properties of medium carbon steel subjected to ECAP // Kovove Materialy.–2013.–V. 51.–N. 6.–P. 343-350
4. G.G. Mayer, E.G. Astafurova, H.J. Maier, E.V. Naydenkin, G.I. Raab, P.D. Odessky, S.V. Dobatkin. Grain refinement and mechanical properties of low-carbon steel by means of equal channel angular pressing and annealing // International Journal of Materials Research (formerly Z. Metallkd.).–2013.–V. 104.–N 5.–P. 457-461.
5. G.G. Maier, E.G. Astafurova, H.J.Maier, E.V. Naydenkin , G.I. Raab, P.D. Odessky, S.V. Dobatkin. Annealing behavior of ultrafine grained structure in low-carbon steel produced by equal channel angula rpressing // Materials Science and Engineering A.–2013.–V. 581.–P. 104–107.
6. A. Etienne, B. Radiguet, C. Genevois, J.-M. Le Breton, R. Valiev, P. Pareige. Thermal stability of ultrafine-grained austenitic stainless steels // Materials Science and Engineering: A.–2010.–V. 527.–N 21–22.–P. 5805-5810.
7. S. Dobatkin, W. Skrotzki, V. Terent'ev, O. Rybalchenko, A. Belyakov, D. Prosvirnin, E. Zolotarev. Structure and Fatigue Properties of Cr-Ni-Ti Austenitic Steel after Equal Channel Angular Pressing and Heating // Materials Science Forum.–2014.–V. 783-786.–P. 2611-2616
8. Dobatkin S.V., Kaputkina L.M., Rybal'chenko O.V., Komlev V.S. Phase and structural transformations in corrosion-resistant steels upon high-pressure torsion and heating // Russian Metallurgy (Metally).–2012.–V. 2012.–N. 9.–P. 763-771
9. Dobatkin S.V., Terent'ev V.F., Skrotzki W., Rybalchenko O.V., Pankova M.N., Prosvirnin D.V., Zolotarev E.V. Structure and fatigue properties of 08Kh18N10T steel after equal-channel angular pressing and heating // Russian Metallurgy (Metally).–2012.–V. 2012.–N. 11.–P. 954-962.
10. S.A. Nikulin, S.O. Rogachev, V.M. Khatkevich, A.B. Rozhnov. Structure and Hardness of Corrosion Resistant Ferritic Steels Subjected to High Temperature Nitriding // The Physics of Metals and Metallography.–2014.–V. 115.–N. 2.–P. 186–191.

# THE COMPREHENSIVE TECHNIQUE FOR QUANTITATIVE ANALYSIS OF THE STRUCTURE IN COMPOSITE SUPERCONDUCTORS BASED ON $Nb_3Sn$

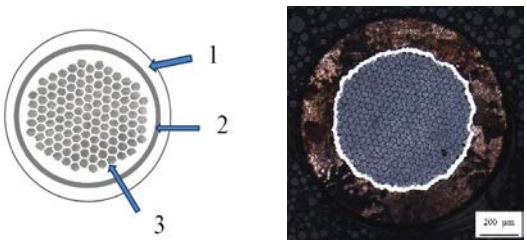
# КОМПЛЕКСНАЯ МЕТОДИКА КОЛИЧЕСТВЕННОГО АНАЛИЗА СТРУКТУРЫ КОМПОЗИЦИОННЫХ СВЕРХПРОВОДНИКОВ НА ОСНОВЕ $Nb_3Sn$

S.A. Nikulin[1], prof., Dr. Sc., A.B. Rozhnov[1], Ph.D., S.O. Rogachev[1], Ph.D.,
V.I. Zabolotnikova[1], postgraduate student
E.A. Dergunova[2], Ph.D, R.T. Aliev[2]
[1]NUST "MISIS"
[2]A.A. Bochvar VNIINM
viki.zabo@gmail.com

**Abstract:** *The complex technique for study of the structure in $Nb_3Sn$-based composite superconductors is developed. Technique is based on scanning and transmission electron microscopy on different scale levels. The possibility of using the method of focused ion beam for TEM sample preparation is confirmed.*
KEYWORDS: $NB_3SN$, FILAMENT, STRAND, SUPERCONDUCTOR, MICROSTRUCTURE, ITER

## *1. Introduction*

The $Nb_3Sn$-based superconductors obtained by "bronze process" are complex composite materials, having tens of thousands superconducting filaments in the cross-section of a wire with a diameter of 1 mm [1-7]. Filaments are usually collected in bunches (strands) and distributed evenly in a bronze matrix, surrounded by a niobium diffusion barrier with tantalum inserts and a stabilizing copper shell (Fig. 1.). Each filament of $Nb_3Sn$ superconducting compound (with a diameter of ~2-3 μm) has an ultra-fine grain structure with a grain size from ~50 to 500 nm. Material having such a complex structure demands a comprehensive approach for quantitative analysis of structure characteristics, including studies on different scale levels: macro, micro and nano.




1 - copper wire sheath
2 - a diffusion barrier
3 - a bronze matrix with strands (bundles) of niobium fibers

Fig. 1. Macrostructure of superconductors

## *2. Methods and Results*

Images of macrostructure by optical microscopy (magnification x100 - x1000) were obtained for a quantitative analysis of superconductors at the macro level. The following parameters have been measured on the obtained images: diameter of the wire, thickness of copper shell, thickness of diffusion barrier, diameter of strand.

The quantitative analysis of the structure on the micro level was performed using SEM in the electron backscatter mode (magnification x1000 – x5000) (Fig. 2.). For images obtained the following parameters have been measured: diameter of filaments, distance between filaments, a volume fraction of Nb in filaments. Such measurements have been performed including at layer-by-layer polishing with a step of 50 μm.

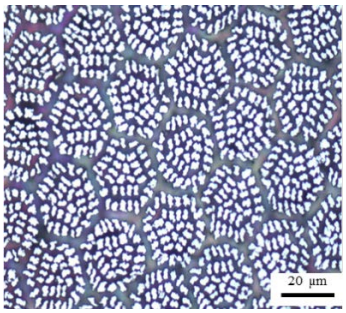



Fig.2. Microstructure of superconductors (SEM)

The analysis of structure on the nano level included study of ultra-fine grain structure of superconducting filaments. The analysis of grain structure on the filament fracture surfaces of annealed superconductors was performed using high-resolution field emission scanning electron microscopy in secondary electron mode at magnification x25000. The obtained images of the fracture surfaces were quantitatively analyzed using a specialized software ImageExpertPro. The quantitative analysis included measurement of the diameter of equiaxed and columnar grains, measurement thickness of different morphology layers, measurement of volume fraction of residual niobium (Fig. 3.).

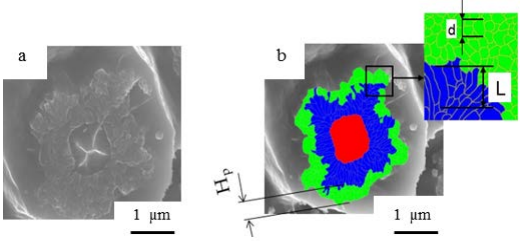



Fig. 3. Image of fracture: a - original of fracture surface; b - image after processing in AdobePhotoshopCS3 (TEM)

The possibility of using the focused ion beam method for wire samples preparation to study the structure of superconductors by transmission electron microscopy (TEM) also has been shown. Foils have been prepared on a scanning ion microscope with gallium liquid metal ion beam. Sample was cut to obtain a thin plate (lamella) (5-15) μm in size and (1-2) μm in thickness. After receiving the lamella it was further thinned and explored by the TEM method (Fig. 4.).

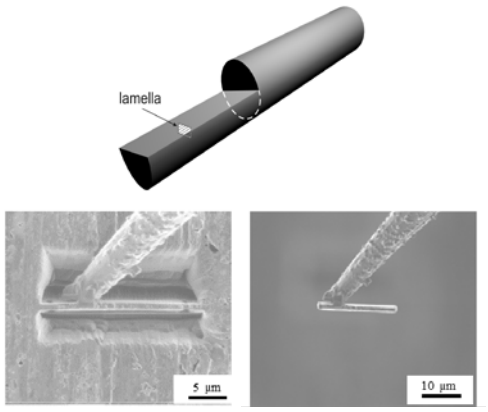



Fig. 4. The main stages of sample preparation for TEM studies

## *4. Conclusion*

The comprehensive technique for quantitative analysis of the structure of composite superconductors based on $Nb_3Sn$ is developed. The developed technique included study of structure by optical microscopy, scanning electron microscopy, transmission electron microscopy on different scale levels.

Comparative study of the structure of $Nb_3Sn$-based composite superconductors manufactured using different modes of deformation and heat treatment have been performed in the current work. Those superconductors were fabricated at JSC "Chepetsky Mechanical Plant" and verified at A.A. Bochvar VNIINM.

## *4. References:*

1. ITER Magnet Design Descripption Document Part 1. ITER IDM reference 2NPLKKM. Version 1.8, Sept 2009.

2. Zauter R., Muller H., Kudashov D.V. Spray-Formed High-Tin Bronze - A Homogeneous Pre-Material for $Nb_3Sn$-Based Superconductor Wire // App. Superconductivity.– 2007.–V. 17.– № 2.– P. 2572 – 2575.

3. Fischer C.M. Investigation of the Relationships Between Superconducting Properties and $Nb_3Sn$ Reaction Conditions in Powder-in-Tube Nb3Sn Conductors: M.S. thesis.– Univ. of Wisconsin, Madison WI.– USA, 2002.– 110 p.

4. Microstructure, composition and critical current density of superconducting $Nb_3Sn$ wire / R. Flükiger, D. Uglietti, C. Senatore e.a. // Cryogenics.– 2008.– V. 48.– № 7-8.– P. 281-396.

5. Diffusion and growth mechanism of $Nb_3Sn$ superconductor grown by bronze technique / T. Laurila, V. Vuorinen, A. Kumar e.a. // Appl. Phys. lett.- 2010.– V. 96.– № 23.

6. Okamoto H. Nb-Sn (Niobium-Tin) // Journal of Phase Equilibria.– 2003.– V. 24.– №4.– P. 380.

7. Mitchell N., Devred A., Libeyre P., e.a. // Appl. Supercond.– 2012.– V. 22.– №3.

# INCREASE WEAR RESISTANCE HARD ALLOYS T15K6 BORIDE COATINGS

Prof. Dr. Chernega S.[(1)], Poliakov I.[(1)], Grinenko K.[(1)], Krasovskiy M.[(2)]
[1]National Technical University of Ukraine "Kiev Polytechnic Institute", 03056, Ukraine, Kiev, Polytechnique st., Bldg. 9, e-mail: smchernega@mail.ru; polykov_igor@mail.ru
[2]The Frantsevich Institute for Problems of Materials Science of NAS of Ukraine, 03680, Ukraine, Kiev, Krzhizhanovskogo st., 3

***Abstract:*** *The results of studies on the application of complex boron coating powder method on hard alloys. Defined phase and chemical composition, thickness and microhardness of the coating on alloys.*

*It was established that after diffusion saturation of hard alloy in boron mixture for 4 hours formed coating with boride phases TiB, WB, CoB and WC, TiC, whose thickness is 50-60 microns. At complex saturation with boron and copper for 4 hours diffusion saturation formed coating with boride phases TiB, WB, CoB and WC, TiC and separate inclusions of copper with a thickness of the diffusion layer up to 70-80 microns.*

*Boriding and complex saturation with boron and copper allows in 2 – 2.5 times increase the microhardness of the surface layers of hard alloys, that in turn leads to increased wear resistance.*

***KEYWORDS:*** *BORON CARBIDE, BORIDING, BORON LAYER, COPPER, STRUCTURE, DIFFUSION, FRICTION, MICROSTRUCTURE, MICROHARDNESS, WEAR RESISTANCE, CRACK RESISTANCE.*

## 1. Introduction

Hard alloys provide high capacity under different operating conditions. Hard alloys WC-TiC-Co – titanium tungsten is used for the treatment of viscous materials: steel, brass [1 – 2], but their application field is narrowed due to low strength. One of the ways to improve the operational characteristics alloys are applying coatings, such as the use of chemical – heat treatment (CHT) [3 – 5]. However, doesn't definitive data on the positive effects of this method CHT to improve wear resistance hard alloys products [6 – 7]. To create technology of boriding hard alloys that gives stable results, it is necessary to investigate the mechanism of boride layer, processes of diffusion and redistribution of elements in boride layer and the transition zone hard alloy.

The aim of this work was to investigate the structure and characteristics of complex diffuse boride coatings on hard alloys obtained in boriding powder mixtures with the addition of various copper containing elements: $Cu_2O$, $Cu_3P$ and installation of saturating powder environment impact on parameters wear resistance, thickness and microhardness coating obtained after a complex saturation with boron and copper.

## 2. Materials and Experiment

Integrated borating powder method performed in a special container under reduced pressure at a temperature of 975 °C for 4 hours using fusible valves. The investigate was conducted on samples from hard alloys T15K6.

Saturation alloys boron and copper performed in mixtures containing technical boron carbide $B_4C$ and powders $Cu_2O$, $Cu_3P$. As the activator used ftoroplast.

Heating the crucible and the subsequent isothermal exposure was carried out in a laboratory furnace type SNOL – 1,6,2,5.1/11M.

After the isothermal exposure container with details removed from the furnace and cooled to room temperature in air, disclose and took out details with clean surfaces that do not require further purification.

This method has the following advantages: simplicity of the process, allows the processing of products of different configurations can be obtained diffusion layers of different thickness.

Polishing was performed on samples of diamond polishing circles paste grit from 28 to 1 micron, that provided to obtain high surface quality research. As a reagent for chemical etching using 3...5% - solution was nitric acid in ethanol; exposure – 90 sec.

Visual study, measuring the thickness of diffusion layers and microstructure coatings investigate performed on metallographic microscope OLYMPUS GX-41, producer Japan, in the range the increase 100...1000.

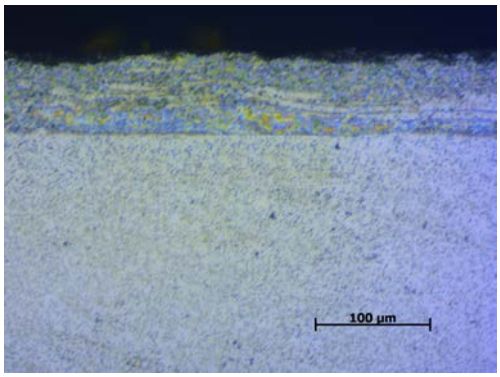
Microhardness measurements were performed on microhardness DuraScan, the company EMCOTEST, Austria, with a load of 50 grams.

Phase composition of coatings analyzed on X-rays diffractometer Ultima-IV, of Rigaku, Japan, in copper $K\alpha_1$, $K\alpha_2$ monochromatic radiation and chemical composition was determined by scanning electron microscope SEM – 106I.

## 3. Results and discussion

In this paper was investigate the structure, phase composition and properties of boride coatings obtained on hard alloys T15K6.

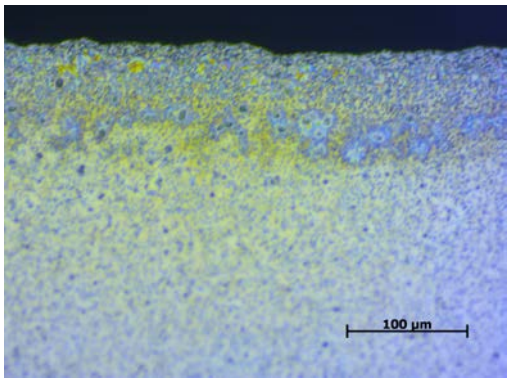
It was established that after the diffusion saturation hard alloys in boriding mixture for 4 hours formed coating from boride phases TiB, WB, CoB and phases TiC, WC, coating thickness of 50-60 microns. After a complex saturation with boron and copper 4 hours diffusion saturation formed coating from boride phases TiB, WB, CoB and phases TiC, WC, and separate inclusions of copper with diffusion layer thickness to70- 80 microns (Fig.1).




*a*

***Table.*** *Chemical composition diffusion layer obtained after complex saturation with boron and copper*

| Elements | Position | | | | | |
|---|---|---|---|---|---|---|
| | ***Fig*.2 (*a*)** | | ***Fig*.2 (*b*)** | | | |
| | **+ 1** | **+ 2** | **+ 1** | **+ 2** | **+ 3** | **+ 4** |
| | **wt. %** | | **wt. %** | | | |
| Ti (K) | 0.80 | 0.55 | 25.39 | 30.40 | 0.69 | 2.17 |
| Co (K) | 10.89 | 0.37 | 1.49 | 4.02 | 0.23 | 96.25 |
| W (K) | 85,10 | 99.08 | 73.10 | 65.57 | 99.08 | 1.58 |
| Cu (K) | 3.21 | 0. 00 | 0.01 | 0.00 | 0.00 | 0.00 |

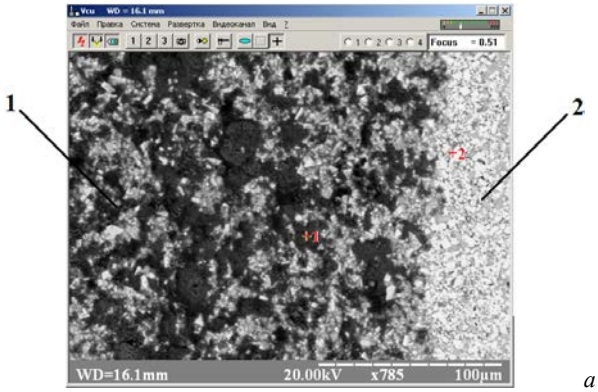



*b*

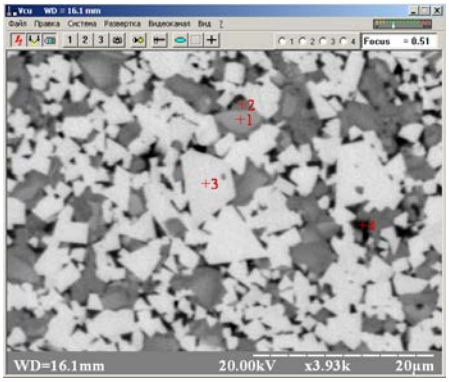
***Fig.1:*** *Microstructures boride coatings on hard alloys T15K6: a – coatinga after boriding, 4 hours, x200; b – after complex saturation with boron and copper, 4 hours, x200*

To determine the chemical composition of the coating was applied microanalysis by using scanning electron microscope – SEM-106I with increasing in 2000 time, accuracy 0.01 wt. %. Determination of the chemical composition performed by EDS, calculation of quantitative chemical composition – the method ZAF.

Microrengenospectral analysis has established presence copper on the surface of boride coating (Fig.2, Table). Formation separate inclusions copper leads to increased wear resistance, such as copper in the coating under dry frictional wear acts as solid lubricant.




*a*

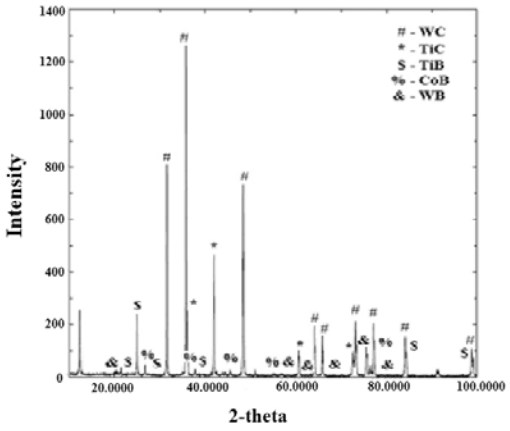



*b*

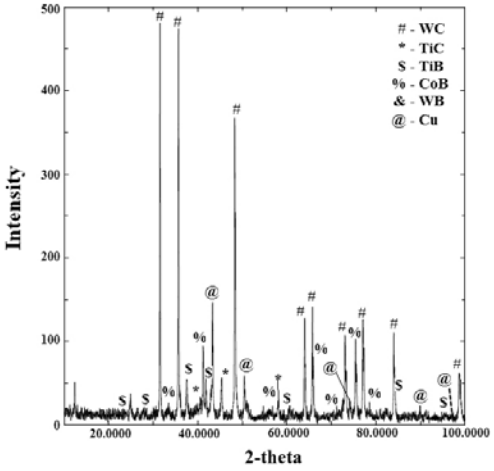
***Fig.2:*** *Surface topography (a - (1 – surface (surface area 1 is at an angle of 18° from the subsurface zone, 2) 2 – subsurface zone); chemical analysis determined the points +1, +2) and the structure of the surface area (b – chemical analysis determined the points +1, +2, +3, +4)* hard alloys *T15K6 with boride coating obtained at introduction of the saturating powder environment* $Cu_2O$

To establish a relationship between the phase and structure, diffusion layers obtained after complex saturation with boron and copper, conducted X-ray analysis (Fig.3).

Diffraction patterns taken from the sample surface after boriding (Fig.3, *a*) shows the presence of diffraction peaks from phases TiB, WB, CoB, WC, TiC, and the samples after a complex saturation with boron and copper in the environment with the addition copper containing powder $Cu_2O$ or $Cu_3P$, fixed phase TiB, WB, CoB, WC, TiC and Cu (Fig.3 *b*).




*a*




*b*

***Fig.3:*** *Diffractograms taken from the surface of hard alloys T15K6 with boride coatings in Cu* $K\alpha_1$, $K\alpha_2$ *monochromatic radiation: a – coating after boriding; b – coating after complex saturation with boron and copper in the environment with the addition copper containing powder* $Cu_2O$*, diffraction peaks of Cu line (111), (200), (220), (311), (222)*

Established that boriding and complex saturation with boron and copper allows in 1.5 – 2.5 times increase microhardness of the surface layers of hard alloys, which in turn leads to increased wear resistance. After boriding on the surface hard alloys obtain coating microhardness which is 31 - 33 Gpa, base – 13 – 13.5 GPa. At the complex saturation with boron and copper obtain coating microhardness which is 24 – 25 GPa (Fig.4).

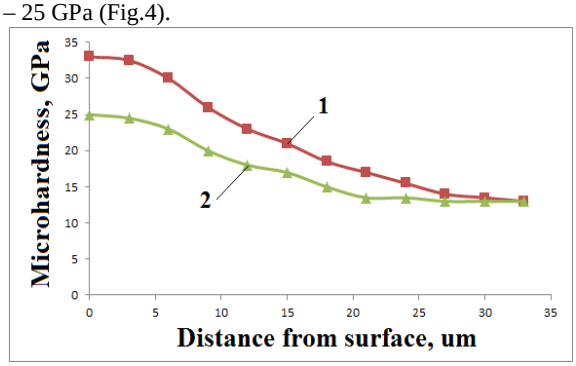
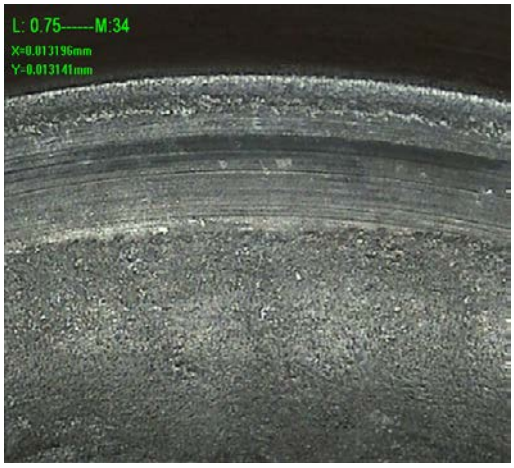



***Fig.4:*** *Microhardness boride* coating*: 1 – coating after boriding; 2 – coating after complex saturation with boron and copper*

Testing wear resistance were carried out on rollers produced of hard alloys, which are used to rolling aluminum profiles (Fig.5 and Fig.6).

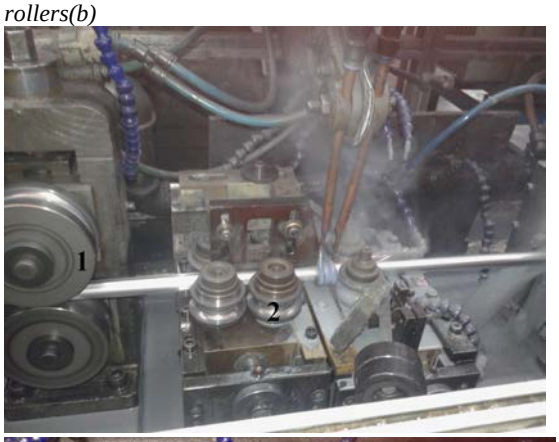


*a*

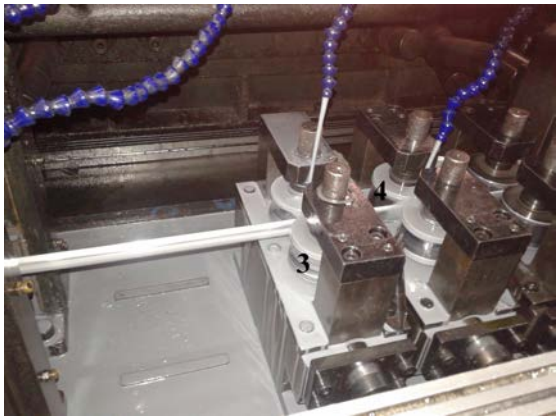



*b*

***Fig.5:*** *Rollers (a) and topography surface wear coating on the rollers(b)*




*a*




*b*

***Fig.6:*** *Section rolling machine for aluminum profiles: 1, 2, 3, 4 – rollers in the work*

Investigations have shown that the boride coating allow in 2 times increase the term of operation rollers. When the rollers working without coating can be made of 10 tons aluminum profiles, whereas at the application of the boride coatings is reached value of 21 tones.

## 4. Conclusions

Investigate the structure and characteristics boride and complex saturation with boron and copper coatings on hard alloys T15K6 obtained in environments powder with the participation boron carbide and copper containing powder $Cu_2O$ or $Cu_3P$. X-ray phase analysis established that at diffusion saturation in the surface layers of hard alloys formed phases: TiB, WB, CoB, WC, TiC and respectively Cu. At the addition in environment for boriding copper containing powder identification of clear lines Cu (111) (200) (220).

X-ray analysis confirmed the local distribution of copper in the surface zone boride coatings obtained after complex saturation with boron and copper.

Boriding and complex saturation with boron and copper allows forming of boride phase in the surface zone hard alloys and increase the microhardness to 33 GPa and 25 GPa (respectively) compared with basic material (13.5 GPa) and thus increase the wear resistance of hard alloys in 2 times.

## 5. References


[1] Bogoduhov S.I. Improving the performance of hard alloys by heat treatment / S.I. Bogoduhov, A.S. Kills, E.A. Shein, A.S. Yasakov,
R.R. Khaibullin // Bulletin of the Orenburg State University. – №5 (124). – 2011. – P. 164 – 170.

[2] The use of plasma ceramic coatings in friction pairs of end seals / O.A. Zelenkevich, N.G. Taran, G.E. Lazarev, B.M. Kudryavtseva // Chemical and petroleum engineering. – 1990. – № 4. – P. 28 – 30.

[3] Klinskaya-Rudenskaya N.A. Comparative analysis of the composite coatings based alloys Ni-Cr-B-Si with refractory borides, obtained by different methods / N.A. Klin-Rudenskaya, V.A.Kopysov // Physics and Chemistry of Materials Processing. – 1995. – № 3. – P. 63 – 68.

[4] Moiseenko O.I. Tool materials / O.I. Moiseenko, H.O. Chkalov.–K.: Higher school, 1982. – 196 p.

[5] Berzina I.G. Distribution of boron, tungsten, titanium and cobalt alloys in solid borated / I.G. Berzina, E.B. Gusev, B.V. Zakharov, G.N. Fedin, V.M. Fedin // Physics of Metals and Metallography.–1984 – T.57, # 4. – P. 713 – 718.

[6] *Zakhariev Z.* Preparation and some properties of boride diffusion layers hard WC – TiC – Co alloys / Z. *Zakhariev, K. Petrov, M. Christov* // J. Less-Common Metals. – 1981. – 82. – P. 57 – 62.

[7] Berzina I.G. On the distribution of boron diffusion zone borated hard alloys used for the manufacture and machining of rolling stock / I.G. Berzina, E.B. Gusev, B.V. Zakharov and others // Proceedings of the Institute of Railway Engineers, Engineering. – 1982. – Vol. 701 – P. 24 – 27.

# MICROSTRUCTURE AND MECHANICAL BEHAVIOR OF TIG BIMETALLIC JOINTS

M.F. Benlamnouar, R. Badji, M. Hadji, A. Boutaghane, N. Bensaid
*Welding and NDT Research Center (CSC), PB 64, Chéraga, Algiers, Algeria*
***E***-mail: csc.farid@yahoo.fr

***Abstract:*** *Bimetallic weld techniques have progressed a great deal in the last decade. In this work, the effect of the filler metal composition on microstructure and mechanical behavior of dissimilar HSLA-X70/304L stainless steels weld joint is investigated. The dissimilar weld joints are fabricated using austenitic, duplex and low Carbone filler metal. The mechanical behavior is investigated through microhardness, charpy impact and tensile test.*

*The results show that, the weld metal composition has a great influence on mechanical properties and microstructure of weldments, in particular the grain size and phases nature, changes with filler metal composition. In addition presence of martensitic slats in the FZ when using the low Carbone filler metal, detailed microstructure examination is carried out and related to the mechanical behavior of the dissimilar joints.*

**KEYWORDS**: TIG WELDING, BIMETALLIC WELD, HSLA, DSS, HAZ, MICROSTRUCTURE, MICROHARDNESS.

**Nomenclature**: *HAZ: heat affected zone, I: average intensity (A), FZ: fusion zone, MV: medium voltage (V), TIG: tungsten inert gas,*

*D: Argon flowrate (l/min),* Φ : electrode diameter(mm), *K: Charpy impact energy (J), V: weld speed (mm/min)*

*HV0.2: Microhardness (load of 0.2 kg),* $\sigma_m$ *(MPa): maximum stress,* $\varepsilon_m$ *(%): maximum strain, S: Sample (S3: third sample)*

| Elément(%) | C | Si | Mn | P | S | Al | Cu |
|---|---|---|---|---|---|---|---|
| **X70** | 0.08 | 0.7 | 2.39 | 0.01 | 0.001 | 0.06 | 0.01 |
| **304L** | 0.07 | 0.75 | 1.85 | 0.045 | 0.03 | - | - |
| **Elément(%)** | **Cr** | **Mo** | **V** | **Nb** | **Ti** | **N** | **Ni** |
| **X70** | 0.04 | 0.1 | 0.05 | 0.4 | 0.09 | - | 0.02 |
| **304L** | 18.5 | - | - | 0.08 | - | 0.08 | - |

***Table 1:*** *Chemical composition of base materials*

## *1. Introduction*

High strength low alloys (HSLA) and Austenitic stainless steels have been used widely by the fabrication industry owing to their high resistance to corrosion combined to excellent mechanical properties. Some of the typical applications of these steel include their use as pipelines, oil refining, pressure vessels, chemical and process industries ….etc.

Homogeneous weld applications require the use of filler metal which contains the same chemical composition with base metal in order to get more mechanical resistance of welded material, this resistance depending on a number of factors like mechanical properties, wear and friction characteristic... ... etc. In this regards There are numerous investigations on the characterization austenitic or HSLA steel using arc welding regardless of any assembly between them [1, 2]; however, there are little data on the evaluation of mechanical properties to weld together HSLA/Stainless steel.

At present, some Studies have been conducted on welding of stainless steel with HSLA steel, almost all common fusion welding techniques can be used to weld duplex stainless steel through selecting appropriate welding parameters, corrosion resistance... or residual stresses condition, in this study we interest to filler metal selection.

Filler metal composition has a great influence on the solder properties. Mechanical properties and toughness of weldment depend of microstructure of weld metal and heat affected zone.

The welding process used was Tungsten arc welding (TIG). These were chosen because each process is one of the most commonly used welding techniques in industry.

## *2. Experimental Procedure*

Bases material used in present work is austenitic (304L) and ferrite-perlitic (X70) steels. Their chemical composition and mechanical properties are given in Table 1. The steel is welded by semi-automatic tungsten arc welding (TIG), According to moved table in order to set welding speed.

Based on partial plates of base materials, TIG welding was carried with three filler metal, namely, austenitic stainless steel 308, (Sample 1:S1), duplex stainless steel 2209 (S2), low Carbon E7018 (S3), and the fourth sample (S3) is intended to cover welding process without filler metal.

Filler metal selection is based on the homogeneity of chemical composition with each base metal: for X70 we take and for E7018 we take 304L.

In order to maintain similar welding parameters conditions, the weld cou- pon dimensions were fixed at 100 mm X 60m X 2mm (Fig. 1) and the electrodes diameter fixed at 1.5 mm.




***Fig.1.*** *Plates of Sample number two (S2)*

Our welding has one pass based on TIG welding with to avoid cracking, supercooling and excessive penetration. Before welding, Pairs of plate were welded together (edge to edge) width-wise at each filler metal (Fig. 2).

Chemical composition of filler metal is given in Table 2. The welding is carried out with fixed parameters (Table 3).

***Table 2:*** *Chemical composition of filler materials*

| Elément (%) | C | Si | Mn | Cr | Ni | Mo |
|---|---|---|---|---|---|---|
| **E308L** | 0.19 | 0.46 | 1.72 | 20.80 | 10.10 | |
| **E2209** | 0.03 | 0.46 | 0.9 | 22.5 | 9.3 | 2.8 |
| **E7018** | 0.12 | 0.80 | 0.90 | - | - | 0.5 |

***Table 3:*** *Welding parameters*

| I (A) | MV (V) | V (mm/min) | Φ (mm) | Temps (s) | D (L /min) |
|---|---|---|---|---|---|
| **72** | 11.68 | 2.515 | 1.5 | 53 | 8 |

The tensile specimens were tested on a servo hydraulically controlled digital tensile testing machine. Three specimens per each filler metal were machined out from the weld plate. Each tensile specimen size was prepared in accordance with ASTM E08 standards [5] as illustrated schematically in Figure 2.

The Charpy test was performed according to standard test methods for notch bar impact testing of metallic materials [6]. The total length of the specimen is 55mm and the rectangular cross-section area is 5mm×2mm. Specimen has a V-shaped notch with a flank angle of 45° and depth of 2mm (Fig. 3) in the HAZ and FZ.

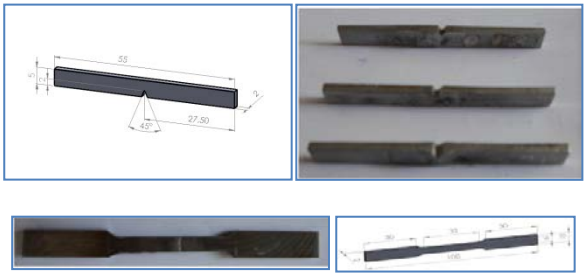
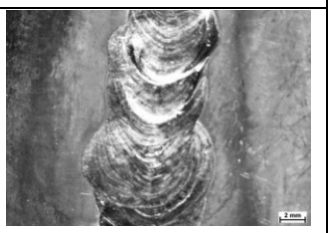


***Fig.2*** *Specifications of Charpy and tensile specimens [6-8].*

## *3. Metallography*

For the observation of microstructural changes that take place during welding, corresponding to each filler metal; specimens were taken from the welded plates. The microstructures of the joints were captured with the help of optical microscopy. Standard polishing procedures were used for microstructural observations, Glycerine reactif was used with the conditions (20ml of nitric acid, 30 ml HCl acid and 30ml of glycerol) for 3min.

***Table 4:*** *Morphology of solders*

| S1 | S2 |
|---|---|
|  |  |
| S3 | S4 |
|  |  |

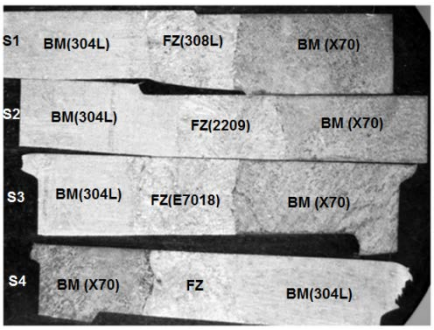



***Fig.3*** *Attacked samples*

These micrographs show that the weldments are free from welding defects like lack of penetration, undercut, cracks…etc.

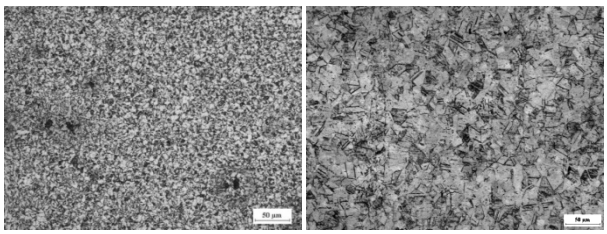
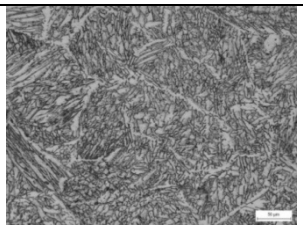
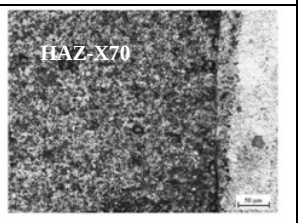
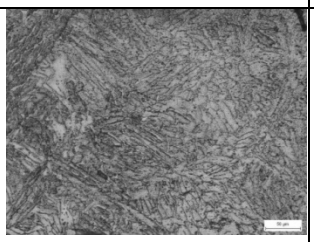
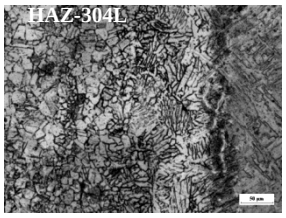
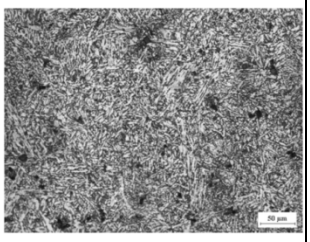
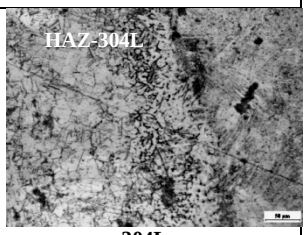
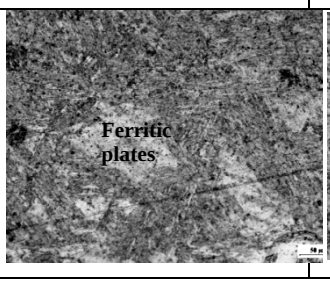
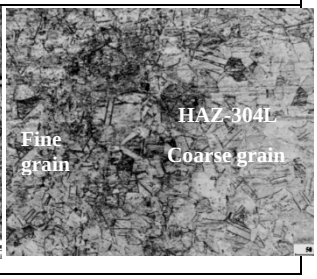


***Fig.4*** *Optical microstructure of the two materials (in the left HSLA-X70, 304L SS in the right)*

Micrograph of X70 base metal describes polygonal ferrite–pearlite containing about 70% ferrite, while the microstructure of 304L consists of polycrystal of single-phase which consists of equiaxed austenitic grains with an average diameter of 17µm.

***Table.5:*** *Micrographs of weldments*

| | FZ | HAZ |
|---|---|---|
| S1 |  |  |
| S2 |  |  |
| S3 |  |  **304L** |
| S4 |  |  |

Polished samples were scanned on the optical microscope along the weldments zones of the fusion zone and the HAZ, and at a few places microphotographs were taken in the middle of fusion line (Fig.3). As a result, this study has many microstructures of dissimilar joints in accordance with various mechanical properties.

The microstructure of the (HAZ-X70) undergoes a decrease in grain size when it becomes close to the base metal, the latter is characterized by a ferritic-pearlitic structure with large ferrite content. it's also distinguished by the presence of acicular ferrite and the formation of martensitic slats, this presence is even greater in S4 with carbides formation in fusion line.

Microstructure of duplex fusion zone revealed that the principal constituents are austenite and columnar ferrite with fine intermetallic precipitation in ferritic phases. Moreover,

Microstructure evaluation of austenitic fusion zone reveals essentially a dendritic ferrite in austenitic matrix. With regard to the fourth sample, With regard to the fourth sample, fusion zone presents a continuous casting structure.

## *5. Mechanical behavior*

### *Microhardness*

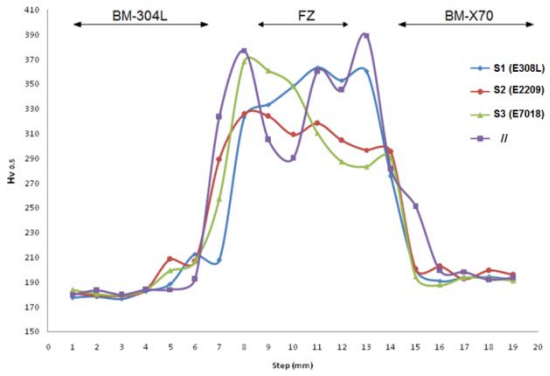



***Fig.5*** *Microhardness profiles*

The microhardness measurements are schematized relative to solder center of the four samples. For the S1 and S3, there was an increase in the microhardness of both the fusion lines and heat affected zones (HAZ). These higher microhardness values in fusion line are related to the higher Carbon content of 304L and X70 base materials (Table 2), which produced a large amount of Carbide precipitation.

In S4 fusion zone, Microhardness values is severly disrupted, this can be explained by the presence of ferrite plates and martensite lattices in this area.

As regards the austenitic HAZ of samples, Austenite grain growth increased from small ratio in S2, and S3 to big ratio in S4, this phenomenon can be explained by cooling rate and solubility modes of filler metals in 304L SS (Table 5).

The fuzion zone of S2 is characterized by balanced level of microhardness. Otherwise, In the other samples, microhardness is characterized by high level values.

A brittle microstructure was formed in FZ-S4, which contains primarily large ferritic plates (about 27µm) surrounded by lamellar martensite. This can be explained by the strong instability in microhardness values with the presence of intermetalic inclusions which were found in fusion zone (dark spots in FZ-S4, Table.5).

In fusion line of 304L SS, there is a similar properties of microhardness of duplex filler metal and austenitic filler metal, this is due to the presence of same nature of phases which formed during TIG welding, these phases consist principally of delta ferrite and Secondary austenite. The inclusions also were found on fusion line of 304L SS.

### *Tensile test*

The tensile strength of joints has been evaluated. In each sample three specimens were tested, the tensile strength and their elongation are mentioned in Table 6.

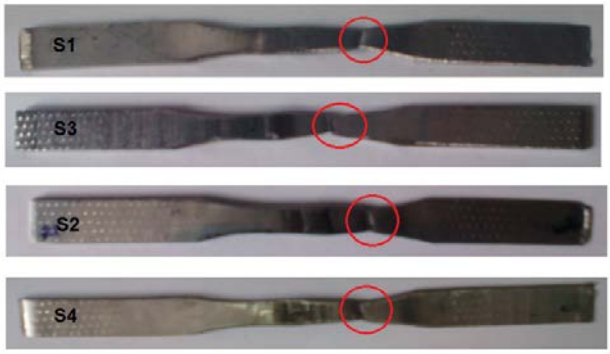



***Fig.6*** *Broken specimens*

The Ultimate strength and elongation of S1, S2, S3 and S4 specimen are shown in Table 2. therefore, the tensile properties change significantly with the filler metal nature, which can be attributed on one hand by the Difference between the four microstructures of fusion zones, and on the other hand by the joining zone, which is influenced, primarily by connection zone (FZ/HAZ), and in secondary consideration: by austenitic grain growth (in HAZ-304L) and ferritic grain growth (in HAZ-X70).

Among the different testes, a duplex filler metal clearly gives a better combination of strength, ductility compared to the other filler metals (Table.6).

***Table.6:*** *Tensile properties of the weld joints*

| Sample | S1 | S2 | S3 | S4 |
|---|---|---|---|---|
| $\sigma_m$ (MPa) | 522.40 | 642.02 | 671.77 | 487.13 |
| $\varepsilon_m$ (%) | 15.1 | 14.8 | 11.8 | 9.3 |
| Location of fracture | MB(X70) | MB(X70) | BM (304L) | BM(X70) |

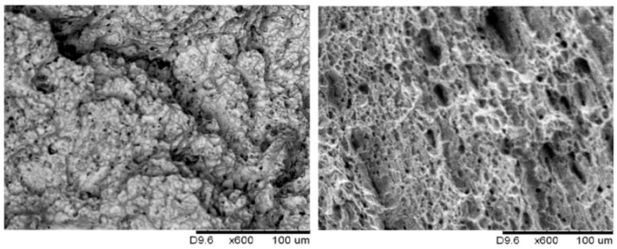



***Fig.7*** *SEM fractographs (X70 in the right)*

Examination of the fracture surfaces of the broken mechanical test specimens showed that Transgranular brittle failure and intergranular ductile failure occur in 304L-S3 specimen, which contains Clefts and river forms, with the presence of several crack arrest lines.

The fracture surface in X70 base metal indicated a ductile failure with granular aspect, which is consistent with significant ravelling of material. Therefore, ductile cleavage indicates that cracks growth phases were relatively slow compared to S3 specimen.

### *Charpy impact*

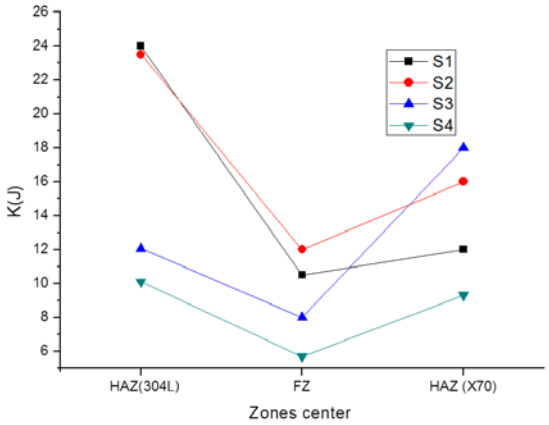



***Fig.8*** *Measurements of Charpy Impact*

The impact tests presented in figure 6 indicated that the combination of impact resistance (K) in second sample (S2) is better than the other samples. However the lower energy was found in S4 fusion zone. Furthermore, it is also apparent that homogeneous bimetallic joints have excellent impact properties (low Carbone fusion zone with X70 base materials and stainless fusion zones with 304L base material) compared to the heterogeneous joints.

## *6. Conclusion*

Based on the results obtained, it was possible to conclude that:

Duplex filler have a good weldability with 304L SS/ HSLA-X70 dissimilar joints compared to austenitic low Carbone filler metal by medium energies of TIG process.

This study investigates the effects of filler metal composition on 304L SS/ HSLA dissimilar welds and the formation of microstructures at various weld zones of different filler metal composition, Variation in morphology of microstructures across the fusion zone and heat affected zone is evident within solder. Microhardness profiles charpy test tensile test are made and linked with the formation of the microstructures in different weld zones.

As regards the mechanical behavior, At Samples welded by filler metals, there was an increase in the hardness of both the FZ and the HAZ with the best characteristic given by duplex filler metal. This filler metal combines between improvement in maximum tensile and amelioration of impact resistance.

In welded sample without filler metal, we find a significant decrease in mechanical properties. That phenomenon can be explained mainly by existence of ferrite slabs and martensite lattices in fusion zone.

To understand more realistically the application of dissimilar weld joints in industry, electrochemical tests will be very important to evaluate the resistance of weldment against corrosion degradations.

## *References*

[1] Subodh Kumar, A.S. Shahi. “Effect of heat input on the microstructure and mechanical properties of gas tungsten arc welded AISI 304 stainless steel joints” Materials and Design 32 (2011) 3617–3623

[2] S. Jana “Effect of heat input on the HAZ properties of two duplex stainless steels”, Journal of Materials Processing Technology, 33 (1992) 247-261

[3] V.S.R. Murti, Y.R. Sastry “Some studies on the service weldability of HSLA steels using 18Cr, 8Ni, 6Mn type austenitic electrodes”, Journal of Materials Processing Technology, 37 (1993) 759 765.

[4] Sindo Ko “Welding metallurgy”, Second Edition. ISBN: 0-471-43491-4 (2003).

[5] Rahul Unnikrishnan, K.S.N. Satish Idury. “Effect of heat input on the microstructure, residual stresses and corrosion resistance of 304L austenitic stainless steel weldments” materials characterization 93(2014)10–23

[6] ASME “Qualification Standard for Welding and Brazing”, An International Code of ASME Boiler and Pressure Vessel Committee on welding and Brazing, USA, 2010.

[7] ASTM International E08-03“Standard test methods for tension testing of metallic materials”.

[8] ISO 148 “teste d’impact sur échantillons iso en V”, NF EN ISO 148-2 (2009).

# HOT FORGING OF POWDERED $Fe_3Al$ INTERMETALLIC ALLOYS

Prof., Dr.Sc. Bagliuk G.A., PhD. Tolochin A.I., PhD. Iakovenko R.V., M.Sc. Tolochina A.V., M.Sc. Kurikhin V.S.
Institute for Problems of Materials Science, National Academy of Science of Ukraine
gbag@rambler.ru

***Abstract:*** *The capabilities of powder hot forging for manufacturing of $Fe_3Al$ intermetallics and effect of forging and following thermal treatment routines on their structure and properties had been investigated. $Fe_3Al$ intermetallic powders were produced by means of thermal synthesis at 1000 $^0C$ in vacuum from a mixture of Fe and Al elemental powders. Hot forging of consolidated preforms had been carried out from 1000, 1050, 1100 and 1150 $^0C$ and afterwards the hot forged preforms were subjected to supplementary sintering in vacuum at 1100÷1450 $^0C$. It is foud, that thermal synthesis of Fe + 14 % Al powder mixture results in formation of $Fe_3Al$ phase. Sintering of hot forged specimens result in increasing of strength and crack growth resistance, which values enhance with increasing of sintering temperature. Otherwise the hardness of hot forged intermetallics decreases after their sintering. The influence of modes of treatment on the structure and properties of the materials was investigated. It has been established that the strength and fracture toughness of the intermetallics obtained from milled blend after hot forging had the higher values as compared with the alloy made from the batch without its milling.*

***Key words****: INTERMETALLICS, IRON ALUMINIDES, POWDER, HOT FORGING, SINTERING, STRUCTURE, STRENGTH.*

## *Introduction*

The development of modern technology requires implementation of new materials which combine the chemical resistance, high wear resistance and heat resistance, which possess intermetallic compounds, in particular - iron aluminide. These intermetallic compounds are becoming more attractive to modern industry due to their unique combination of physical, chemical and mechanical properties, such as low density, high corrosion resistance, heat resistance and heat-temperature strength [1-3].

However, the widespread commercial use of such materials obtained by casting is currently limited due to the inherent fragility, low values of ductility and toughness at room temperature [1, 2].

At the same time, there was a series of works, pointing to prospects for the use of products from Fe-Al intermetallic powder metallurgy techniques such as hot isostatic pressing, extrusion, hot forging or pressing and injection molding [4-6], spark plasma sintering (including the combination with mechanical alloying) [7, 8]. However, the limited information in this field leads to the need for comprehensive research in the development of new effective technologies for manufacturing products from Fe-Al intermetallic compounds and study of the impact of technological modes of manufacturing on the structure and properties of the resulting materials.

It is known, as well, that the basic physical and mechanical properties of materials and performance attributes are largely dependent on the size and morphology of the structural elements of the alloy and increases with increasing dispersion past due, in particular, intensive grinding of the initial powders accompanied by their mechanical activation [8-10].

In this regard, the aim of this work was to study the impact of technological modes of processing the initial powder mixture and thermomechanical processing of sintered iron aluminide with the use of methods of hot forging on the structure and properties of the resulting materials.

## *Experimental procedure*

The initial powders of iron with particle size 80-160 microns, and aluminum having a particle size of 30-70 microns in the ratio (%, wt.) of 86Fe + 14Al were mixed in a tumbling mixer for 60 minutes in an alcohol.

Thermal synthesis of the intermetallic $Fe_3Al$ powder from the mixture of Fe and Al elemental powders was performed under vacuum at a temperature of 1000 °C with isothermal exposure 60 min.

As a result of synthesis porous sponge was received, which was crushed and the obtained alloy powders were pressed at 600 MPa to porous billet for subsequent hot forging. The billet was heated in argon to 1000, 1050, 1100 and 1150 $^0C$ and hot forging was performed in the semiclosed die on the screw arc-type stator press.

The samples after hot forging were divided into four groups, one of which did not respond to further heat treatment, and the other three were subjected to additional sintering in vacuum in accordance with the following modes:

– sintering at 1100 °C - 180 min.;
– sintering at 1300 °C - 10 min.;
– sintering at 1450 °C - 10 min.

To study the effects of dispersion and the morphology of the structural elements on the structure and properties of the intermetallic compounds for their preparation were used the powder mixtures of two types: in the first case the initial iron and aluminum powders were mixed in a tumbler mixer for 60 minutes (mixture I), in the second - the same initial mixture was milled in a planetary mill for 20 minutes in alcohol (mixture II).

The obtained after hot forging samples of both parties were subjected to the following modes of processing:

– mode 1 – hot forging without additional treatment;
– mode 2 – hot forging + sintering in vacuum at 1100 °C for 180 min.;
– mode 3 – hot forging + sintering in vacuum at 1300 °C for 10 min.

After implementation of each operations process for all of the obtained samples their density was investigated (by means of hydrostatic method), electrical resistivity (by measuring the voltage drop), the Vickers hardness with a load of 100 N, bending strength, fracture toughness. Bending and fracture tests was performed testing machine Ceramtest system. X-ray phase analysis of samples was performed on DRON-3 difractometer in Co-Kα radiation. The structure of the material investigated by the scanning electron microscope JEOL Superprobe 733.

## *3. Results and Discussion*

The results of XRD analysis of samples obtained after various processing steps showed that the synthesis of Fe-Al powders mixture at 1000 °C leads to the formation of intermetallic compound with an ordered B2 type structure, which is typical for phase FeAl, with interplanar spacings [110] constituting 2,044 Å (fig.1). Superstructural lines which characterize structure of the $D0_3$ type, and free aluminum and iron in the synthesized sample it was not revealed. The samples after hot forging from temperature 1000–1150 °C had the identical phase structure.

The application of subsequent sintering of forged samples allows ordering of the structure of the intermetallic compound of the type and appearance of $D0_3$ phase $Fe_3Al$, which is noted by the presence of X-ray diffraction patterns superstructure lines.

The density of the samples after forging at 1000 °C was about 6,62 g/cm$^3$, and a further increase in temperature is almost unchanged (fig. 2). Subsequent sintering at 1100 °C and 1300 °C led to some decrease of density is more distinct for the samples forged at lower temperatures. Decrease of the porosity may be associated with degassing of samples during sintering in vacuum after forging and ordering process structure B2 type to type $D0_3$. Sintering of compacted samples at 1450 °C leads to increased

density up to 6,71 ÷ 6,72 g/cm$^3$ for all temperatures of forging that correspond to the theoretical density of the intermetallic $Fe_3Al$.

.

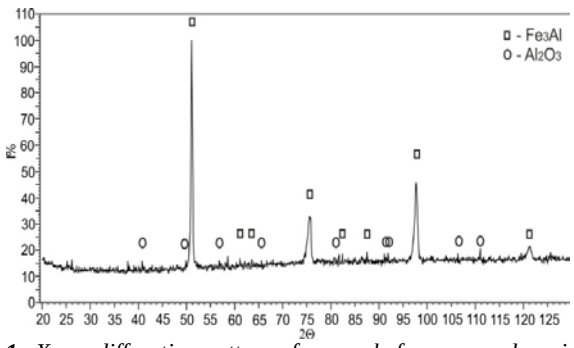



***Fig. 1.*** *X-ray diffraction pattern of a sample from a powder mixture Fe + 14% Al after thermal synthesis and forging at a temperature of 1050 °C*

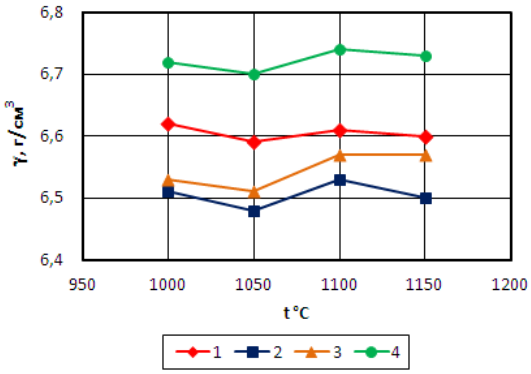



***Fig. 2.*** *Relationship between materials density and forging temperature for the samples after: 1 – hot forging (HF); 2 – hot forging + sintering at 1100 °C; 3 – forging + sintering at 1300 °C, 4 – forging + sintering at 1450 °C*

The analysis of microstructure of samples after forging didn't show noticeable influence on it forging temperature, while their subsequent sintering led to a considerable increase of degree of interparticle fusion: in the continuous grid of brittle interparticle contacts of hot forged intermetallic (fig. 3a) after sintering at a relatively low temperature of 1100 °C interparticle fusion elements was observed (fig. 3b), while after sintering at increases temperature the interparticle mesh was converted markedly into a discontinuous (fig. 3c, d). Increasing of sintering temperature also leads to some consolidation of the structure.

Quality of borders or degree of contact interaction between particles in material are reflected indirectly by the characteristic of electrical resistivity. According to the results of investigations, the samples after forging showed some decrease in electrical resistivity with increasing of forging temperature to 1100÷1150 °C (fig. 4), which may be caused by increasing the degree of adhesion between particles at higher temperatures. However at forging temperature of 1050 °C there is some increase in the electrical resistivity of the intermetallic compound, the increased porosity received after forging from 1050 °C samples (see fig. 2) can be one of the reasons of that. Thus, the defects which led to the increased value of the electrical resistivity of the intermetallic compound after forging from 1050 °C doesn't improve the subsequent sintering neither at high, nor at a low temperature.

Sintering of the samples compacted by forging shows decrease electrical resistivity from 129÷132 mkOm·sm to 112÷116 mkOm·sm, respectively for forged intermetallic compound before and after sintering. The reason for this decrease of electrical resistivity can both improved quality of interparticle borders and decrease in their length, as noted on fig. 3.

The characteristic of material strength also is sensitive to quality of interparticle borders. Bending tests of the samples showed that their strength after forging without subsequent sintering appeared at the level of 400 MPa and practically didn't depend on forging temperature (fig. 5, a). Sintering of the forged samples at 1100 °C resulted in an increase in strength to 620÷700 MPa and the sintering temperature increases to 1300 and 1450 $^0$C increased the level of strength of materials to 900÷1050 of MPa. Presumably, this increase of strength associated with a change of state bounderies by improving the adhesion between the particles and a decrease in the length of such boundaries, which is particularly noticeable for higher sintering temperatures.

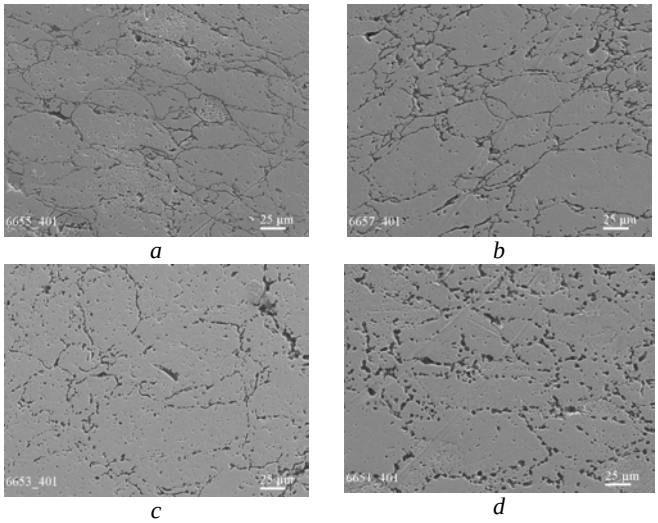



***Fig. 3.*** *The structure of the samples after forging at 1100 °C (a) and subsequent sintering at 1100 °C (b); 1300 °C (c) and 1450 °C (d)*

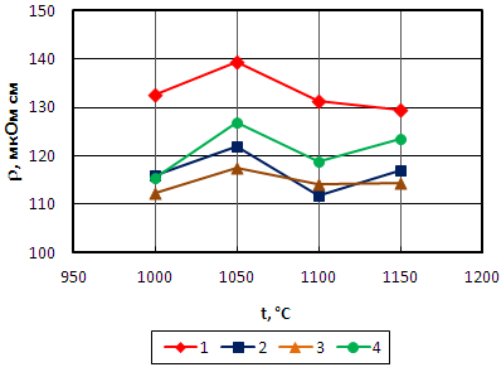



***Fig. 4.*** *Relationship between electrical resistivity and forging temperature for the samples after: 1 – hot forging (HF); 2 – hot forging + sintering at 1100 °C; 3 – forging + sintering at 1300 °C, 4 – forging + sintering at 1450 °C*

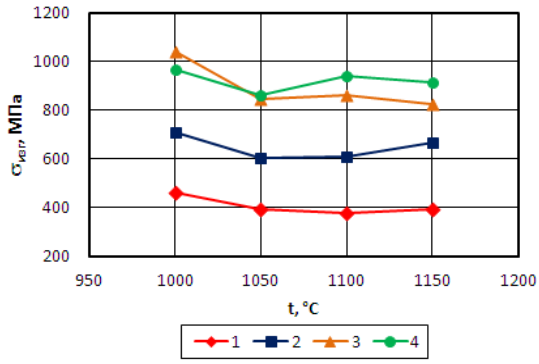



***Fig. 5****. Relationship between bending strength and forging temperature for the samples after: 1 – hot forging (HF); 2 – hot forging + sintering at 1100 °C; 3 – forging + sintering at 1300 °C, 4 – forging + sintering at 1450 °C*

Other characteristic which can estimate strength of boundaries and shows ability of material structure to resist crack promotion is a fracture toughness. Furthermore, the intermetallics are the materials of low ductility and fracture toughness is the most appropriate characteristic, that describes the behavior of brittle materials under loading.

The fracture toughness assessment of the samples after hot forging shown that they possess $K_{1C}$ values at 10÷11 MPa·m$^{1/2}$ for the whole range of forging temperatures (1000÷1150 °C) (fig. 6). Their sintering allowed to increase this characteristic and with the increase of sintering temperature there is a marked increase in fracture toughness of 14÷15 MPa·m$^{1/2}$ after sintering at 1100 °C , till 17÷ 20 MPa·m$^{1/2}$ – at 1300 $^0$C and till 22÷ 33 MPa·m$^{1/2}$ – at 1450 °C, which, in our opinion, is associated with a significant improvement in the quality of interparticle boundaries.

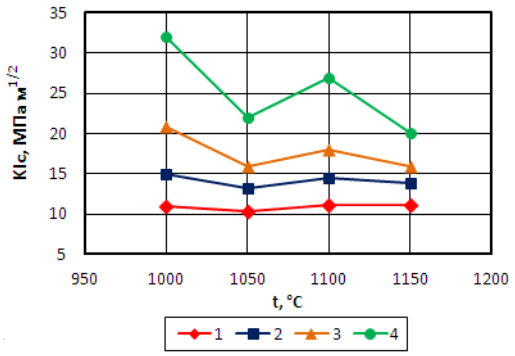



***Fig. 6**. Relationship between bending fracture toughness and forging temperature for the samples after: 1 – hot forging (HF); 2 – hot forging + sintering at 1100 °C; 3 – forging + sintering at 1300 °C, 4 – forging + sintering at 1450 °C*

Unlike previous characteristics of the intermetallics, which had insignificant dependence on forging temperature, evaluation of hardness values indicate an increase in the latter with increasing temperature deformation. In case of sintering of hot forged samples there is a decrease of hardness in compare with unsintered materials (fig. 7).

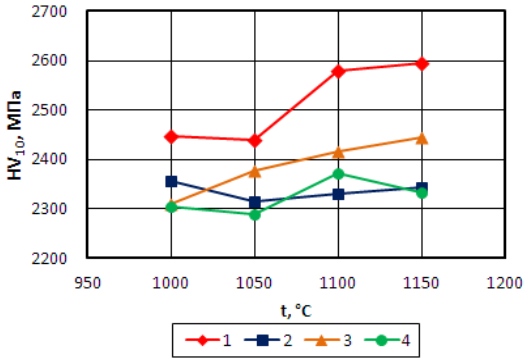
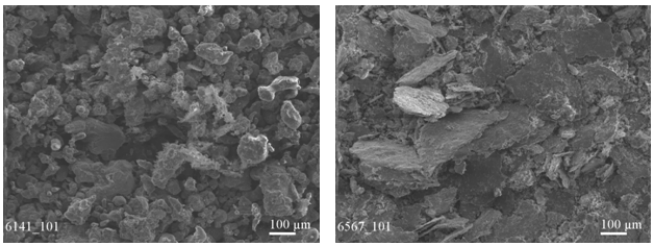



***Fig. 7**. Relationship between hardness and forging temperature for the samples after: 1 – hot forging (HF); 2 – hot forging + sintering at 1100 °C; 3 – forging + sintering at 1300 °C, 4 – forging + sintering at 1450 °C*

When studying the influence of preliminary processing of initial powder mixtures on the structure and properties of the resulting material it was shown that milling in a planetary mill did not lead to a noticeable refinement of mixture components compared to mixing in a tumbling mixer (fig. 8). However, due to intense exposure of local plastic deformation of powder particles the significant amount of lamellar conglomerates appeared in the blend composition that is caused by rather high plasticity of mixture components.

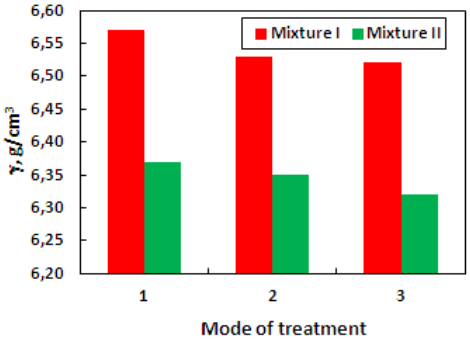



*a* *b*

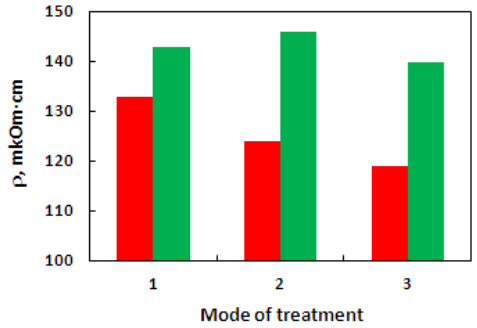
***Fig. 8.** The morphology of initial powder mixtures after mixing in a tumbling mixer (a) and milling in a planetary mill (b)*

The analysis of results the density of the samples after each mode of processing showed that application of hot forging for densification of iron aluminide obtained from a mixture of Fe and Al elemental powders (mixture I) and the mixture after milling in a planetary mill (mixture II) allowed to obtain intermetallics density of 6,57 g/cm$^3$ and 6,37 g/cm$^3$ respectively (fig. 9a).

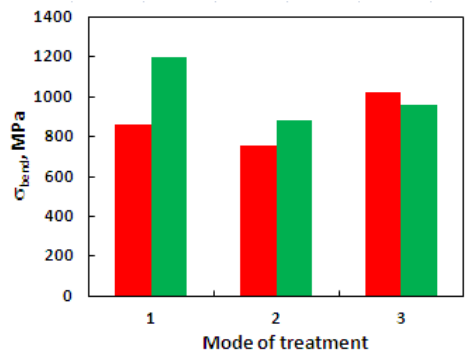
Application of vacuum sintering for samples after forging led to some reduction in density - to 6,52 g/cm$^3$ and 6,32 g/cm$^3$ for the alloys obtained from the first and second mixtures, respectively, which may be due to the partial degassing of the samples so and by the formation of oxide phases in the grain boundaries in the presence of residual oxygen in the powder.



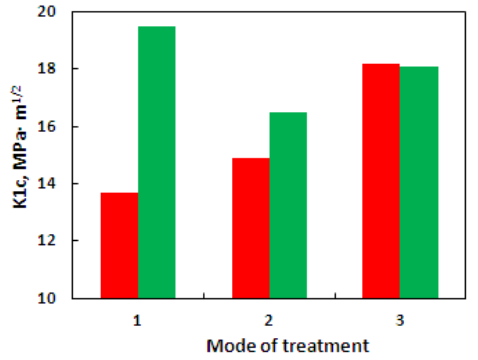

*a*



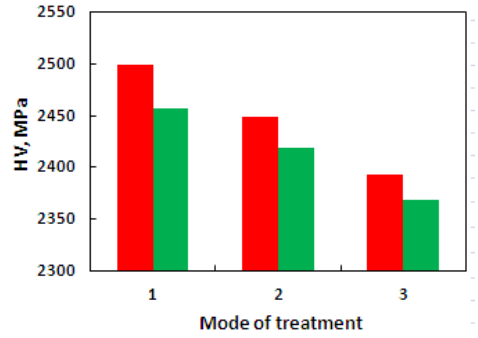

*b*




*c*




*d*




*e*

***Fig. 9.*** *The effect of processing modes and type of original powder mixture on density (a) and the basic physical and mechanical properties (b-e) of intermetallics*

Noticeable increase in the oxygen content for the material after intensive milling in a planetary mill compared with the initial powder and the material, obtained from the simple powder mixture was confirmed by the data in Table. 1.

***Table. 1.*** *The oxygen content in the initial powders of iron and aluminum and intermetallic compounds of two compositions after sintering at a temperature 1000* °C

| Powder | Al | Fe | Mixture I | Mixture II |
|---|---|---|---|---|
| Oxygen content, % | 0,2 | 0,4 | 0,2 | 0,9 |

The data of microstructural analysis of hot forged intermetallics had shown, that after forging of initial powders (mixture I) structure is observed with near-equiaxed particulate size of 50-150 microns (fig. 10,a). After forging of milled powders (mixture II) structure seems like substantially lamellar with 10-20 microns thickness of lamellas (fig. 10,b). Thereby in the structure of the intermetallics obtained from milled powders the lamellar particles thin layers of obviously oxide phase were observed. Subsequent sintering the samples at 1100 °C and 1300 °C led to some enlargement of the structure as well as a marked increase in the degree of interparticle splicing of material obtained from unmilled powders: in a continuous grid of brittle interparticle contacts in hot forged intermetallic (fig. 10a) interparticle splice elements after sintering at a relatively low temperature of 1100 °C is observed (fig. 10,c), and with increasing of sintering temperature to 1300 °C the mesh was markedly transformed into discontinuous (fig. 10, e).

In case of use of the milled powders noted effect is shown significantly more weakly (fig. 10, b,d,e).

Local X-ray analysis of the intermetallic phases showed that the plates consist of iron with aluminum and dark layers are oxide phase, which can be attributed to the nonstoichiometric spinel $Fe_xAl_yO_z$. The component ratio indicates that the composition of plates consists of several phases - solid solution and intermetallic compound, i.e. B2+α and $D0_3$+α. Furthermore, an increase in the sintering of aluminum and oxygen content in the oxide phase, which further shifts the phase composition of lamellar particles to the area of the solid solution α.

It is obvious that the emergence of oxide phases in the alloy should be manifested in the performance characteristics of the electrical resistivity, which indirectly reflects the degree of interparticle interaction in the material. For all modes of processing the rougher due to the presence of intergranular oxide layer resistivity material with lamellar structure higher than the electrical resistance of the intermetallic forged initial powders (fig. 9b). Thus, if the intermetallic compounds made from untreated powders (mixture I), there is a clear trend noticeable decrease conductivity after annealing of hot-forging preforms and with increasing the sintering temperature for the material obtained from milled powders (mixture II), influence on the sintering resistivity values slightly.

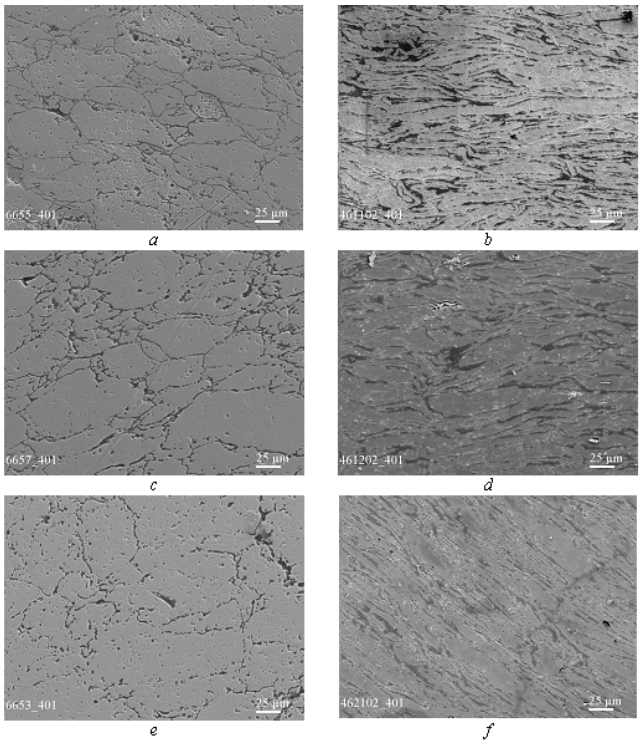



***Fig. 10****. The structure of the mixture intermetallic compounds I (a, c, e) and II (b, d, f) after hot forging (a, b) and subsequent annealing at 1100 °C (c, d) and 1300 °C (e, f )*

These results well correlate with the data on influence of sintering on change of structure of intermetallic compounds shown in fig. 10. Decrease electrical resistivity of intermetallic compound obtained after sintering mixture I apparently due both to the improvement of the contact between the particles and the processes of coalescence of smaller pores into larger at the boundaries between the particles during sintering, as well as decrease in the total duration of the borders due to coarsening of the particles (fig. 10 , a, c, e).

At the same time, insignificant effect sintering the structure of the grain boundaries for materials obtained from milled mixture II (fig. 10, b, d, f) similarly reflected on the nature of the change in the resistance.

Taking into account the higher density and smaller values conductivity for intermetallics obtained from mixture I (not subjected to preliminary intensive grinding) would suggest, and the possibility of providing with such technological scheme and the higher the strength characteristics of the alloy. However, the results of bending tests have shown that the material obtained from mixture II, despite significant intergranular oxide layers, reaching a thickness of 5 microns, after the hot forging has a higher strength (~1200 MPa) as compared with an alloy made from mixture I (870 MPa) (fig. 9c).

Similar regularity is observed for the values of fracture toughness of intermetallics made from powders of different morphology (fig. 9d).

The reason for this phenomenon seems to be something that was born and propagating crack under load in the event of the lamellar structure of intermetallic compound is extremely difficult to fully pass on the grain boundary and go around the plate-like particles, as in the case of destruction of material with considerably less texturing structure .

Sintering the samples after forging at 1100 ℃ causes decrease of strength and fracture toughness for both alloys (fig. 9, c,d) from removing during sintering strain hardening effects and thermal stresses, and increase the sintering temperature to 1300 ℃ leads to an increase of these characteristics improve due to quality and strength of phase boundaries, as evidenced by a decrease in the electrical resistivity of alloys, sintered at high (1300 ℃) temperature (fig. 9b).

The hardness of the intermetallics obtained from the charge I after forging as well as after the subsequent sintering in both modes was higher compared to the intermetallics made from batch II, subjected to milling (fig. 9, e). Sintering after forging leads to a marked decrease of hardness of both alloys, the value of which decreases with increasing the thermal treatment temperature.

## *Conclusions*

1) Thermal synthesis of Fe + 14% Al powders mixture at 1000 $^0$C leads to the formation of intermetallics with an ordered structure, which is maintained even after hot forging.

2) Forging temperature in the investigated temperature range have not any significant impact on the structure of the resulting intermetallics, while their subsequent sintering leads to significant increase in the degree of interparticle splicing. The solid brittle mesh interparticle contacts for hot forged material with increased sintering temperature to 1300 ÷ 1450 $^0$C is converted into discontinuous.

3) The sintering after hot forging of the samples increases material strength and fracture strength values that increase with increasing the sintering temperature, while the hardness after sintering of hot forging of intermetallic reduced.

4) Preliminary processing of Fe and Al elemental powders mixture in a planetary mill essentially changes the morphology both the initial mixture and the structure of intermetallics after hot forging.

5) The strength of the intermetallics obtained from milled charge after hot forging had higher values (~1200 MPa) as compared with the alloy made from powder mixture without milling (870 MPa). Similar pattern is observed for the values of fracture srength of intermetallics produced from powders of various morphologies.

## *References*


1. Deevi S. C., Sikka V. K. Nickel and iron aluminides: An overview on properties, processing, and applications // Intermetallics. – 1996. – Vol. **4**, No. 5. – P. 357÷375.
2. Cohron J. W., Lin Y., Zee R. H., George E. P. Room-temperature mechanical behavior of FeAl: Effects of stoichiometry, environment, and boron addition // Acta Mater. – 1998. – Vol. **46,** No. 17. – P. 6245÷6256.
3. Martinez M., Viguier B., Maugis P., Lacaze J.. Relation between composition, microstructure and oxidation in iron aluminides // Intermetallics. – 2006. – Vol. **14,** No. 10÷11. – P. 1214÷1220.
4. Song H., Wu Y., Tang C., Yuan S., Gong Q., Liang J. Microstructure and Mechanical Properties of FeAl Intermetallics Prepared by Mechanical Alloying and Hot-Pressing // Tsinghua science and technology. – 2009. – Vol. **14**, No. 3. – P. 300÷306.
5. Wang J., Xing J., Qiu Z., Zhi X., Cao L. Effect of fabrication methods on microstructure and mechanical properties of $Fe_3Al$-based alloys // Journal of Alloys and Compounds. – 2009. – Vol. 488. – P. 117÷122.
6. Szczepanik S., Godlewska E., Mania R. Materiały Fe-Al otrzymane z proszków // Kompozyty (Composites). – 2002. – Vol. **2**, No. 4. – P. 242÷248.
7. Grosdidier T., Ji G., Bernard F., Gaffet E., Munir Z. A., Launois S. Synthesis of bulk FeAl nanostructured materials by HVOF spray forming and spark plasma sintering // Intermetallics. – 2006. – Vol. 14, No.10/11. – P. 1208÷1213.
8. *He Q., Jia C., Meng J.* Influence of iron powder particle size on the microstructure and properties of $Fe_3Al$ intermetallics prepared by mechanical alloying and spark plasma sintering // Materials Science and Engineering: A. – 2006. – No. 1-2, vol. 428. – P.314÷318.
9. *Jia C., He Q., Meng J., Guo L.* Influence of mechanical alloying time on the properties of $Fe_3AI$ intermetallics prepared by spark plasma sintering // Journal of University of Science and Technology Beijing. - 2007. – Vol. 14, No. 4. – P. 331-334.
10. *Song H., Wu Y., Tang C., Yuan S., Gong Q., Liang J.* Microstructure and Mechanical Properties of FeAl Intermetallics Prepared by Mechanical Alloying and Hot-Pressing // Tsinghua science and technology. – 2009. – Vol. 14, No. 3. – P. 300÷306.